UQAC

Université du Québec
à Chicoutimi

Effect of grain refiners on the refining performance in aluminum wrought AA6111 alloys

PAR

Chaima Hajji

Sous la direction de M. X.Grant Chen directeur et M. Zhan Zhang codirecteur

Mémoire présentée à l'Université du Québec à Chicoutimi en vue de l'obtention du grade de Maître ès sciences appliquées (M. Sc. A.) en ingénierie

Jury :

M. X.Grant Chen, Directeur de recherche, DSA de l'UQAC, Président du Jury

M. Zhan Zhang, Codirecteur de recherche, DSA de l'UQAC, Membre interne

M. Emad Elgallad, Professeur-chercheur, DSA de l'UQAC, Membre interne

M. Kun Liu, Professeur-chercheur, DSA de l'UQAC, Membre interne

QUÉBEC, CANADA

© Chaima Hajji, 2023

RÉSUMÉ

Étant donné le rôle critique d'affinage des grains dans l'amélioration de la coulabilité et des propriétés des alliages d'aluminium corroyés, ce projet vise à optimiser la pratique d'affinage des grains dans les fonderies d'aluminium. Des efforts ont été dédiés pour déterminer les facteurs clés à considérer lors de l'affinage des alliages d'aluminium corroyés 6111, tout en mettant l'accent sur les puissants raffineurs des grains. De plus, des études comparatives ont été établies sur le pouvoir affinant des raffineurs en termes de la réduction de la taille des grains, la résistance à la fissuration à chaud et la réaction avec les solutés empoisonnants. Pour ces raisons, le présent travail est divisé en deux grandes parties.

Dans la première partie, les effets de différents raffineurs de grains (Al-3Ti-1B, Al-5Ti-1B et Al-3Ti-0.15C) sur la taille et la morphologie des grains ainsi que sur la fissuration à chaud de l'alliage d'aluminium 6111 ont été étudiés, tout en tenant compte des paramètres de la coulée semi-continue à refroidissement direct (Direct Chill): taux d'ajout du raffineur de grain (1, 2 et 3Kg/T), ajout de Ti, et vitesse de refroidissement (0,4 et 4°C/s). Les résultats ont prouvé que les trois raffineurs des grains peuvent réduire efficacement la taille des grains de l'alliage 6111, et le raffineur Al-5Ti-1B est le plus efficace dans toutes les conditions. La caractérisation de la microstructure des alliages mères des raffineurs a révélé que le raffineur Al-5Ti-1B avait de plus grosses particules d'Al_3Ti, une densité numérique plus élevée de particules de TiB_2 avec une distribution de taille plus raisonnable que les raffineurs Al-3Ti-1B et Al-3Ti-0.15C. Avec l'augmentation de l'ajout de raffineur, les morphologies des grains ont évolué d'une morphologie dendritique, cellulaire à globulaire. De plus, en plus du raffineur de grain, l'ajout de titane sous forme de soluté avec une vitesse de refroidissement élevée ont été bénéfiques pour une réduction supplémentaire de la taille des grains. Les raffineurs de grain ont également eu un effet significatif sur la susceptibilité à la fissuration à chaud de l'alliage 6111. Lorsque la morphologie des grains est dendritique, l'ajout du raffineur des grains a diminué la susceptibilité à la fissuration à chaud. Cependant, un ajout supplémentaire de raffineur a entraîné une augmentation de la susceptibilité à la fissuration à chaud malgré la taille très petite des grains.

Dans la deuxième partie, l'effet d'empoisonnement du Cr sur l'affinage des grains a été étudié dans les alliages d'aluminium 6111. Le présent travail a pris en compte les paramètres de la coulée semi-continue à refroidissement direct (Direct Chill): deux vitesses de refroidissement (0,4 et 4 °C/s), ajout de Ti, trois affineurs de grains différents (Al-3Ti-1B, Al-5Ti-1B et Al-3Ti-0,15C) avec différents taux d'addition (1, 2 et 3Kg/T). Il a été constaté qu'une concentration élevée de Cr avait un effet d'empoisonnement sur l'affinage des grains, entraînant une structure à gros grains dans les trois raffineurs de grain. Les résultats SEM-EDS ont révélé que les 3 types d'intermétalliques présents dans les raffineurs (Al_3Ti, TiB_2 et TiC) pourraient contenir du Cr à la surface des particules. Un pourcentage plus élevé de Cr a été trouvé toujours

à la surface des particules d'Al$_3$Ti par rapport aux particules de TiB$_2$ et TiC, ce qui montre que les particules d'Al$_3$Ti étaient le composé le plus susceptible à une telle réaction avec le Cr. Il s'est avéré que la diffusion de Cr dans les particules augmente avec l'augmentation du temps de maintien. Après cela, le modèle d'appariement bord à bord (E2EM) a été appliqué pour examiner l'appariement cristallographique interfacial entre Al et les particules intermétalliques avant et après la diffusion de Cr. Les résultats basés sur les calculs (E2EM) ont montré que la diffusion de Cr dans les particules Al$_3$Ti et TiC réduisait l'appariement cristallographique des particules avec la matrice Al, entraînant une faible efficacité d'affinage. Couplant les présents résultats avec les études de la littérature, des mécanismes d'empoisonnement ont été proposés pour expliquer l'effet d'empoisonnement au Cr.

ABSTRACT

Given the critical role of grain refinement in improving the castability and materials properties of wrought aluminum alloys, this project aims to optimize the grain refinement practice in aluminum casthouses. Efforts have been made to present a number of key points to consider when refining the 6111 wrought aluminum alloys, highlighting the potent grain refiners in terms of their efficiency. Moreover, comparisons were made based on the refiner potency in the grain size reduction, the resistance to the hot tearing and the reaction with the poisoning solutes. For these reasons, the present work is divided into two main parts.

In the first part, the effects of different grain refiners (Al-3Ti-1B, Al-5Ti-1B and Al-3Ti-0.15C) on the grain size and morphology as well as hot tearing of 6111 aluminum alloy were investigated, taking in account of the direct chill casting parameters: grain refiner addition rates (1, 2 and 3Kg/T), Ti addition, and cooling rates (0.4 and 4°C/s). It was found that all three grain refiners can effectively reduce the grain size of 6111 alloy, and the Al-5Ti-1B refiner is the most effective in all conditions. The microstructure characterization of the refiner master alloys revealed that Al-5Ti-1B refiner had bigger Al_3Ti particles, higher number density of TiB_2 particles with more reasonable size distribution than the Al-3Ti-1B and Al-3Ti-0.15C refiners. With the increase of the refiner addition, the morphologies of the grains evolved from dendrite, cellular to globular morphology. Moreover, in addition to the grain refiner, the addition of titanium as solutes and the high cooling rate were beneficial to further grain size reduction. The grain refiners had also significant impact on hot tearing susceptibility in 6111 alloy. When the grain morphologies are dendritic, the addition of the grain refiner decreased the hot tearing susceptibility. However, a further refiner addition resulted in an increase of the hot tearing susceptibility despite the very small grains.

In the second part, the poisoning effect of Cr on the grain refinement was investigated in 6111 aluminum alloys. The present work has taken in account of the DC casting parameters: Two cooling rates (0.4 and 4°C/s), Ti addition, three different grain refiners (Al-3Ti-1B, Al-5Ti-1B and Al-3Ti-0.15C) with different addition rates (1, 2 and 3Kg/T). It was found that a high concentration of Cr had a poisoning effect on the grain refinement, resulting in a coarse grain structure in all three grain refiners. SEM-EDS results revealed that the 3 kinds of intermetallics in the refiners (Al_3Ti, TiB_2 and TiC) could contain Cr in the particles surface. Higher % of Cr was always found in the Al_3Ti particle surface compared to TiB_2 and TiC particles, showing that Al_3Ti particles were the most likely compound to be affected by such reaction with Cr. The Cr diffusion in the particles was found to increase with increasing the holding time. After that, the edge-to-edge matching model (E2EM) has been applied to examine the interfacial crystallographic matching between Al and intermetallic particles before and after Cr diffusion. Results based on E2EM calculations showed that the Cr diffusion into Al_3Ti and TiC particles reduced the crystallographic matching of the particles with Al matrix, resulting in poor refinement efficiency. Coupling the present results with

findings in literature, poisoning mechanisms were proposed to explain the Cr poisoning effect.

TABLE OF CONTENTS

LIST OF TABLES

LIST OF FIGURES

ACKNOWLEDGEMENTS

First and Foremost, praises and thanks to the GOD, the Almighty, for His showers of blessings throughout my journey and master study in Canada. I have experienced your guidance day by day, whenever and wherever I am…

I would like to express my deepest gratitude to my respected supervisor, Professor X.Grant Chen, for his continued guidance and understanding . His professional attitude and immense scientific knowledge have deeply inspired me to acquire a logic and scientific vision. And, I am extremely honored to be accepted as a student in his research group and under his leadership. I extend to deeply thank him for his supervisory style, his generous financial support and for placing his trust and confidence in my abilities. Thank you for being a mentor who cares so much about his students.

I am deeply indebted to my respected co-supervisor, Professor Zhan Zhang, for his assistance during all this period, for discussions and advices, for his time and his patience to teach me, and especially his motivating words that helped me in all the time of research and writing of this thesis. Thanks a lot Sir.

I extend my thanks to my labmates in CURAL, especially for the shared jokes cracking the too serious moments. Special thanks to my friend Cong Li, for her true care and friendship. Also, I would like to thank the technicians of our lab: Messrs. Samuel Dessureault and Félix Tremblay, for their great technical support during the lab activities.

A very deep feeling of gratitude to my parents Salah Hajji and Habiba Hakaoui, for their sacrifices, purest love, prayers and for all their efforts throughout my life. Without them, this day would not have been possible. Also, I am extremely grateful to my uncle Karim Ennaciri, my aunt Nadia Hakaoui, and their beloved daughter Nada, for their unconditional love, support and the precious moments shared together. It was their encouragement that raised me up during this period. Also, I express my special thanks to my sisters, for their love and the keen interest shown to complete this thesis successfully.

Last but not least, I would like to thank my self, Chaima Hajji, for the sleepless nights working and for all the resistance during these years, alone and far from my family…

CHAPTER 1 : INTRODUCTION

1.1-   Background

Grain refinement presents a crucial practice in wrought aluminum alloys. Finer and equiaxed grain structure is well known to result in several benefits comparing to casting with larger and columnar grains [1]. Refining the alloy structure results in a number of attractive properties: (1) Enhancement in mechanical properties and surface finishing, (2) Uniformity to the extrusion and to the heat treatment response [2], (3) Improvement in fatigue life in term of fine distribution of second phases and microporosity [1]. As industrial practice, the grain refinement is performed by adding master alloys to the liquid aluminum before casting. These master alloys contain intermetallic particles that contribute to the generation of fine and equiaxed grains.

The most used master alloy in wrought aluminum alloys is the ternary master alloy Al-Ti-B with the composition of Al-5%Ti-1%B. Commercially, other compositions are available to provide different Ti/B ratios, including : Al-3%Ti-1%B, Al-5%Ti-0.6%B, Al-5%Ti0.2%B [2]. Each composition is made for specific products and applications [3]. The Al-5%Ti-l%B grain refiner is universally considered as the preferred grain refiner, and was reported to act well in controlling the grain size of wrought aluminum alloys [2, 3]. Unfortunately, quality defects such as surface defects in lithographic sheets and porosity in foils for packaging were obtained when using such master alloys that contain boron [2]. It has been reported that the large clusters of TiB_2 particles formed during the Al-Ti-B manufacture are behind such defects [4-6].

Such agglomerates are detrimental especially in products that require special surface finishes [7]. Plates used in the aircraft structure were found to suffer from a decrease in mechanical properties in the presence of large TiB_2 particles [2]. As a result, efforts have been made to develop a new boron-free grain refiner [2, 8].

The Al-Ti-C grain refiner was developed as an alternative, mainly to limit the particle agglomeration[2, 9]. An enhancement in interactions with filtration and degassing systems were also reported from using the Al-Ti-C instead of Al-Ti-B [9]. The master alloy Al-Ti-C was also commercially available with different Ti/C ratios, where the composition Al-3%Ti-0.15%C was the most used in aluminum refinement [2]. The refinement potency of both systems Al-Ti-C and Al-Ti-B are reported to be strongly linked to their microstructures features including the size, morphology and number density of the nucleant particles present in the master alloys, where these factors are controlled by the process parameters during the master alloy preparation [10].

Given the importance of grain refinement in Al production, collaborated efforts between industrials and academic researchers have been dedicated to reveal the grain refinement mechanism. Several mechanisms have been proposed, but no agreement on specific mechanism has emerged as yet. Moreover, none of the proposed theories could explain all the experimental findings [3, 10, 11]. It was stated that the lack of understanding the refinement is because the nucleation event is difficult to detect due to the lack of experimental tools, producing missing points for a complete understanding [3, 10]. In addition, it was suggested that grain refinement can actually

involve more than one mechanism, depending on the casting conditions, the grain refiner used and the tested alloy [10, 12]. Easton and StJohn [10, 11] provided a classification of all the theories proposed in literature. All the theories were classified into two major categories: (1) Nucleant paradigms and (2) solute paradigms. In nucleant paradigm, theories were developed with considering only the potency of nucleant particles that are added through master alloys, as nucleation sites in refinement mechanism. However, solute paradigm incorporates the essential role of solute elements in the grain refinement mechanism. Solute paradigm states that both potent nucleants and solutes are needed for efficient refinement [10, 11]. The solute potency is quantified by its ability in growth restriction of grains during its segregation in front of the growing grains [10, 11].

Titanium element has a much higher growth restriction effect as a solute compared to other elements, which can explain the excess Ti content in grain refiners to allow the presence of Ti into solution [13]. Moreover, segregations of solutes in solid/melt interface was found to provide the undercooling required for nucleation on potent particles [11]. In contrast, some solutes like Cr, Zr were found to have an adverse effect on the refinement potency, resulting in coarser grains [10]. Such alloying elements are generally added to aluminum alloys in the range of [0.1-0.2 mass%] for the deformed grain structure control and the strengthening reason. This adverse effect on grain refinement is generally donated as "poisoning effect" [14].

Different theories have been proposed to explain this poisoning effect where the general agreement was that the presence of such solutes may react with the nucleant

particles in the grain refiners making them ineffective or less effective [15]. The poisoning mechanism has been studied by several authors from crystallographic matching point of view, where it was agreed that the presence of poisoning elements produces a decrease in crystallographic matching between nucleant and Al [14]. However, controversies in this topic remains about the formed poisoning compound, whether it is a new layer that form and cover the nucleant like (Al3Zr,Al8Fe4Zr), or a substitution of Ti elements in the nucleant to form ($Al_3Ti_{1-X}M_X$), where M can be Cr or Zr [14, 16].

The grain refinement is also considered as one of the major method for reducing the hot tearing susceptibility [17]. The hot tearing defect is known to be a serious and common defect in Direct Chill casting, resulting in severe productivity losses [18]. Therefore, significant efforts have made and studies have been dedicated for establishing the correlation between grain refinement and hot tearing phenomena [17]. Grain characteristics (size and morphology) controlled by the grain refinement has been confirmed to affect the hot tearing susceptibility in wrought aluminum alloys [19, 20]. However, there is no definite conclusion about the manner in which grain refinement control the hot tearing problem, and subsequently there is no definite optimum addition rate of grain refiners. Moreover, the findings in literature have not yet provided an agreement on the exact grain structure (size and morphology) required for minimum hot tearing susceptibility [19, 20].

From industrial view, the objective is to obtain the high hot tearing resistance using the minimum of refiners addition, which improves the castings quality with a

reduction in the production cost [21]. However, the question remains in practice about whether it is required to refine until obtaining the equiaxed grain structure, or they should continue refine as much as possible to limit the hot tearing defect [20]. An excessive addition rate of grain refiners was found to increase the cost and resource, and also decrease mechanical properties [13].

Despite the extensive practice of grain refinement in foundries today, the procedure is still determined only by empirical rules [3]. This often make the refiners addition rates more excessive than required. It is fair to conclude from all the facts mentioned above that further studies need to be carried out to shed lights on this important field of grain refinement. Controversies in literature may arise from the difference in alloying elements and different supplied refiners, but also from the inaccurate measurement and the difference in the qualitative nature of experiments and studies. Therefore, standard experimental setups and parameters have to be fixed to limit such controversy. Therefore, it is necessary to find out some definite conclusions that can provide guidelines for aluminum casthouses.

1.2- Objectives

The present work was undertaken to provide a number of key points to be considered to improve the grain refining performance when making grain refinement practice in aluminum AA6111 alloys. Noting that the aluminum wrought AA6111 alloys are known to be one of the most sensitive wrought alloys to the hot tearing due

to their solidification characteristics [22]. Practically, efforts have been dedicated to achieve the goals with the flowing specific objectives:

1.   Find out the most suitable refiner for the aluminum wrought 6111 alloys in terms of type and quantity, considering the different industrial cast parameters (cooling rate, alloying element (Ti)).

2.   Study the effect of the grain refinement on the hot tearing susceptibility in 6111 alloys, highlighting the correlation between the refiners addition rate, the resulting grain structure and the hot tearing susceptibility in aluminum wrought 6111 alloys.

3.   Find out whether the Cr element influences the refinement process in 6111 alloys.

4.   Evaluate the crystallographic matching between the Al matrix and the nucleant particles before and after reaction with Cr. And suggest the possible poisoning mechanisms after coupling the findings with literature.

CHAPTER 2 : LITERATURE REVIEW

2.1-   Fundamentals in grain refinement

2.1.1-   Nucleation

Grains in metals start to form by a process called 'nucleation'. This term is used to describe the first step in the transformation process of the metal from liquid to a solid phase. There are two nucleation types i.e. homogeneous nucleation and heterogeneous nucleation [23]. In both types, the transformation in phase requires the formation of a nucleus [24, 25]. A nucleus is an embryo that reaches a critical radius rc to become stable. To reach such rc, an energy barrier for nucleation requires to be overcomed [26]. This energy barrier is known to be dependent on the interfacial energy between the old phase and the new one. The nucleus formation, in both nucleation types, depends on the temperature. And therefore, governed by the undercooling degree, where a larger undercooling provides a greater driving force for nucleation [27].

In the case of homogenous nucleation, nucleus is formed by evolution of the solidification state without involving any other sources such as the mould wall or any external facts [28]. In contrast, Heterogeneous nucleation is activated by the presence of solid foreign particles in the melt that can be impurities, mold wall or nucleating agent [28]. The surface of these particles represents the nucleation sites of the new solid phase. In real case, the heterogeneous nucleation is the dominant due to the mold walls and the presence of heterogeneous nucleation agents when solidifying the commercial Al alloys [7, 28]. The heterogenous nucleation is also the preferred mechanism because

it is energetically more favourable, and lesser undercooling degree is required for nucleation activation on foreign particles [28]. The presence of heterogenous particles decreases the interfacial energy between the old liquid phase and the new solid one.

Figure 2-1 shows the difference between solid-liquid phases in both homogenous and heterogenous nucleations. In the case of homogeneous nucleation, the surface area between the newly formed sphere and the old liquid is larger than the surface area between the shape of spherical cap and liquid in heterogeneous nucleation [24]. In the case of heterogenous nucleation, a part of nucleus is accommodated by the particle surface on which it is nucleating (as shown in **Figure 2-1**), producing differences in nucleation barriers [1].
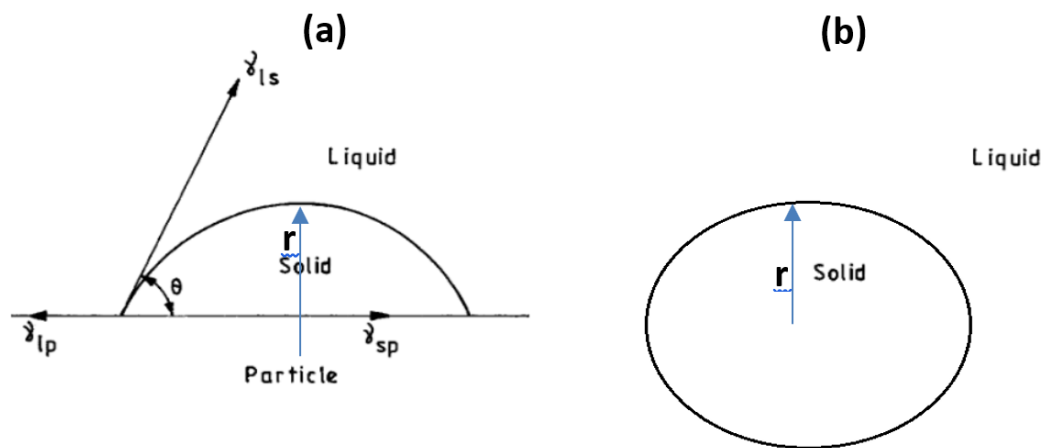
Figure 2-1 (a) heterogeneous nucleation, γ_{lp}, γ_{sp}, and γ_{ls} are liquid/particle, solid/particle, and liquid /solid interfacial energies. θ is the contact angle, (b) homogeneous nucleation. Original Figure from ref [10]

The nucleation barrier is the critical free energy barrier that should be reached by the increasing embryo to be stable. The free energy barrier in homogeneous case, is given by the following Equation [1]:

$$\Delta G^{*}_{homogeneous} = \frac{16\pi\gamma^{3}_{sL}}{3\Delta G^{2}_{v}}$$ (2-1)

where, γ_{sl}: the surface energy of a solid/liquid interface in J/m^{2}. ΔG_{v} is the driving force for solidification and is a function of the undercooling degree, the melt temperature and solidification enthalpy.

The free energy barrier for heterogeneous nucleation is given by the following Equation [1]:

$$\Delta G^{*}_{heterogeneous} = \frac{16\pi\gamma^{3}_{sL}}{3\Delta G^{2}_{v}} f(\theta)$$ (2-2)

Where, f(θ)is a function of the contact angle that takes values only between 0 and 1. θ is the contact angle already shown in **Figure 2-1**, where 0< θ <180 degree [1, 29]. The critical free energy barrier for heterogeneous nucleation is therefore always less than to the one for homogeneous nucleation **[1]**. The more potent heterogeneous substrates are those with lower contact angle (θ) that results in lower nucleation barrier [1].

2.1.2-   Growth of nuclei

During solidification, the growth is the process that takes place after the nucleation event. This step consists of the growth of the nucleated site to macroscopic size, forming the more ordered solid phase. The transformation from liquid to solid phase is accompanied by a release of heat, resulting in an exothermal process [28]. For pure metal, the columnar grains grow in direction antiparallel to the heat flow, starting from the mold wall. Those grains are essentially of planar morphology [1, 28]. However, in the presence of impurities or alloying elements, the zone of columnar grains are of dendritic morphology, and an inner part in the casting central containing equiaxed crystals [1, 28].

During a system solidification, the driving force for grain growth is governed by the total undercooling. In the case of pure metal, this total undercooling is dominated by the heat flow. While in an alloying system, the total undercooling is dominated by constitutional undercooling that arises from solute diffusion [28, 30, 31]. As the grains grow, solutes are rejected in the solid/liquid interface, forming a layer with a higher concentration in alloying elements ahead of the interface due to the segregated solutes. This layer is differentiated from the rest of liquid by its alloying constitution and melting temperature, which causes a local undercooling known by the constitutional undercooling since it is caused by a change in the liquid constitution [30, 31]. The driving force of growth is the constitutional undercooling in an alloying system. Therefore, the growth rate is dependent on the alloy composition [1].

2.2- Aluminum and Aluminum alloys

Aluminum is the most widely used non-ferrous metal in the world and is increasingly replacing steel in a variety of industries such as the automotive and aerospace ones. All this, thanks to its attractive properties including its resistance to corrosion thanks to its natural oxide layer. The corrosion issue is considered as the main reasons for metal failure in service. Adding to its high electrical and thermal conductivity, its low density of 2.7 g/cm3, one third the steel density(7.83 g/cm^3) [32]. Moreover, its high ductility allows it to be casted or machined into a variety of shapes. Add to all the above, Aluminum is 100% recyclable and recycled aluminum is identical to the virgin product. This makes it a much more cost-effective source material for production runs.

 Three independent stages are required to produce the primary aluminium: (1) Mining of the basic raw materials like the bauxite. (2) Processing to produce the aluminum oxide. (3) Processing of aluminum oxide to produce the primary aluminum [32]. Despite all the aluminum characteristics, the poor mechanical properties of pure aluminium limit its wider range of applications.

Therefore, the pure aluminium is alloyed with different percentages of other materials such as (Cu, Mg, Mn, Si...) to improve its mechanical properties (mainly the strength) by combining the characteristics of the different components of alloys [32]. The properties of aluminum alloys are the resulted combination of the chemical

composition and the microstructure characteristics during solidification and thermal treatment [32].

Aluminum alloys are divided into two major categories: The first family is called wrought aluminum alloys. And this term is applied to alloys produced, at first, in billet or ingot form. Then, they are subjected to be worked by any metal working process such as extruding, drawing and rolling to get the semifinished product. After that, the final product can be made from such semifinished product [33]. The second family is named cast aluminum alloys, which are not subjected to subsequent metal shaping work. And generally, they are casted directly to get the final or near final product [33]. Cast alloys are those specially dedicated to be poured into sand or permanent mold or using any other process where the casting presents the final version of the product [32]. Comparing to wrought alloys, casting alloys have larger quantities of alloying elements like the Si or Cu, resulting in a very heterogeneous cast structure [32]. Further differentiation is used depending on the mechanism used for developing the alloy properties.

In both categories (casting or wrought alloys), a number of alloys are heat treatable, where they are subjected to specific heat treatments hardening including the solution heat treatment followed by the aging [32]. These alloys are known by heat treatable alloys [32]. Such alloys present important solid solution and precipitation hardening under the heat treatment effect [32]. While other number of wrought alloys are not heat treatable and subjected, instead, to work strengthening through mechanical reduction, and known to be as work hardenable alloys. In contrast, casting alloys can

not be work hardenable [32]. The work hardenings made on wrought alloys are often accompanied with annealing procedures for developing the wrought alloy properties [34]. The non-heat treatable casting alloys are just casted with modifying some thermal conditions unrelated to solution or precipitation treatment effects [34].

2.2.1- Aluminum wrought alloys

Aluminum wrought alloys are used much more than cast alloys at the industrial scale, where 85% of Al is used for wrought products [35]. Aluminum wrought products include foil, wire, extruded tubing, extrusions, bar, rod, sheet, drawn, etc…. [32]. Ref [32] stated that industrialists prefer wrought alloys if both production methods can be used to produce a part. In fact, wrought alloys contain usually lower percentage of alloying element [32, 36]. 4(pct) is the up-limit proportion of alloying element in wrought alloys, limiting the casting defects including the heterogeneous structure with brittle secondary morphology [36]. While same alloying elements can be found in casting alloys, but with higher proportion. For example, 22(pct) of Si can be found in casting alloys [36]. In addition, tools required for cast alloys are more expensive, and the higher production rates of wrought alloys encourages industrials to select solutions that contain the wrought product [32]. Furthermore, wrought aluminum alloys are reported to retain their mechanical properties including the ductility in the temperature range of [520-590°C] [36]. While, most casting alloys exhibit drastic loss of mechanical properties (shear strength, tensile and impact) within this temperature range [36].

2.1.1.1-   Designation system of Wrought Aluminum Alloys

Industrially, a variety of wrought aluminum alloys arises from the large number of combinations of alloying elements to achieve the desired properties. Therefore, it is very useful for aluminum users, either in research or industry fields, to have a common standard designation for alloy identification. The alloy designation system for wrought aluminum alloys that, currently, in use is adopted by the Aluminum Association [33].

According to ANSI H35.1(American National Standards Institute), the Aluminum Association Wrought Alloy Designation System contains four numerical digits [33]. The first number is used to indicate the major alloying element, where each wrought alloy family is identified by that number and the corresponding main alloying element(s). Alloys designation and their associated meanings based on the main alloying element are as the following [33]:

1xxx: Mostly pure aluminum

2xxx: Copper

3xxx: Manganese

4xxx: Silicon

5xxx: Magnesium

6xxx: Magnesium and Silicon

7xxx: Zinc

8xxx: Other elements (iron or tin)

9xxx: Unassigned

It should be noted that further judgment decisions are required in some cases. If we have same quantity of two or more different alloying elements. Then, the choice of the appropriate series of the alloy shall be in the following order : copper (Cu), manganese (Mn), silicon (Si), magnesium (Mg), magnesium silicide (Mg_2Si) and zinc (Zn) [33]. For example, if a new alloy has the same proportion of zinc and manganese, it will be included in the 3xxx series [33]. Interestingly, the 6xxx series need much more attention to be judged. Alloys that have more silicon than magnesium, but with significant proportions of both, should be assigned to the 6xxx series rather than 4xxx series because of the predominance of the silicon and magnesium combination [33]. Taking the example of 6005 and 6066, where both alloys contain significantly more Si than Mg or other element. However, they are assigned to the the 6xxx series known by the Mg2Si series [33].

The second digit indicates a modification in impurity levels or in one of the alloying elements to control some properties. For series from 2xxx to 8xxx, if the second digit is (0), it indicates that it is the original or the basic composition. While, a one (1) indicates the first variation, a two (2) for the second variation, and so on. The sequence here describes the chronology in the alloy variations. An example for this is given by the sequence of alloys: 7075, 7175, 7275, 7375, and 7475, arising from modifying various impurities, principally the Si and Fe to increase the fracture toughness, especially in 7175 and 7475 [33]. For the 1xxx series, if the second digit is 0, this indicates a natural impurity limit. While if the second digit is between 1and 9, it indicates that special control was performed on the impurity levels [33].

The third and fourth digits are significant in the 1XXX series, but not in other alloys. In 1xxx series, the last two digits indicate the level of purity of the alloy. For example, the designation 1070 or 1170 indicates that 99.70% minimum aluminum is in that composition. 1050 or 1250 means 99.50% minumum aluminum in those alloys. For other wrought series from 2xxx to 8xxx, the third and fourth digits serve only to identify the different alloys in the series. Thus, alloys 3003 and 3004 are different Al-Mn alloy [33].

To show what processing has been performed on aluminum alloys to achieve the desired properties, there is also the temper designation that will be presented briefly because it doesn't concern the main themes of the present project. The temper designation takes the form of letters and digits that are added as suffixes to the alloy number. Basic temper designations consist of capital letters, indicating the general category of treatment performed on the alloy. (F) designation indicates as fabricated condition, which means that no special processing (strain-hardening or thermal conditions) has been performed to obtain specific properties. (H) designation means strain hardened, where the(O) designates an annealed aluminum alloy. The (W) indicates that the alloy was solution heat treated, and it is applied only when alloys exhibited natural aging after solution heat treating. The (T) means thermally treated. A subdivision of those basic tempers is also adopted, using digits that describe and follow the letters used for the basic temper. For example, (T1) describes an alloy that was cooled from an elevated temperature shaping operation followed by natural aging [33].

It is fair to mention that such designation system provides several benefits. Just from knowing the series of which the alloy is a member, a great information will be known about it including its chemical composition, the hardening mechanism that can be performed on that alloy, its characteristics and its applications.

2.3-   Limitation of the traditional techniques and Direct Chill Casting process for aluminum wrought alloys production

Initially, the permanent mould was the casting technique used for production of aluminium ingots. The molten aluminum was subjected to be poured in a permanent mold, which was also the same process used for copper and steel before that [37]. After that, the World War I and then, the increased need for speedy mail delivery were the cause to fuel the increased demand for wrought aluminum production [38]. By the end of 1930s, industrialization of all-metal designed aircraft, was dominant by the aluminum [38].

It became clear since then that mass production of wrought aluminum alloys is very necessary for making military and also civil airplanes. Thus, larger sizes of wrought aluminum billets and ingots are needed to be processed (extrusion, rolling, forging) in order to provide larger aluminum parts and therefore greater planes number [38].

Literature [38] confirmed that in the period between 1924 and 1939, the average weight of an aluminum ingot cast increased from 20 to 500 kg using the permanent mold. Billets and ingots were casted using the permanent mold [37, 38]. However, the very large dimensions (volume and cross section) of such casting resulted in a very serious casting problems that affected the cast structure and properties of the metal [37, 38]. The principles problems caused by casting in a permanent mold were reported to be (1): Turbulence during the metal pouring. (2) The poor heat transfer that leads to a slow solidification. The low cooling rate results in a coarse structure that contains large intermetallic particles. Then, fracture problems can appear during processing such as rolling or later, in the final product [37, 38]. After that, several casting techniques were developed to overcome such serious problems. However, negative results such as low casting speed, inhomogeneous structure, macrosegregation and high thermal gradient were still present. The main cause was that the heat was, in all those developed methods, still extracted by the walls of the molds [38].

A new technology, called (Direct chill casting) was thereafter developed, presenting a new concept of solidification. The new point is that the heat could be extracted principally through the solid casting itself [37, 38]. This casting method (direct chill casting) has resolved the problems related to slow solidification, where the quality of the ingot improved significantly [37]. However, application of this new technology (Direct Chill casting) has shown limitations, where some casting problems still remain up to date, which are basically hot tearing and cold cracks. Up to now, the direct chill casting technology remains the primary tool for producing ingots for rolling and billets for extrusion from the wide range of aluminum wrought series [38]. Now,

it is essential to provide the principal steps of the direct chill process, which will be presented in the following section.

2.4-   Description of the Direct Chill Casting Process for aluminum alloys

A number of modifications have been made on the basic direct chill casting technique to improve the products quality. However, the main concept of direct chill technology, including the technique features and prototype that was developed in the 1930s, remain the same in the modern industrial Direct chill machines [38]. The basic concept of DC casting is the fact that the ingot is cooled by a running water as it emerges from the bottom of the open mold [37]. DC casting is a semi-continuous process used extensively in the aluminum industry to produce ingots from a wide range of aluminium alloys for subsequent rolling into sheet products as well as cylindrical billets for extrusions and forgings. A 200 mm was reported as a typical diameter for the cylindrical extrusion billets, while the dimensions of the rectangular rolling ingots were reported to be 1500 × 500 mm [39]. A schematic diagram of the DC casting machine is shown in **Figure 2-2**.
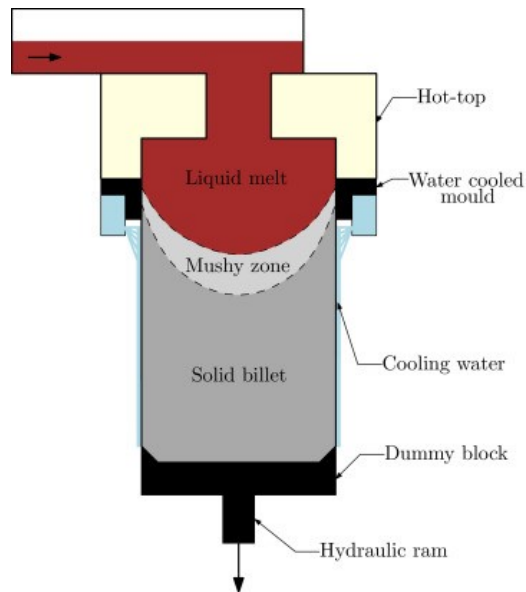
Figure 2-2. Schematic of the DC casting (open access) [40]

At first, the molten aluminum metal (690-725°C) is poured from the furnace into water cooled aluminum or copper mold [7, 39]. The block, shown in **Figure 2-2** is initially located slightly close to the lower lip of the mold, closing off the bottom of the open mold. As the molten metal fills the mold, metal starts to solidify, forming a semi-solid shell along the mold wall. The heat, here, is extracted from the molten metal to the mold walls, where the mold is cooled by water. This solidification step is known by the primary cooling [37, 39]. When the solidified shell becomes strong enough to hold the molten metal inside, the block is lowered gradually accompanied with the solidifying ingot. After leaving the bottom of the mold, the cooling water(direct chill) is directly sprayed on the surface of the ingot, producing very higher cooling rate. The direct contact between water and metal is the main cause behind the largest quantity of heat extraction. This step is known by the secondary cooling [39]. The increasing demand for higher quality of aluminum products lead to the development of further

innovative tools to optimise the DC casting process. For example, the introduction of electro-magnetic moulds instead of the classic ones, or also injecting gas onto the mold top to enhance some problems of surface quality [37].

2.5- 6xxx aluminum wrought alloys, AA6111 alloy in particular

2.5.1- Characteristics and applications

6xxx aluminum wrought alloys contain both magnesium and silicon as main alloying elements. The alloys in this series are heat treatable. The formation of Mg_2Si in this series leads to the precipitation hardening of alloys, resulting in moderately high strength coupled with an excellent resistance to corrosion. The proper ratio for Mg_2Si formation is reported to be Mg/Si=1.73, but this is not achievable in practical. Thus, commercial alloys have always either silicon or magnesium excess. Magnesium excess produces higher resistance to corrosion with lower formability and lower strength. In contrast, silicon excess leads to higher formability coupled with higher weldability and strength with some corrosion tendency between grains[7].

Moreover, 6xxx alloys are characterized by a great extrudability which make them among the first choices in architectural and structural construction. Furthermore, they can be joined by the majority of the processes. 6xxx alloys can be easily welded using GTAW and GMAW methods [33]. the high flexibility of aluminum magnesium silicon alloys (6xxx) allows them to be extruded into very complex shapes, making them widely used in automotive structure. 6111 aluminum alloys are chiefly promoted

in the automotive sector for products like body panels, reducing the whole weight of vehicles [33]. It was reported in ref [40] that 6111 was developed by the research laboratory of Alcan situated in Canada. It is widely used by the famous Jaguar Land Rover in their aluminum models, using the copper as the alloying element(0.5-0.9 wt.%). Strength of 6111 alloys is reported to be higher than 6016 strength. In addition, 6111 are known with the good quality of surface after the stamping and paint bake processes [40]. The 6111 automotive body panels are subjected first to stamping, which is a working process to form various products from sheet metal [40]. After that, they are assembled and then, finished by the paint baking heat treatment for curing the paint and adhesives used for structure joining. To ensure the stamping processes, 6111 alloys are supplied with low strength (T4P temper) for successful formability. After that, the yield strength of the stamped parts increases thanks to the precipitation hardening that happens during the paint baking process [40].

2.6- Defects of DC cast products

The DC casting technique has been used for a long time. However, casting the semi-finished products (ingots and billets) with higher quality is still a challenging issue for casthouse engineering. There are several defects that occur during the DC casting process, and some of these defects are considered as detrimental defects [41]. Such severe defects present serious productivity losses. Once they are obtained, the casting has to be repaired or even scrapped [18]. The industrial relevant defects are

known to be: Macro-segregation, micro-segregation, porosity, hot tears and cold cracks formation [41].

Cold cracking is a fracture that occurs below the solidus temperature when the metal has completely solidified. Whereas the hot tearing is a failure that develops during solidification when some metal liquid is still present [41]. Hot tearing problem is further explained in the following section since it will be evaluated for 6111 alloys in the present work. Porosity occur because of the gas precipitation during solidification [42]. Macro and micro-segregations are both problems coming from the non homogeneity in chemical composition [38, 41]. The difference is that micro-segregation is measured in micrometers(scale of a single grain or dendrite), while macro-segregation problem is measured in centimeters(along the cross-section of the DC cast billet [38, 41]. The micro-segregation defect is caused by the high cooling rate of solidification in DC casting, resulting in a composition variation across grain or dendrite as well as in the formation of a wide range of intermetallic phases [43].Such defects impact the extrudability of the as-cast part, producing surface defects during extrusion [43]. Fortunately, such defects of micro-segregation can be partially or totally removed thanks to the application of a suitable thermal treatment, known by homogenization on the as cast billets before extrusion. Such homogenization operation has been reported by literature [38, 43] and applied in industries, confirming that micro-segregation can be removed by this thermal technique [38, 43]. In contrast, macro-segregation can not be removed by such homogenisation treatment. In DC cast aluminum ingots and billets, the macrosegregation is often characterised by the enrichement of the periphery of casting by solutes compared to the lower content of

solutes in the center of the casting [38]. This is known by (inverse macrosegregation), since the normal segregation is the opposite in which solute content increases from surface to center [38]. The inverse macrosegregation is frequently observed in DC casting and known to be controlled by the grain refinement degree, the casting speed, the casting temperature and the ingot thickness [38, 41].

It is worth noting that controlling the quality of the as cast structure is critical and requires a deep understanding and mastering of the different casting facts that influence the resulted microstructure and mechanical properties. From a productivity view, the industrial prefer to produce the largest ingots with the highest casting speeds as possible. However, the casting speed and the ingot size are limited by the occurrence of several defects [7].

2.7- Hot tearing susceptibility in 6xxx alloys

Hot tearing is considered as one of the most serious and common defects faced in DC cast aluminum alloys [38, 41, 44]. Once a hot tear is present, component should even be scrapped in most cases, leading to a severe productivity loss [18, 41] Hot tearing, termed also hot cracking or hot shortness is an irreversible fissure that occurs in the semi solid state of casting [38]. The main features of a hot tear were described to be as follows [41]: (1) A hot tear propagates principally in an intergranular path (2) Hot tears are frequently found in the hot spots areas, which are the regions of casting that solidify in the end. (3) Visually, hot tears are of branching and ragged failures.

Thermal contractions during solidification are considered among the major facts involved in hot tearing formation [38, 41, 45]. The higher cooling rate using water in DC casting produces a high thermal gradient in the different parts of the cast, resulting in dissimilar thermal contraction of the solid during solidification [38, 41]. This thermal contraction produces stress/strains regions, where tension and compression occur in different parts of casting. Hot tearing defect occurs mainly in regions in which there are tensile stresses [38, 41, 45]. During solidification, a semi solid region that is subjected to tensile stresses is the most vulnerable to hot tears. Hot tearing location depends on the shape of DC cast product, whether it is ingot or round billet. In the case of billet, hot tearing usually occurs in the central section of the billet. In this round shape(billet), the periphery is subjected to compression, while the center experiences tensile stresses. However, the stress distribution in the ingot shape is not that simple. Tension in ingots is concentrated closer to short side surface and corners. Tensile stresses can be found also in the central section of ingots, but the short side surface is reported to be much more vulnerable to such tensile stresses in ingots [38].

When transforming from liquid to solid, there is temperature and time ranges in which the material found in both solid and liquid phase, known by (semi solid). This semi solid state contains two steps, where the second step is known to be vulnerable to hot tearing. The two steps are as follows: (1) the material in this step is termed slurry, in which the newly solidified grains are suspended and can move freely in the liquid. This phase extends with decrease in temperature until the grains start to make contact between them. This event is characterized by the coherency temperature. (2) Below the coherency temperature and above solidus temperature, material is known to be mushy,

creating hot tears conditions [38, 41, 45]. Temperature range between coherency and solidus is known to present "brittle temperature range", confirming that it is the vulnerable region for hot tears formation [46, 47].

The behaviour of the semi solid material can be understood by studying the different steps of solidification in metal alloys. The solidification process is divided into 4 steps based on the permeability of the solid network [38, 41, 47]. The steps are as follows: (1) Mass feeding, in which the microstructure is mainly of solid particles suspended in liquid. Both liquid and solid are free to move. (2) Interdendritic feeding, in which grains start to contact each other, and the remaining liquid should flow through the formed solid network, controlled by grain size and shape. However, the permeability at this stage still large enough, preventing hot tear formation. (3) Interdendritic separation, in which hot tears may form. The higher solid fraction hinders the liquid flow by surface tension or isolated liquid pockets can exist. Thus, hot tears formed by the thermal contraction of solid can not be healed due to the very poor permeability in such environment. (4) Solid feeding or Interdendritic bridging, in which the material develops considerable strength. And further contraction is compensated by solid state creep [38, 41, 47]. **Figure 2-3** shows clearly the different characteristic steps during solidification, where the vulnerable step is between the upper boundary of rigidity and the lower boundary of solidus as shown [48].
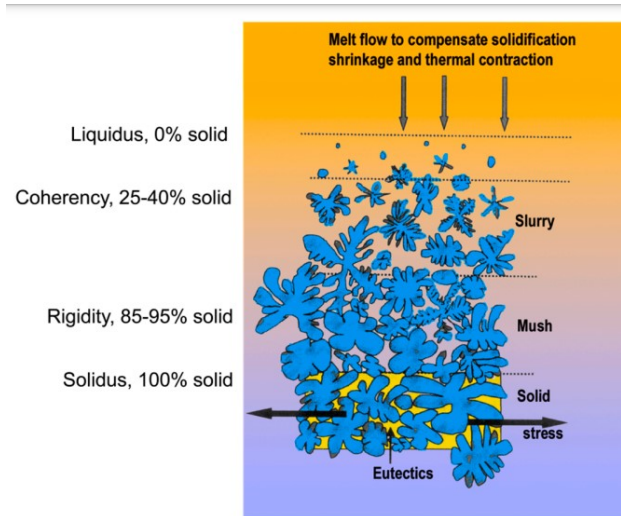
Figure 2-3. Characteristic steps during alloys solidification, the original Figure comes from [48]

It appears therefore that the hot tearing phenomenon is strongly related to the liquid amount during last solidification stage as well as to the permeability in the mushy zone. Hot tear will not occur as long as there is a good feeding of the solid phase with the liquid. This approach was adopted by Miyama and Feurer [38], where the feeding depends on the permeability of the mushy zone. In this approach, the permeability is largely dependent on the solid structure [38]. A number of authors considered the lack of feeding of the solid phase as the major fact for hot tearing formation [46]. Adding to the mechanical properties of the mushy zone that indicate if the material can resist to the thermal stresses and accommodate the thermal strain, or it will form hot tears [45]. In fact, hot tearing can be prevented if the ductility or strength of the mushy zone are greater than the thermal stress/strain induced on it. And a hot tear can be healed if the liquid amount is sufficient and the permeability is large enough to fill the hot tears induced in the mush zone by deformation [41, 45].

Experiments on Al alloys [41, 47] have confirmed that at the semi solid state, there is a critical temperature range in which ductility and tensile strength are extremely low, known by brittle temperature range. Cracks may therefore appear when the thermal stresses exceed the low strength and ductility of the vulnerable semi solid phase [41, 47]. Thermal analysis and radiography studies have confirmed that hot tearing happens at temperatures closely above solidus, where the liquid film surround the solid phase. The presence of such film decreases the strength of the network producing hot tears. This solidification stage is termed as the film stage [46]. The solid fraction was reported to be close to one in this vulnerable stage [49].

In addition, the correlation between the hot tearing susceptibility and the alloy composition has been confirmed in several occasions [38, 50]. Alloys that have a large solidification range are more sensitive to hot tearing since they spend more time in the vulnerable state. 3104 and 6111 alloys were evaluated in terms of hot tearing susceptibility by ref [51]. 3104 was found less prone to hot tearing with smaller brittle temperature range that was less than 10 °C. While alloys 6111 were found more prone to hot tearing with larger brittle temperature range between 20 and 50 °C. Thus, a wider brittle temperature range with the low mechanical properties of the mush under thermal stresses results in hot tear formation. A multicomponent alloy has a complicate influence on the hot tearing depending on its solidification behaviour. Findings indicate that factors influencing the hot tearing are mainly the freezing range and the amount of the final eutectic [49]. Final eutectic amount reflects the quantity of the remaining liquid that feeds the network and solidify at the end of solidification. Higher freezing range and small amount of final eutectic result in higher susceptibility to hot tearing

[49]. Investigations have been performed on the Al-Si-Mg alloys to study the relation between the Si/Mg ratio with the susceptibility to hot tearing. Results showed that the Si/Mg ratio is not a critical factor for HTS, while the freezing range and amount of the final ternary eutectic were found to determine the HTS [49].

It appears from the ongoing section that hot tearing formation presents a complex phenomenon, associated with several facts including the produced stresses/strains, strength and ductility in the mushy zone. Adding to the permeability of the mushy zone that depends largely on the grain structure. The grain structure, in turn, is controlled by the casting parameters (grain refiners, cooling rates, chemical composition…). Results based on tensile tests have confirmed that the strength of the semi solid material depends strongly on the microstructure size and morphology, the fraction solid, and alloy chemistry [52]. Grain refinement was also known to influence the hot tearing since it controls the size and morphology of the solid network. And further information about the correlation between hot tearing and grain refinement will be provided later in another part of the present literature review.

Moreover, DC processing parameters were reported to have an effect on the hot tearing, including the casting speed, the water flow rate and melt temperature [38, 41]. Casting speed was reported to be the most processing parameter that influence strongly the hot tearing susceptibility [38, 41]. The casting speed has to be controlled, especially for some aluminum alloys that present high susceptibility for hot tears [53]. Water flow rate is reported to have much less influence. Higher water flow rate increases the cooling at the billet surface, but it increases the thermal gradient between the center

and periphery of the billet. Thus, the periphery cools and contracts much more faster than the center, resulting in higher thermal stresses and strains in the billet center [41]. All these mentioned facts confirm that productivity using DC machine is limited by the occurrence of a number of casting defects, where the master of the linked complex parameters is a real challenge for controlling the solidification process.

Given the severity of hot tear defect, it has been extensively studied over many decades. A considerable number of efforts have been conducted to find out the hot tearing criterion that relate the DC casting parameters and properties of the mush to the hot tearing occurrence [38, 41]. The hot tearing criteria were reviewed by Eskin and can be summarized as follows [38, 49]. These hot tearing criteria can be divided into two categories: mechanical and non-mechanical. The mechanical criteria were developed mainly based on the mechanical behaviour of semi-solid material, involving the critical stress, critical strain and critical strain rate. While the non mechanical criteria involve the vulnerable temperature range and process parameters such as pouring temperature [38, 49]. However, hot tearing has been showed to be a result of both mechanical and non mechanical facts [38, 41].

A combined (mechanical and non mechanical) criteria were therefore developed to incorporate simultaneously these different facts [38, 41]. The most accurate criteria was developed by Rappaz, Drezet and Gramaud (RDG), and was modified by Grandfield and others [20, 21]. According to author [49], RDG model has the greatest potential in terms of qualitative prediction of hot tearing susceptibility. This modified model was reported to better describe the complex environment of the

mush, incorporating different parameters, including the vulnerable temperature range, the feeding and permeability in the mush depending on the size and morphology of solid grains and other parameters such as (viscosity, surface tension). The mechanical behavior of the mush was also involved in this criterion. To calculate the HTS in this model, the formulation incorporates the permeability equation of Carman Kozeny that involve the grain size and morphology [41]. This relation will be used in the present work, to evaluate the permeability of the mush for globular grains with different size. In addition, the strain rate was used as critical mechanical factor for hot tearing occurrence. The dependence of hot tearing on strain rate in DC casting has been experimentally confirmed [20, 49]. In fact, it was proposed that a void is formed only if the mushy zone can not accommodate the induced strain at a given strain rate [38]. The high solidification rate in DC casting doesn't give enough time for liquid to limit the casting strain, resulting in hot tear formation. Therefore, it exists a critic strain rate at which voids occur [38]. In this recent modified RDG model, hot tearing criteria is based on the maximum strain rate that can be sustained by the mushy zone before the hot tearing occurrence [49].

Despite the qualified nature of the modified RDG, it is still not able to predict quantitively the hot tearing, where it fails to predict correctly in some situations [38, 49]. In addition, such theories depend on how much the chosen values are correct like: The surface tension between solid and liquid and the mush permeability. These parameters can not easily be determined experimentally because of the limited existing experimental tools [38]. Therefore, a further improvement for the hot tear prediction criteria is still needed and remains a high challenging quest for the researchers.

2.7.1- Experimental methods for hot tearing evaluation

In addition to the theoretical studies and the mathematical models, a number of experimental tests were developed to evaluate the hot tearing susceptibility of alloys. These tests can be divided into two major categories: Partial remelting tests and solidification casting tests. Further information about these categories is available in the following section.

2.7.1.1- Partial remelting tests

This kind of tests focus on evaluating the mechanical properties of the material in semi solid state, because the hot tears are believed to occur in the weak semi solid state (low strength due to the presence of liquid film around grains) as mentioned before. In this kind of test, samples are partially remelted to a certain temperature above the solidus. Then, mechanical tests (shear, compression, but basically tensile tests) are performed to evaluate the strength of the semi solid material [38]. As experimental tools, Gleeble machine equipped with modern tools controlling the strain/stress and temperature were used recently for HTS evaluation in aluminum alloys. The use of such modern tools are known to produce accurate and reliable results due to the parameters control and the rapid melting of the sample using Joule heat [38, 52]. Such partial remelting tests were reported to be the most adequate techniques for evaluating the semi solid constitutive behaviour. However, the conditions that occur during remelting(fraction solid in terms of temperature) are different from the ones that occur during solidification. Moreover, such techniques can be performed only at high solid

fraction [52]. Ref [52] has the belief that such tests may lead to different results from those actually occurring during solidification because there is no liquid feeding that respond to the deformation to contribute to the hot tears healing.

2.7.1.2-   Solidification casting Tests

In these casting tests, the liquid metal is poured into a mold that present a special design. After the complete solidification of casting, an evaluation is performed on the resulted hot tears present in the casting. The major advantage in these tests is that they simulate the industrial solidification conditions [52]. The concept is that the molds used in such tests are designed in a specific geometry that induces stresses in castings during solidification. Produced tensile stresses in casting may lead to hot tears formation in the weak regions indicating the alloy susceptibility for hot tearing. Some casting parameters can be modified in such tests like the pouring temperature and the refinement addition rate, which help to establish correlation between some casting parameters and HTS in DC cast. Several kinds of molds were designed, where the most common used are summarized in this section.

A- Ring testing Mold

The ring mould has been used in many studies to characterize the HTS in ferrous and non ferrous alloys [22, 46, 49]. This technique is considered as the most classic method for hot tearing evaluation [22]. The ring mold is shown in **Figure 2-4**. The mold consists of a core and a ring made with strong and high melting material,

placed on a flat plate. Pouring of the liquid metal, to a certain height, is performed in the annular space between the core and the ring. During solidification, the thermal contraction of the cast ring around the core imposes tensile stresses, and therefore leads to hot tears formation on the casting surface. The numerical value attributed to HTS in this technique is the total length of cracks formed on the casting surface. The ring mold technique is still present in several research projects and casting-houses, basically, due to its simplicity. In addition, the whole process of solidification can be visually observed since the top of the test mold is open [22]. However, such technique was reported to give only qualitative results for hot tearing susceptibility. Moreover, results don't consider the crack severity in terms of width and depth [22, 44]. In addition, the metal has to be poured in each casting to the same height in order to limit the metallostatic effect [46].
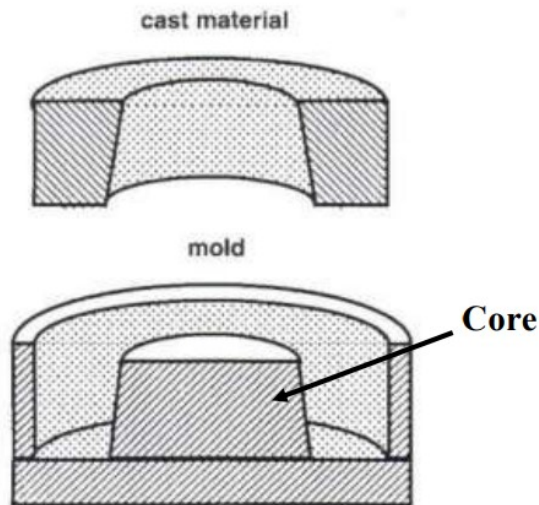
Figure 2-4. Ring mold for hot tearing evaluation [54]

B- Dog-Bone testing Mold

The name (dog-bone) was attributed to such mold due to its resemblance in shape to the bone of the dog. The **Figure 2-5** shows an example of this mold. As shown, the mold contains a bar restrained at both ends. Liquid metal is poured into the center, spreading out toward both edges. Solidification starts in both ends, inducing stresses along the center of the casting bar. The resulted length of crack was measured to indicate the HTS of the tested alloy [46].
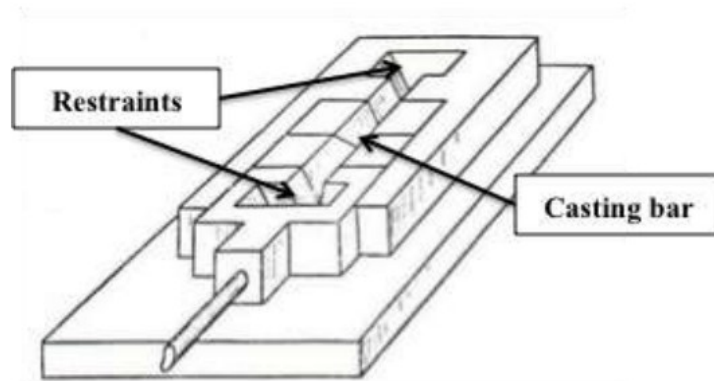
Figure 2-5. Dog-bone mold for hot tearing evaluation [54]

Modified version of the dog-bone mold was made by Clyne and Davies [46], where they inserted a heater in the center of the mold, and a cooler in both ends of the mold. Such modifications have the advantage of controlling the cooling rates and be closer to the actual conditions of DC casting. The similar setup was used by Spittle and Cushway [46] with a feeder placed in the casting center, close to the hot spot region. Such modification simulates closely the actual casting where the feeder is present to control the liquid amount for feeding [46].

Another modification was added to the dog- bone mold by combining a number of dog bone molds in the same setup [46, 54]. The modified design is shown in **Figure 2-6**.
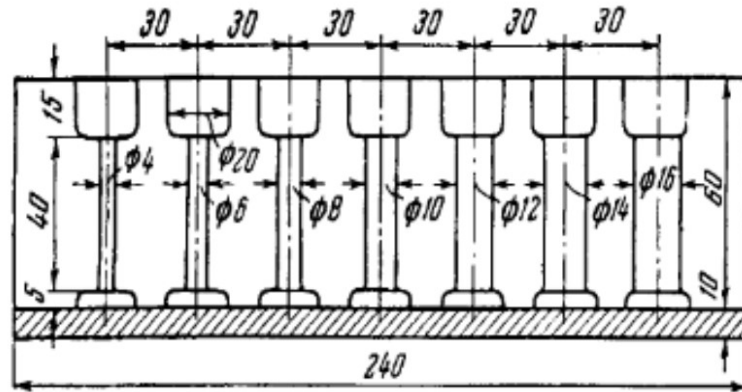
Figure 2-6. Combined dog-bone molds in the same setup for HTS evaluation, casting are with different diameters[54]

As shown in the **Figure 2-6**, the design is characterised by variation in the samples diameters. The length is kept constant with value of 40mm, while diameter vary in the range of [4-16mm]. the maximum critical diameter (D_{cr}) of the sample in which hot tears occur, reflects the severity of HTS [46, 54]. The advantages of the dog-bone test arises from the simplicity of its setup configuration, adding to the ability of controlling some parameters(insertion of heaters and chills, varying diameters…) [46].

It was reported that other methods were also developed like Cold finger test as techniques for evaluating the HTS. These relatively simple techniques in configuration were preferred in several researches. However, results arisen from such techniques are only qualitative in nature. Therefore, new developed methods occurred to furnish more quantitative results [46].

C- Constrained rod casting testing mold

In this kind of test, a constrained rod casting (CRC) mold is used. In terms of design, the mold was made based on the dog-bone shape shown before [46]. **Figure 2-7** represents an example of a typical constrained rod casting mold used for hot tearing evaluation. The CRC mold consists of parallel and cylindrical bars (rods) with different lengths. Bars are constrained from both sides. One side by a sprue, and the other side by a spherical shape(ball). The feeding of bars is performed through the long sprue [22].

Figure 2-7. Mold for constrained rod casting (open acess) [55]

During solidification, thermal contraction induces stresses along the bar constraint between the sprue and the ball. Hot tears may therefore form near the sprue or near the ball or in the bar middle, but frequently in the region close to the sprue end [50]. In fact, Hot tears occur more at the sprue end as a result of the higher stress concentration induced by the higher thermal contraction of the larger cross section of the solidifying sprue [50]. After complete solidification, resulted cracks should be evaluated to can calculate thereafter the HTS index. Hot tearing measurement in such test considers the crack severity, the crack location and the bar in which the crack

occurs [49, 50]. Hot tearing occurs much more frequently in the longer bars since they are more prone to hot tears. And therefore, tears in the shorter bars reflect the higher severity of hot tearing in the tested alloys [50]. Further details about the numerical measurement of HTS index of this test method are given in the methodology chapter, because it is the test method used to evaluate the HTS in 6111 aluminum alloys in the present work.

Testing technique using CRC molds are known to produce repeatable results thanks to the specific design of the mold. The manner in which the rod decreases in diameter from the sprue was reported to decrease the friction effect between the casting rod and the mold wall [46]. In addition, the mold is generally placed vertically to perform the pouring. However, ref [22] mentioned that placing the mold inclined with a certain degree from the vertical position when pouring, ameliorates the reproducibility by ensuring the good filling of mold cavities and reducing casting defects such as gas and filling shortage. HTS indexes measured in this kind of test are known to be comparable and reliable. However, further important information concerning the hot tearing occurrence can not be determined with such technique, including the temperature and time in which the hot tears occur [46, 49].

D- Instrumented constrained rod casting testing mold

To overcome the limitation of the conventional CRC mould, Cao et al. [46, 49] developed more sophisticated tools to be added to the CRC mold. The main objective was to evaluate the HTS quantitatively with detection of the temperature and time in which hot tears occur. The developed tools were joined to the simple CRC mold in the same setup to record the temperature, load and time during solidification process. Such recorded details help to detect the initiation of hot tearing [46, 49, 56, 57]. The experimental setup is shown in **Figure 2-8**. The setup contains basically a CRC mold, a thermocouple and a load cell. The upper four rods are used for evaluating the HTS in the same way as in the simple method shown before. While the bottom rod is for collecting temperature and load data to can thereafter detect the hot tearing onset [46, 49, 57]. By pouring the melt, metal liquid will enter and solidify into the threaded rod which is attached to the load cell. The thermocouple is located in the bottom rod, close to the sprue end (position A), as shown in **Figure 2-8**. During solidification, the solidified threaded rod was reported to restrict the free contraction of the casting rod. The contraction force along the casting rod is recorded in terms of time. **Figure 2-9** is the resulted plot of such setup, combining the (temperature and contraction) Vs Time. The load curve of contraction force shows a sudden drop that indicates the hot tear initiation, where the corresponding temperature represents the temperature of the hot tearing onset [46, 49, 57]. In fact, cracks(hot tears) initiation causes the relief of the contraction, producing such sudden drop [46, 49, 57].
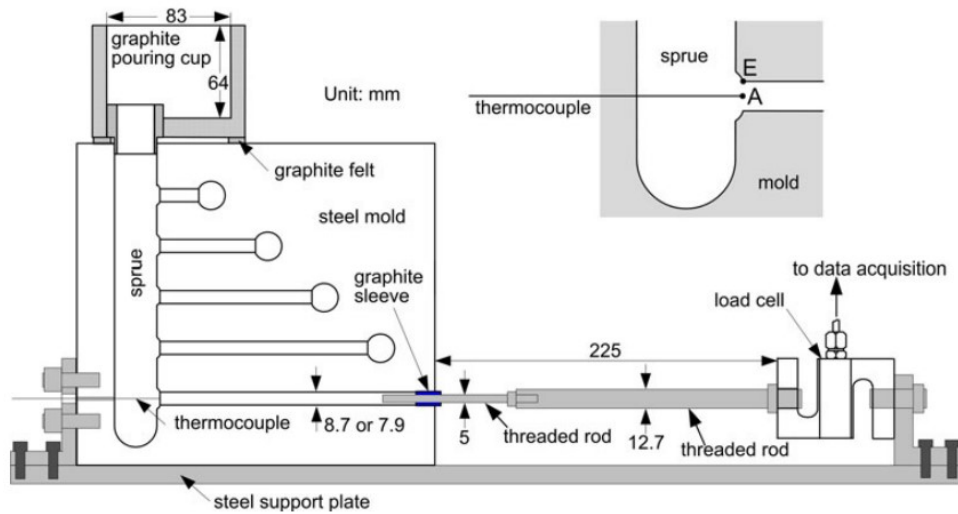
Figure 2-8. Instrumented CRC mold [57]
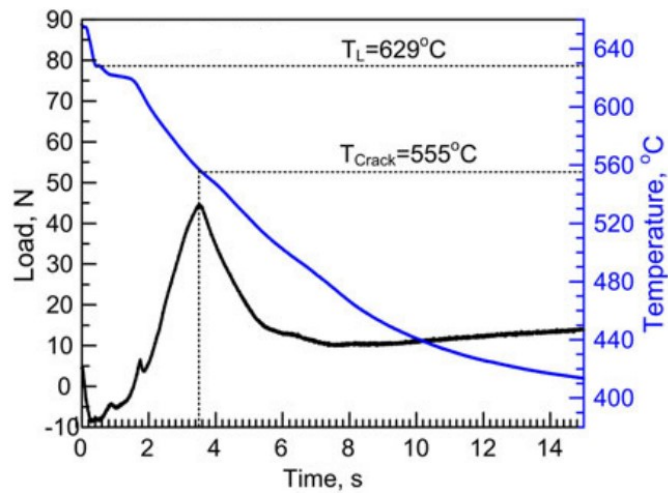
Figure 2-9. An example of cooling and load curves resulted from the instrumented CRC mold[57]

Further development of the instrumented CRC mold was performed to record the displacement, as an addition to the load and temperature records as shown before. Such measurement was found to present an agreement with HTS results of the tested

alloys [49]. There is no doubt that such enhancement in CRC mold setups provides valuable data about the hot tearing, which contributes to a better understanding of the hot tearing phenomena.

2.8- Grain refinement of aluminum alloys

A coarse grain structure is known to lead to a variety of surface defects and reduced mechanical properties in aluminum alloys. Grain refinement has, since then, gained much attention in the aluminum industry to improve the alloys properties [58]. The most evident impact by grain refinement is the increase in alloys strengthening, which is explained by the Hall–Petch theory [58]:

$$\sigma_y = \sigma_0 + k_y \cdot d^{-\frac{1}{2}} \qquad \text{(2-3)}$$

Where σ_y is the yield stress, σ_0 is the material constant of the starting stress for dislocation movement, k is a constant, d is the average grain diameter. Compared to precipitation strengthening, grain refinement can in the same time improve strength, toughness and reduces casting defects like the segregation and porosity with better fatigue life [58]. Moreover, an homogenous distribution of second phases and uniform anodized surface is achievable in refined alloys [59]. A number of methods have been proposed as aluminum refinement techniques. All the methods can be classified as follows [58]: Grain refining by vibration and stirring during solidification, rapid solidification, severe plastic deformation and the addition of grain refiner. Grain

Refiners addition has become a common industrial practice where several theoretical and experimental studies have been dedicated to investigate this industrial process [58, 60].

Despite the extensive work on grain refinement, there are still missing points for a complete understanding, which limits the better mastering of the refinement industrial practice [58, 60]. These collaborated efforts between industrials and academic researchers continue until this moment. And the present section will present a comprehensive review as possible on the grain refinement by grain refiner addition in wrought aluminum alloys, highlighting the main concepts and findings in this field.

2.8.1- History

History of the grain refinement of aluminum alloys started in 1930. it was realised by Rosenhain et al [10] that titanium addition to the aluminum liquid results in smaller solidified grains. By Ti addition before casting, the coarse columnar grains were replaced by smaller and equiaxed grains. While the other elements like (B ,V, Ta, W, Ce, Zr, Nb) were found to contribute to a slighter grain refinement of pure aluminum [10], adding to their higher cost compared to the Ti element [10]. Therefore, Ti has been identified as a potential grain refiner for aluminum comparing to these various elements. Rosenhain et al, were the first to identify the Ti potential effect. However, Cibula, according to ref [10], is the pioneer in the grain refinement field due

to its extensive and systematic work that investigated the possible grain refinement mechanisms and the effect of different elements on the grain refinement [10].

Experimental results have found that the grain refining effect of Titanium in aluminum alloys could be significantly ameliorated by adding small amounts of boron [10]. For this reason and since the early stages of refinement practice, both of titanium and boron were added to the melt in the form of reducible halide salts, such as KBF_4 and K_2TiF_6 [10]. However, such kind of practice was stopped later because of the drawbacks of these reducible halide salts addition, including the large fumes, the high dross and the inability to control the content of titanium and boron [10]. To overcome these disadvantages, The addition of titanium and boron to aluminium were performed using the master alloys such as Al-Ti and AL-Ti-B instead of the salt form. This resulted in better melt quality and also in higher effectiveness of grain refinement, when comparing to the salt effect [10]. Studies performed by Jones and Pearson revealed that the ternary master alloy Al-Ti-B has a higher potency in grain refinement compared to the master alloy Al-Ti, which confirms that the boron presence increases the refinement potency of Al-Ti master alloy [10]. Moreover, the Al-Ti-B was found to have a higher efficiency than the salt form that contain both Ti and B. This has confirmed that an efficient grain refinement can be achieved not only by a simple addition of Ti and boron, but most probably thanks to the heterogenous nucleation exhibited by the TiB_2 and Al_3Ti particles present in the ternary master alloy(Al-Ti-B) [10]. This fact has been further confirmed by experiments, in which an absent of refinement was found after the dissolution of Al_3Ti and TiB_2 particles compared to an efficient refinement in the particles presence [10].

2.8.2- Types of grain refiners, forming process, efficiency and limitations

2.8.2.1- Al-Ti-B

The most common grain refiners for wrought aluminum alloys used in industries are the ternary master alloys Al-Ti-B [2]. The Al-Ti-C master alloys were developed to present an alternative of the Al-Ti-B master alloy in specific industrial applications that will be shown later in this section. Other master alloys including the Al-Ti-Si and Al-Ti-Be have been studied by some investigators without resulting in an efficient grain refinement [10]. The Al-Ti-B is commercially available in the form of rods and ingots [10]. And it consists of an α-aluminium matrix with embedded intermetallic particles of TiB_2 and Al_3Ti [2, 10]. In general, it is believed that the contact of such master alloy with Al melt results in the dissolution of the aluminium matrix of the master alloy including the Al_3Ti particles, while the TiB_2 particles survive to act as heterogeneous nucleant particles [2]. Commercial Al-Ti-B master alloys present wide variation in the Ti/B ratio, resulting in different compositions including the following ones: Al-5Ti-1B, Al-3Ti-1B, Al-5Ti-0.6B, Al-5Ti0.2B, and Al-3Ti-0.2B [2, 61]. All these compositions contain Ti/B ratio greater than the ratio required for TiB2 formation, which is reported to be (%Ti/%B = 2.22) [2, 61]. While the remaining titanium participates to the Al_3Ti formation in the master alloy [2, 61]. Therefore, Al-Ti-B master alloy that present Ti/B ratio lower than 2.22 contain only TiB_2 particles dispersed in the Al matrix. The actual available master alloys have always Ti/B ratio larger than 2.22 [61].

On a universal scale, the Al-5%Ti-l%B grain refiner is the preferred grain refiner and the most widely used for Al alloys [2, 3, 62]. The higher efficiency of Al-5Ti-1B has been confirmed experimentally, showing better results in terms of grain size reduction in wrought aluminum alloys [10]. Where the higher efficiency was attributed to the larger fraction of nucleating agents present in the Al-5Ti-1B [10]. However, Al-3Ti-1B was found to perform better when refining alloys that contain (Li, Zr or Cr) [10].

Refinement potency of Al-Ti-B grain refiners are known, in general, to be impaired or poisoned by chromium, zirconium, vanadium. This poisoning concept will be discussed in a later section. Another drawback was found during the grain refinement practice using Al-Ti-B is the fading phenomenon [10, 61]. After refiners addition, the mixture (refiners and liquid metal) is subjected to be held for a specific duration before pouring, called (contact time). If a longer contact time results in a coarser grains, instead of the finer structure obtained after a shorter time. This phenomenon is known by fading [10, 61]. The fading degree can be very high, resulting in a completely columnar grain structure [10, 61]. Such grain coarsening indicates that the higher contact time decreases the number of the nucleating agents [10, 61]. Fading can be due to either dissolution or settling of nucleant particles [10, 61]. Fading issue in Al-Ti-B is often caused by agglomeration and settling of TiB_2 particles under the effect of longer contact time in the Al melt [10, 61]. Experimental have proven that the dispersed TiB_2 particles tend to stick one to each other to form larger agglomerate during a long holdig time in Al melt [61]. This results in formation of TiB_2 layer that settle down in the bottom of cast [61, 63]. In addition, the TiB_2 particles are known to

have a higher density than Al melt which increases their sedimentation behavior in the bottom of the cast [61, 63]. Stirring was reported as a solution that can limit partially this fading issue after a long time [10]. Interestingly, the large clusters of TiB_2 were found to occur not only during the holding time after their addition to the Al melt, but also during the forming process of the master alloy itself. The main reason for agglomerated particles of TiB_2 is the salts used in their manufacture [2].

There exist many ways to produce Al-Ti-B master alloy, where the most widely common method used in industries is the one that uses halide salts with aluminium. The industrial route consists of adding the inorganic salts potassium fluoborite and potassium fluotitanate(KBF4 and K2TiF6) to molten aluminum. As a result, Al reduces these salts to form Al-Ti-B master alloy(dispersed $TiAl_3$ and TiB_2 in Al matrix), and a KF-AlF3 flux [61, 64]. It was reported that using such route, instead of introducing titanium and boron in elemental form, presents both technical and economic advantages [64]. Cleanliness of the melt and the control of alloy composition are often obtained using such industrial routine [64]. However, there are some drawbacks resulted from such forming process, where the major issue was reported to be the agglomeration tendency of TiB_2 particles. Such agglomeration can be caused due to the flux induced by the reaction of Al with KBF4 and the engulfment of the KF-AlF3 flux [65]. It was found experimentally that wetting the TiB_2 particles by the potassium cyrolite flux contributes to their agglomeration [64].

Other factors were reported to cause the TiB_2 agglomerations, including the attachment to oxide films, particle collision and surface adhesion by the aluminide

layer and growth in filters [9]. Such agglomeration issue decreases the refiners potency by influencing the number and number density of the nucleant particles in the master alloy. In addition, this issue influences the final properties of the cast product. Large clusters of TiB_2 particles were found to result in reduced mechanical properties and quality problems like surface defects in lithographic sheets and porosity in foils for packaging [2]. Moreover, filtration systems in industries were found to have difficulties in the presence of such agglomerates [9]. Detrimental inhomogeneity is caused by agglomerates, particularly for wires and thin sheets, and in general for products that require special finish of surface.

In the forming process of Al-Ti-B master alloy, salts addition of K2TiF6 and KBF4 to molten aluminium are performed at temperatures above 700°C. TiB2 particles are hexagonal, and their morphology doesn't depend on the addition temperature in such salt route [61, 66]. Author [61] reported that addition temperatures of 1100°C and 750°C produced the same aspect of TiB_2 particles, including the same size, frequency and morphology. However, TiB_2 morphology was reported to be influenced by the time duration of the reaction. An increasing in the reaction time from 30 s to 5min during the forming process transformed some of the regular hexagonal TiB_2 particles to bigger collided particles [66]. For Al_3Ti particles, Liu and Xie [66] have reported that produced Al_3Ti particles present 2 different morphologies. Liu added that low temperature smelting produce blocky Al_3Ti, while high-temperature smelting can quickly form rod-shaped $TiAl_3$ particles [66]. It was reported by ref [61] that salt addition at 750°C, produces blocky $TiAl_3$, while a higher addition temperature (above 900°) leads to the formation of acicular or flaky Al_3Ti particles. To obtain uniform

dispersion of TiB_2 and Al_3Ti particles, good stirring of the melt is required to prevent the sedimentation of these particles due to their higher densities.

2.8.2.2- Al-Ti-C

The history of Al-Ti-C grain refiner started in the early of 1980s when Alcoa collaborated with its grain refiner suppliers to develop a boron-free grain refiner. The main drive for such program was to reduce the particle agglomeration found in the Al-Ti-B system [2, 9]. In 1986s Anglo-Blackwells made a new commercial Al-Ti-C grain refiner to meet the industry demand. The primary composition was at that time: Al-6Ti-0.02C [2]. However, such composition presents a high ratio of Ti/C, and consequently high amount of titanium addition is required [2, 61]. To reduce the addition rate of Ti with sufficient TiC particles, Al-3Ti-0.15C composition was commercially introduced. Other different ratios of Ti/C are also available, including the Al-5Ti-0.25C. By 1996, Al-3Ti-0.15C has been widely used in the aluminum refinement [2].

The microstructure of Al-Ti-C grain refiners is an aluminium matrix, containing $TiAl_3$ and TiC particles dispersed in the aluminium matrix [2, 61]. Compared to the Al-Ti-B master alloy, Al-Ti-C showed a smaller tendency for agglomeration coupled to smaller number of nucleant particles due to the absence of the salts in their manufacture, which has been demonstrated to improve the melt fluidity, the castability and also to reduce blockage in filtration system [9]. A better

surface finish and less segregation effect were also reported as advantages from such refiners change from Al-Ti-B to Al-Ti-C [9].

Al-3Ti-0.15C are found to have higher efficiency in some 7xxx plate applications and present the good alternative, especially in aerospace applications [9]. Using the Al-Ti-C instead of Al-Ti-B has shown in some findings more uniform microstructure and more uniform eutectic, which reduce the segregation effect and decrease homogenisation times with enhanced uniform properties. Further advantage was reported is that Al-Ti-C master alloy has a higher resistance to the poisoning effect of Zr and Cr in high strength alloys [3, 9]. The superiority of Al-Ti-C efficiency has not been proven in all wrought aluminum alloys. And it is often reported that Al-Ti-C grain refiners are used as an alternative to Al-Ti-B master alloys for critical applications. Al–Ti–C master alloys were reported either less efficient or as potent as conventional Al–5Ti–1B master alloy in terms of grain size reduction [67].

Each producer has his own forming process in producing the Al-Ti-C grain refiner. Therefore, there is no details about the forming process. However, in general it is known that two steps are mainly performed in their forming process: First, melting Al with Ti scrap. Then, the addition of Carbon, either as graphite or some other form of carbon [61]. The problem of using Al-Ti-C master alloy was often reported to be related to the TiC stability in the melt. TiC particles were found to transform to other compounds at the normal melting temperature below 1000°C. The higher free energy of formation of TiC compared to Al4C3, is the driving fore for such transformation [61].

To achieve better results, temperature control is required when using this titanium carbide master alloy. It should be at the low degree as possible [3, 9]. There is still a debate about the TiC stability in Al melt. In general, carbides (TiC) are considered as stable, but with a lesser degree compared to the borides(TiB_2) in contact with Al melt.

To sum up, Al-Ti-B grain refiners can be considered as the preferred refiner than Al-Ti-C grain refiners in terms of grain size reduction of wrought aluminum alloys. While Al-Ti-C can be considered as the most promising grain refiner commercially available, which can avoid the boron clusters, but also can limit poisoning problems made by elements such as chromium according to some findings. Al-Ti-C grain refiner are most used to limit the defects in foil and lithographic sheet alloys (1xxx and 8xxx), can stock alloys (3xxx and 5xxx) and bright trim alloys (5xxx and 6xxx) [2, 3].

2.8.3- Evaluation and tests of refinement efficiency

To act as an efficient nucleating particle, there exist some basic requirements to meet: (1) The master alloy used should contain sufficient number of nucleating agents. (2) The melting point of the nucleant particle should be higher than that of the alloy to refine. (3) nucleant particle should be able to nucleate grains at minimum undercooling degree. (4) Size of nucleant agents should be higher than a critical value, depending on the undercooling degree of the melt [61].

Measurements of grain size of the refined as-cast structure is an indication to evaluate the grain refiner performance. Standard Test Methods for Determining Average Grain Size are provided by ASTM Standard E112 [68]. The different methods for measurements based on this standard give results that can be reported in different ways, including the mean intercept distance, average diameter, number of grains per unit area or ASTM grain size number [61]. The measured grain size is a function of a number of factors including the casting process parameters (cooling rate, casting speed, addition temperature, holding time). It depends equally on the features of the grain refiner including their microstructure (the morphology and size of nucleant particles), adding to the chemical composition of the nucleant particles and its subsequent reaction with different alloying elements.

A number of methods have been developed to evaluate the grain refinement. The aluminum company of Canada firstly developed a refinement test, known today by the Alcan test. Following this, a number of other tests have been developed including the Alcoa test, the KBI ring test and the Aluminium Association test [10, 61]. The most widely popular and acceptable refinement tests are the Alcan and Alcoa tests [61]. These two tests (Alcan and Alcoa) were developed in a specific way that simulate the DC casting route used for producing aluminium and its alloys. Both tests involve high cooling rate, which mimic the conditions of the Direct Chill casting. In the Alcan test, the test procedure consist of melting 10 Kg of pure aluminium (99.7 %) in a furnace to be heated to 718±5°C. The grain refiner is added, and the mixture (Al melt with refiners) is subjected to mechanically stirring for 30 s. After that, a preheated conical mold(ladle) is used to be filled with the melt. Then, the ladle or the mold filled

with the melt is introduced in a specific container, where the mold base is cooled by cold water for directional solidification. The chilled test specimens are sectioned transversely 25 mm from the bottom. Macro and micro evaluations including the grain size measurement are performed on the sectioned surface after sample preparation (grinding, polishing and etching). This method is mostly considered and used as quality control test for suppliers of grain refiners, in which a predetermined grain size should be obtained in the test to can consider the tested grain refiner as passable [10]. It is difficult to applicate such test procedure in a smaller scale of laboratory, because the necessary starting amount in Alcan test consist of batches of 10 kg pure aluminium. While feasible amounts in laboratory scale are of 1,2 or 3 Kg [10]. The Alcoa test procedure uses a water cooled copper cone to achieve the directional solidification, where this water cooled copper cone is inserted into the Al melt. In such test, directional solidification is performed vertically from the top to the bottom of the mold.

It is worth noting that both tests (Alcan and Alcoa) were developed to simulate solidification conditions experienced in DC casting. However, the very higher cooling rates in such tests result in further refinement and smaller grains, which make difficult to detect the real grain refining efficiency of the tested grain refiner [10].

2.8.4- Grain refinement mechanisms

Much of work has been dedicated to explain the involvement of the nucleant particles in the nucleation event, and consequently to reveal the manner in which nucleant agents nucleate the Al grains. Therefore, several nucleation mechanisms have

been proposed. However, none of these theories is able to explain all the observations obtained in the grain refining experiments. In fact, the proposed nucleation theories for aluminium have been proposed based on specific facts of some experiments. Moreover, the quantitively detection of nucleation event and nucleation centers is difficult due to the subsequent growth of solidified grains. It is interesting to mention that despite the extensive practice of grain refinement in industries, it is still a routine that controlled mainly by empirical rules. Mechanisms of grain refinement have been the subject of several review papers, where several mechanisms have been postulated. Until now, the subject presents controversies, and there is still no total agreement between researchers on the exact mechanism that contribute to the nucleation event [3].

The proposed mechanisms have been reviewed by Easton and StJohn [10, 11], and were classified into two major groups. The first group is termed "nucleant paradigm". In this first group, nucleant agents are considered to be the ultimate contributor in nucleation event. Therefore, these theories are related only to the nucleant particles present in the master alloys, including (Al_3Ti, TiB_2 and TiC). While, the second group is termed "solute paradigm". In this second group, the solute, combined to the nucleant particles, are believed to contribute in the refinement event. Several theories have been proposed in the light of the first group (nucleant paradigm). The proposed theories are as follows: (1) Boride/carbide theory, (2) Phase diagram theories(based on peritectic reaction), (3) Peritectic hulk theory, (4) Hypernucleation theory, and (5) Duplex nucleation theory.

2.8.4.1-   Nucleant Paradigm

A- The boride/carbide theory

This theory was first proposed by Cibula, and supported by others like (Jones and Pearson) [10, 11]. According to this theory, TiB_2/TiC particles are the responsible for the Al nucleation by heterogeneous nucleation. In the beginning, borides TiB_2 are thought to be provided by the master alloy addition of Al-Ti-B, while TiC particles were considered as the result of the reaction between residual carbon and the added titanium in the melt [10, 11]. This TiC formation was explained on the fact that carbon amount coming from impurities that always present in the melt are sufficient to form TiC [10, 11, 61]. After that, Al-Ti-C master alloy was produced by Banerji and Reif, resulting in an efficient grain refinement [10]. The Al-Ti-C producers have shown that carbon and titanium were found in the centers of solidified grains, which confirm the earlier Cibula view about the TiC potency in refining [10].

When using the Al-Ti-B grain refiner, borides particles present in such master alloy are believed to be AlB_2 , TiB_2 and $(Al,Ti)B_2$ [10]. It was reported that TiB_2 and AlB_2 are hexagonal, having a very close lattice parameters [11]. Several researchers were not able to make difference between them, and therefore could not identify whether borides particles are TiB_2 or AlB_2 [61]. The mixed boride $(Al,Ti)B_2$ is believed to form by the substitution of titanium atoms by aluminum atoms, and they finish by transforming to TiB_2 [11, 61].

Cibula, Jones and Pearson had the belief that TiB_2 particles disperse in the Al melt, and act as nucleating agents for Al grains. This view was confirmed by radiography experiments, in which, boron and titanium were found in the grains centers of Al [10]. In return, Maxwell, Hellawell et al., indicated that the presence of Al_3Ti particles in the melt can nucleate Al with little or even no undercooling degree, while TiB_2 and TiC particles are known to need some undercooling to nucleate aluminum [10]. This confirms that Al_3Ti particles are more efficient than the TiB_2/TiC particles, where Al_3Ti particles were found in the grains centers of Al based on the observations of Davies and others [10]. A number of investigations in the literature, including the ones of Kobyashi, Arnberg and others have confirmed the higher potency of Al_3Ti in Al refinement based on the existence of multiple orientation relationships between Al_3Ti and Al, while no orientation relationship was found between TiB_2 and Al for many years [10, 11]. Compared to AlB_2, TiB_2 and TiC, Al_3Ti are known to present greater number of planes that posses a good matching with Al. Experimental results have shown that in the presence of aluminide particles(Al_3Ti), borides were pushed to the grain boundaries, whereas Al_3Ti were found in the center of the solidified Al grains [10]. It was cited in [3, 11] that lattice matching between the aluminum and the borides is large which indicates that borides are poor nucleants, or at least much less effective compared to the refinement efficiency of Al_3Ti particles.

B- Phase diagram theories (based on the peritectic reaction)

From all the evidence above, it became generally agreed that Al_3Ti particles are much more better in Al refinement. And once they are present, Al nucleation occurs on

these powerful aluminides particles. To ensure the Al nucleation on the particles of Al$_3$Ti, these particles have to be stable in the melt. α-Al nucleation is reported to form by the peritectic reaction on the stable Al$_3$Ti particles, the peritectic reaction is as follows [10, 11, 61]:

$$L + TiAl_3 \longrightarrow \alpha\text{- Al}$$

However, the stability of these particles (Al$_3$Ti) faces problems of dissolution, when they are in contact with Al melt. When the master alloy of grain refiner is added, the typical concentrations of Ti in wrought aluminum alloys is below 0.15%, which is the minimum Ti amount required for peritectic reaction based on the phase diagram of Al-Ti. Below this concentration of 0.15%, Ti is present at hypoperitectic amount, and Al$_3$Ti are thermodynamically not stable, where they finish by dissolving. To face this problem, the phase diagram theories were developed to find explanation about how Al$_3$Ti could act as nucleant agent for Al, even at hypoperitectic compositions. All the theories of this group start from a common belief, suggesting that grain refinement is the result of the peritectic reaction.

One school of thought has suggested that the peritectic point can be shifted to lower concentration of titanium, where 0.05 pct Ti was proposed as the new shift peritectic point due to the boron presence [11]. The boron presence and its contribution in changing the peritectic point was able to explain some obtained findings. However, phase diagram calculation doesn't match with such explanation. In addition, efficient

grain refinement was found to occur even below that proposed concentration [11]. Thermodynamic and theoretical studies have been performed by Sigworth, Jones and Pearson , confirming that phase diagram of Al-Ti can not be modified due to the boron presence [11].

An alternative school had the belief that Al_3Ti particles can nucleate Al before their dissolution, even at hypoperitectic amounts. According to this school, increasing the holding time of master alloy in Al melt before casting results in coarser grain size since there is more time for further dissolution of Al_3Ti. This phenomenon is known by fading, making the refinement poor. The debate here is about the time required for total dissolution of these particles. A variety of times durations were proposed, showing that there is no agreement on the dissolution rate of aluminides particles. Starting with Mondolfo et al. who proposed that dissolution takes hours, despite the fact that holding temperature was higher than 800°C [11]. While 30 min was found as the duration time for Al_3Ti dissolution with temperature of 700°C, according to Guzowski et al. [11, 12]. However, Johnsson suggested that 5 min is, definitely the dissolution time duration, at temperature of 775±10°C. Wanqi et al, performed calculations to find 10 min as the duration time [11]. Microstructural studies have been performed by Jones and Pearson to show that 30 seconds is the dissolution duration time [69]. Based on several experimental findings, it seems that the dissolution rate of Al_3Ti depends on the holding temperature, the Ti level in the melt and also on the size and morphology of Al_3Ti [11]. Vader et al. [11] consider the particles size, melt temperature and Ti level when calculating the dissolution rate of Al_3Ti particles. They found that dissolution time can vary between 1 and 30 min, depending on the mentioned parameters.

It appears from all the facts mentioned above that the problem with the phase diagram theories is that the Al nucleation on Al$_3$Ti based is the peritectic reaction can occur only in short holding time and specific conditions.

C- The Peritectic Hulk Theory

The peritectic hulk theory was considered as the most popular theories that could explain grain refinement mechanism in the late 1980s and beginning of 1990s. This theory was supported by Vader et al. and Backerud et al. [11]. As believed before, the Al$_3$Ti particles are more potent for Al nucleation and they nucleate grains by peritectic reaction. The new point in this school of thoughts is that they proposed a new way that explain how the borides increase the stability of the Al$_3$Ti when the Al-Ti-B master alloy is added. The peritectic hulk theory suggests that the borides TiB$_2$ form a shell around the dissolving aluminides Al$_3$Ti, which slow down the dissolution rate of aluminides. The aluminides dissolve by time, but with leaving a cell of liquid into the boride shell that presents approximately the peritectic composition. The peritectic reaction can then take place to form the α-Al, where subsequent grains growth can occur after that. Such mechanism was found to agree with several experiments, where shells of TiB$_2$ were found in Al grains in some cases [10, 11]. In contrast, TEM studies performed by Mayes et al., [10] have shown that TiB$_2$ particles are found in the center of Al$_3$Ti. In addition, Johnson et al. [70] have shown that solidification potency didn't decrease after a successive number of melting and solidification cycles on an

hypoperitectic alloy. If the refinement was based on peritectic hulk theory, melting and solidification cycles would decrease the refinement potency, since the number of cycles would cause the titanium diffusion out of the hulk. Moreover, such mechanism can not satisfy the refinement after long holding time, since the titanium content inside the hulk would disappear. Therefore, peritectic hulk theory was supposed not to be the principle mechanism in Al grain refinement [10, 11].

D- The hypernucleation Theory

The hypernucleation theory was proposed by Jones [11]. It was reported that this theory was named like that to highlight the disproportionate effect made by the very small addition rates of Al-Ti-B master alloy on the grain size of Al [11, 61]. According to this theory, Al nucleation happens on the borides particles (TiB_2), where the segregation of solutes to melt/inoculant interface provide a suitable interface for Al nucleation. The atomic size of the segregating solutes was supposed to be the critical factor in the hypernucleation theory [11]. Solutes that have a similar atomic size to Al induce the hypernucleation refinement mechanism. While, elements with big difference in size compared to Al will be detrimental for refinement process. Titanium has very close atomic size as aluminium, which promotes the hypernucleation mechanism. Whereas, Zr and Cr are very different in size compared to Al, which destroy the hypernucleation mechanism [10]. Such results fit well with the poisoning mechanism obtained when using Al-Ti-B master alloy. The hypernucleation theory seems to explain most of the observed phenomena in Al refinement, and elements

segregation to the interface are known to occur. However, the activity gradient produced by TiB_2 addition to the melt is thermodynamically not logic, and it is difficult to make experimental evidence for this theory, as Jones confirmed [10, 11].

E- The duplex Nucleation theory

The duplex nucleation theory is the most recent mechanism among all the proposed mechanism. It seems that it is the most attractive by researchers, however it is still problematic and was refused by some of other researchers [10, 11]. The basic concept of this mechanism is that the Al nucleates on the Al_3Ti, which in turn is fixed on the borides particles of TiB_2. Evaluation of the refinement efficiency was performed by Mohanty et al., [10, 11] with different levels of titanium. Results have shown that the presence of TiB_2 with no added Ti didn't lead to any grain refinement. And, TiB_2 were found in the grain boundaries during those experiments, which confirmed well that TiB_2 are poor nucleant. However, Ti addition resulted in a significant refinement efficiency, where TiB_2 were found in the centers of grains.

At hyperperitectic level of Ti, the presence of Al_3Ti layer between Al grains and TiB_2 was confirmed experimentally. At hypoperitectic Ti level, the layer found between Al and TiB_2 was presumed by the same researchers Mohanty et al., [11] to be Al_3Ti too. To explain this phenomenon, Mohanty et al., proposed that the formation of Al_3Ti layer is caused by the Ti segregartion to the melt/TiB_2 interface. They also suggested that the Ti concentration in the melt and particularly close to the

interface(melt/TiB$_2$) would exceed 0.15% inducing the stability of Al$_3$Ti. And therefore, the peritectic reaction can take place to nucleate Al grains. Experimentally, they confirmed the higher Ti concentration in areas close to borides particles [11]. Sigworth supported this segregation findings. However, he refused the formation and stability of Al$_3$Ti layer between Al and TiB$_2$ particles based on thermodynamic arguments [11, 71]. Simulation of the nucleation mechanism was performed by Schumacher and Greer using metallic glass experiments, where they added Al-Ti-B master alloy to an aluminum rich metallic glass(Al85Ni5Y8Co2). Results have shown borides particles that were surrounded by Al$_3$Ti layer, which, in turn, was surrounded by Al. They supported the same nucleation sequence proposed by Mohanty et al., [10].

The orientation relationships, including the matching planes and directions between the different compounds (Al, Al$_3$Ti and TiB$_2$) were also determined [11]. Schumacher and Greer [3, 11] suggested that Al$_3$Ti formation can explained by chemical attraction such as the adsorption effect at the Al$_3$Ti/TiB$_2$ interface. However, such reason is not yet that clear and question remains about whether such observations are related to specific casting conditions, or can be relevant to normal conditions.

To sum up, it appears that there was no total agreement on one mechanism in the light of the nucleant paradigm, and no consistent theory has been developed until now. The proposed mechanisms were based on experimental findings and observations related to different casting conditions, resulting in different interpretations when guessing the possible mechanism of the grain refinement. The following **Figure 2-10**

presents a sum up of the different theories proposed in the light of the nucleant paradigm.
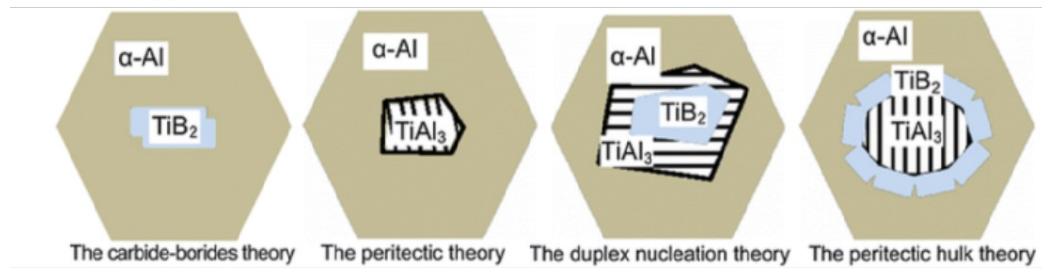
Figure 2-10. Nucleation of Al in different theories [58]

2.8.4.2- Solute paradigm

All the discussed theories above were proposed in the light of the nucleant paradigm, which consider that refinement process depends only on nucleant particles. This nucleant paradigm was modified thereafter to become the solute paradigm. In solute paradigm, nucleants are still of important fact. However, solutes effect is considered also as important contributor to the refinement process. It was suggested and agreed by jonhsson and others [11, 72] that effects of both nucleant and segregants elements can explain the grain refinement process, including the nucleation event and the grain growth [11].

The change from nucleant paradigm to solute paradigm was the result of the incomplete understanding of the refinement mechanism in isolation from chemical facts of alloying elements. Interestingly, it was reported that the presence of the most efficient nucleant particles in pure aluminum was expected not to succeed in refining

since there is no solutes in the melt. And the presence of an adequate amount of solutes has been proved to be essential for obtaining the desired fine grain structure [11].

To understand the role of solutes on grain size, there are two key concepts that should be considered. The first one is the control of the grain growth by the segregating elements due to its growth restriction effect. The second is the constitutionally undercooled zone produced by these segregating elements. More details on these two points and their contribution in the grain refinement are given in the following section.

A- Growth restriction

According to the solute paradigm, it is believed that solute elements are able to restrict the grain growth. During solidification, solutes segregate in the interface of (growing grain/melt), restricting further growth of grains. Cibula [73] confirmed that there are concentration gradients around the solidifying dendrites that retard the crystal growth. The growth restriction factor (GRF) was suggested as a measure to quantify the effect of the segregating elements on the growth of the solid/liquid interface. Experimental results performed by Pearson and Keans [10] confirmed that aluminum grain size drops drastically with increasing this growth restriction factor. Ti element is known to have the highest growth restriction effect than any other elements, which explain the use of excess Ti in industry when practicing the refinement procedure. The growth restriction effect of a solute is quantified in the following equation:

$$GRF = mc_0(k-1) \qquad\qquad (2\text{-}4)$$

where m is the gradient of the liquidus, k is the partition coefficient between the equilibrium concentrations of the solid and liquid at the growing interface(k=cs/cl at the interface temperature), and c_0 is the solute concentration [11]. Ti presents the largest GRF as a solute in the melt, where its corresponding (k-1)m is equal to 245.6, while the corresponding values of Si, Mg, Fe and Mn are: 5.9, 3, 2.9 and 0.1, respectively [11]. In the presence of a number of solute elements in the melt, the GRF for an alloy is measured as the summation of the growth restricting factors for the individual elements, where interaction between solute phases is neglected [10, 11]. Hence, the GRF for a multi solutes alloy becomes as the following [11]:

$$GRF = \sum mc_0(k\text{-}1) \qquad\qquad (2\text{-}5)$$

B- Development of constitutional supercooling(CS)

It is agreed that a sufficient undercooling is required to trigger nucleation on the potent nucleant agents, where solutes were found to provide this required undercooling. While segregating to the solid/liquid interface, solutes build up an undercooled zone close to the interface. This undercooling phenomenon was called by Ivantsov (diffusional undercooling), because it is due to the diffusional process that takes place in the melt layer neighboring the solidification front [73]. This phenomenon is very known also by (constitutional supercooling) since it is created by the alloy constitution. Once the CS reaches a certain amount, the nucleation occurs on the neighboring nucleant agent. The constitutional undercooling therefore presents the driving force

that induces many nucleating sites, resulting in a wave of fine equiaxed grains from the mold edge to the casting center [11, 61].

In the beginning of solidification, the driving force for nucleation is believed to be the thermal undercooling, close to the mold walls [61]. After that, thermal undercooling will be dissipated under the effect of latent heat. In pure aluminum, coarse grains will grow towards the casting center. However, in the case of aluminum alloys the formed CS by the solute rich layer that surround the growing crystal surface activate the nucleation event on particles. It has been recognized that grain refinement is strongly influenced by the alloying elements, where the nucleation event itself is considered now only, as a part of the refinement process [11].

2.8.5- Poisoning effect by solutes on the grain refinement

The most common belief in the refinement field is that a refined grain structure is the result of two essentials steps: (1) Al heterogeneous nucleation by potent nucleant particles present in the refiners and (2) the grains growth that is controlled by the solutes presence. Unfortunately, some solutes were found to weaken the potency of nucleant particles, including Zr, Cr, and to lesser extent Li, Ta, Mn and also a high levels of Si in Al melt [16]. This weakening effect on grain refinement is generally termed in the literature by the term 'poisoning', resulting in a poor grain refining response and hence in a coarser grain structure [3, 16].

Cr is considered as a poisoning element when refining Al alloys using the commercial refiners that contain Ti. However, most of researchers in the literature have performed tests using the Zr element, where they expect that Cr, as a poisoning element, would react in the same manner of Zr [74]. Therefore, more literature is provided for the Zr element and its poisoning effect that hinder the refinement mechanism. At concentration level of about 0.1 to 0.2 mass%, solute elements like Cr, Zr are added basically to increase the alloys strength. However, such small amount was reported to impair the grain refining efficiency when using the commercial grain refiner Al-Ti-B [14]. For example, in the study of Ahmady et al., the grain size in 7050 alloys without Zr was the half compared to the size measurement obtained after the Zr addition to the same alloy using the Al-Ti-B grain refiner [14]. Similar poisoning effect was found by Birch and Fishers when refining Zr containing 7xxx with Al-5Ti-1B grain refiner [75]. Results of Abdel Hamid et al., have also confirmed the detrimental effect of Cr and Zr in aluminum alloys refinement [75].

For several decades, efforts have been dedicated to reveal the exact poisoning mechanism. However, the exact mechanism remains unclear and different thoughts were proposed in the literature concerning this issue. Trying to find the possible poisoning mechanism, Abdel Hamid have proposed that Ti atoms were substituted in both Al_3Ti and TiB_2 particles by poisoning elements, such as Cr, Zr forming less potent compounds: $(Ti_{l-x},Me_x)Al_3$ and $(Ti_{l-x},Me_x)B_2$, where Me=Zr,Cr,Ta [16]. This mechanism has been proven by experimental findings [16]. Arjuna et al., have found, in the grain centers, the aluminides Al_3Ti that contain Zr element, confirming the possible diffusion of such element into the nucleant particles [16]. Moreover, Johnsson

shared the same belief, attributing the grain refining deterioration by Zr to the $(Ti_{1-x},Zr_x)Al_3$ formation after the substitution and the Ti dissolution into the matrix [16]. Murty et al., share also the same concept of poisoning when explaining the poisoning effect of Zr, Cr [16]. In contrast, Jones and Pearson believed that the Zr poisoning effect is coming from the TiB_2 surface coating by ZrB_2. Where they attribute the formation of such ZrB_2 layer to its higher thermodynamic stability compared to TiB_2 [75]. And such coating is thought to result in larger lattice parameters, hindering the TiB_2 to act as nucleating agents [75].

The Al-Ti-C grain refiner was considered in some studies as immune to such poisoning effect. Refining the 7xxx containing (0.006% Zr) using the Al-3Ti-0.15C resulted in very fine grain structure without showing any poisoning impact. However, in other experimental tests a Zr quantity above 0.03% has been found to weaken the efficiency of Al-5Ti-0.4C grain refiner [14]. Al-Ti-C master alloy was reported to be also poisoned since it contains the same vulnerable Al3Ti particles [14].

Interestingly, there exists a second school of thought believing that the poisoning issue results from the Fe or Si presence in the melt. In fact, a combination between Fe/Si and the poisoning elements (Cr, Zr) is thought to be happened, resulting in the surface modification of inoculants agents [14]. In study of Arjuna Rao et al., the Cr presence in an Al alloy containing Fe and Si was found to result in a poisoning effect when refining Al and using the Al-Ti-B as refiner, while the Al alloy without Fe and Si were refined better [74]. In the Spittle and Sadli findings, a 0.15% Zr has improved the grain refining efficiency of Al-5Ti-1B when casting an ultra high purity Al (99.99

pct), while the addition of Fe (0.15 to 0.25 %) to the Al melt in the presence of Zr has lead to the poisoning mechanism [14]. Qiu et al., [14] have also attributed the poisoning mechanism to the Fe presence, where the Al_3Ti was found to be partially or totally coated by a thermodynamically stable layer Al_8Fe_4Zr. This layer was therefore thought to limit the Al_3Ti dissolution. And hence reduce the Ti, which is considered as the main contributor to the grain refinement. Moreover, such poisoned layer was found to have good crystallographic matching with Al_3Ti but poor one with the aluminum matrix. Several experimental observations support this poisoning mechanism, where complex aluminide particles that contain Al, Ti, Zr, and Fe were found rejected in the grain boundaries and thought to be the poisoned nucleants particls [14].

Despite differences found in thoughts above, all the findings agree on the fact that using Ti-containing grain refiner in the presence of poisoning element should make the existing nucleant particles less potent. The potency of these nucleant substrates is one of the basic requirements to achieve an efficient grain refinement [76].

As a potent nucleant, the energy of the newly formed interface (nucleant-crystal solid) should be lower than the existing interface energy between nucleant and liquid, which facilitates the phase transformation [76]. For lower interfacial energy, a certain orientation relationship between these two phases is required. This requirement is associated with providing a good crystallographic matching in the interface. A large atomic mismatch results in a significant strain and significant energy in the interface, while a minimum atomic mismatch result in relaxed and completely or partially coherent interface [76].

It appears therefore that crystallographic matching in the refinement system (inoculant/metal matrix) represents a critical significance in the evaluation of the grain refinement efficiency in addition to other competing factors including the wetting ability, roughness, size distribution of inoculants particles, interactions between nucleant and alloying element, surface segregation and the inoculant particles settling [14, 77].

For simple crystal structures, lattices matching evaluation has been used in order to predict the refining potency based on lattices correlation rather than atoms. However, most of the inoculant particles have complex crystal structure and atoms that are in the interface between crystals were not considered in this lattice evaluation model. Therefore an Edge to Edge model (E2EM) has been developed to solve this issue, examining the atomic matching in the interface of the adjacent surfaces of inoculant and metal based on the crystallographic features of both phases [14, 76]. The basic concept of the E2EM model is that the crystallographic relationship in the interface is controlled by the minimization of interfacial energy through the matching of atomic rows of both phases. And based on this model, these atomic rows should be parallel [77]. For maximizing this condition, the matching rows should represent close packed or nearly close packed directions, i.e., they have close interatomic spacing. Moreover, the model requires that these 2 close packed directions are coming from 2 close packed planes, i.e., planes that have close interplanar spacing [77]. More details of evaluation method of this model are in the methodology section, since it is the method used for poisoning evaluation.

Findings have proven that the E2EM has shown a very significant success in the refining evaluation [14, 76, 77]. Poisoning effect by Si was also examined using the E2EM in Al-Si cast alloys [14]. The success of this model in orientation relationship prediction makes it a very good tool to develop more potent grains refiners for Al alloys, especially for those in which grain refinement is found difficult such as the case for Al-Si and Al-Li [76].

2.8.6- Effect of grain refinement on the hot tearing susceptibility in wrought aluminum alloys

The grain refinement process is considered as one of the major method for decreasing the hot tearing susceptibility defect [17]. Hot tears defect is known to be a severe and common defect in alloy casting, resulting in serious productivity losses. Once it is obtained, the casting has to be repaired or even scrapped [18]. The possible causes of hot tearing formation during solidification were already presented in section (2-7). Significant efforts have been focused to understand the correlation between the grain refinement and hot tearing over the past years [17]. It was found and agreed that grain structure (size and morphology of grains) resulted from the refinement process, influences the hot tearing behavior of aluminum alloys [19].

In general, it is commonly agreed that columnar grains are very prone to hot tearing due to the easy crack path through such large grain structure. Therefore, a transition from columnar coarse grains to an equiaxed structure induced by refiners

addition is highly recommended to prevent the hot tearing issue [20]. However, it is not agreed on whether the refinement has to be the maximum as possible to obtain the smallest grain size, or it is only required to have an equiaxed grain structure with a certain grain size that prevent hot tearing [20]. Published studies in literature are contradictory [18]. In practical use, it is still not clear what is the preferred grain size and morphology, and subsequently how much of refiners quantity is enough to produce that preferred structure in terms of hot tearing reduction. Li et al. [18] found that the more we add grain refiners, the more the hot tearing tendency decreases in AlCu alloys whatever the size and morphology are. In return, studies [19, 21] performed on 6060 series alloys have confirmed that the grain refinement decreased the hot tearing severity to a certain extent, where an excessive grain refinement increased the hot tearing susceptibility due to the permeability decrease through the very smaller globular grains. Rosenberg et al., found, surprisingly, that grain refining did not have any effect on hot tearing in their experimental work [19]. Ref [78] has found that the addition of more grain refiners will promote the formation of more intermetallic phases at grain boundaries, which, in their turn block the liquid flow of the mushy alloy and decrease the permeability, which increases the hot tearing susceptibility HTS.

It is fair therefore to conclude that there is no definite conclusion about the correlation between the grain refinement and the resulted hot tearing behavior. Further work is required to be performed on this important topic. Moreover, such contradiction in findings may arise from the complex area and the competing factors that influence the hot tearing, adding to the differences in the nature of test methods and the inaccuracy of some measurements, resulting in different experimental results [18].

One of the main objectives of this project is to find out the exact addition rate of refiners, and therefore the morphology and size that reduces as possible the hot tearing susceptibility in 6111 alloys.

CHAPTER 3 : EXPERIMENTAL PROCEDURES

The experimental section is sub-divided into three main parts, principally based on the different objectives of the project: **(1)** Experimental part for the performance comparison of the different grain refiners in the 6111 aluminum wrought alloy with/without presence of Ti as solute. **(2)** Experimental part for the hot tearing susceptibility evaluation in the 6111 alloys. **(3)** Experimental part for studying the Cr effect on grain refinement of 6111 aluminum alloys.

3.1- Experimental for comparison of the grain refiners performance

3.1.1- Experimental alloys and grain refinement experimental procedure

The chemical composition of the experimental base alloy is listed in **Table 3-1.** Three master alloys were used as grain refiners for comparative studies: Al-3%Ti-1B, Al-5%Ti-1B and Al-3%Ti-0.15%C, where the Al-6%Ti master alloy was used for Ti addition. In the beginning, an addition rate of 2 Kg/t of each grain refiner was added to the base alloy. After analyzing the grain size of each combination in the 2 different cooling rates(0.4 et 4°C/s), 200 ppm of Titanium was added to the base alloys to analyze again the grain structure modification in the presence of titanium as a solute with modifying the addition rate of grain refiners (1 Kg/t, 2 kg/t and 3Kg/t) at both cooling rates. A schematic diagram is given by **Figure 3-1** to simplify the experimental conditions in each cooling rate.

**Table 3-1**. Chemical composition (wt.%) of 6111 aluminum alloy

Mg	Si	Cu	Mn	Fe	Cr	Al
0.76	0.74	0.51	0.28	0.19	0.004	bal.
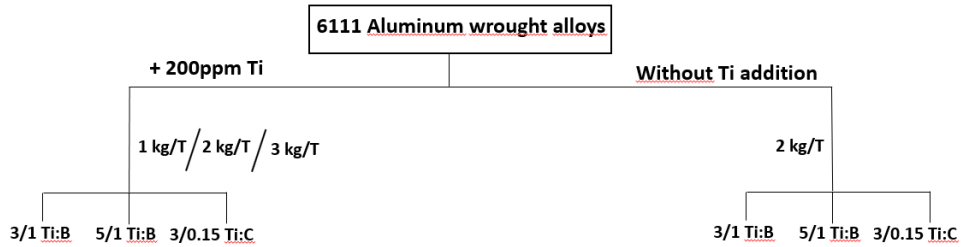
Figure 3-1. A schematic figure of the experimental conditions of Ti/Refiner addition.

First of all, the base alloys were received from the industrial partner. Each time, 700 g was melted in a crucible of 1 Kg capacity in an electrical resistance furnace, to be held thereafter at 720°C. The metallic bath was degassed with argon to insure minimum hydrogen content. After degassing, oxides on the surface of the melt were skimmed and the grain refiners were inoculated into the melt. After 2 min of contact, the melt was stirred for homogenization prior each casting. The mixture is allowed thereafter to cool into 2 different stainless-steel molds preheated to 200°C. The mold parameters are shown in **Figure 3-2** where the resulting weight of casting is 163.4 g. One of these molds was covered by insulation materials (Ceramic and fiber) to obtain a lower cooling rate(0.4°C/s), the second mold was cooled by compressed air to insure higher cooling rate (4°C/s). Cooling rates were measured through the slope of cooling curve close to the liquidus temperature. The temperature-time data were recorded during

cooling through the thermocouples located in the middle of each mold and linked to the Graphtec GL240 data acquisition system.
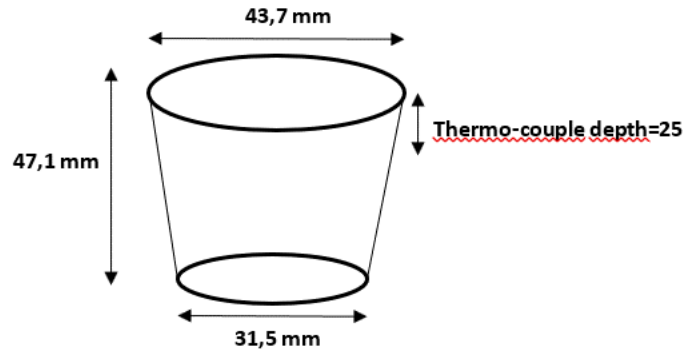
**Figure 3-2**. The Test mold parameters.

3.1.2- Grain size measurement and microstructure analysis

At each rate of grain refiner addition and at both cooling rates, samples were sectioned at the tip of the thermocouple (25 mm from the top) and then prepared by mechanical standard grinding and polishing procedures. The polishing was performed using 6 and 3 μm diamond suspensions followed by final polishing step using 0.5μm colloidal silica suspension in order to obtain higher surface quality. The polished specimens were then subjected to an electrolytic etching using a Barker solution (3% HBF4) for approximately 4 min at 40 V. The grain structure was analyzed thereafter using the optical microscope (Nikon, Eclipse ME600) equipped with a light polarizer placed in the optical pathway between the specimen and the microscope lamp. For grain size measurement, The ImageJ software was used based on the standard linear intercept method (ASTM 112). The dendrite arm spacing (SDAS) was measured by finding a number of adjacent dendrite arms from primary dendrite and measuring the distance

between the dendrite centres. The macrostructure was examined using the Poulton etchant for 30 s.

All the experimental steps starting from melting to grain size measurement can be summarized in the following **Figure 3-3.**
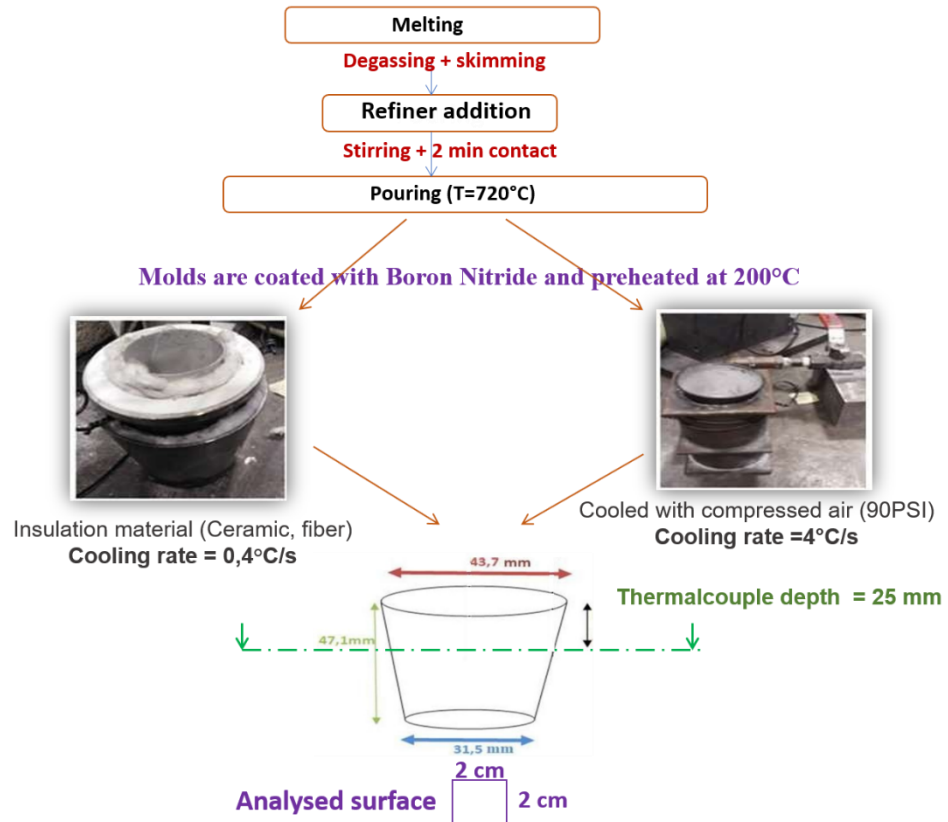
Figure 3-3. A schematic diagram of casting procedure

The 6111 alloy was evaluated from non-grain-refined to fully refined state. A scanning electron microscope (SEM, JEOL-6480LV) operated at 20kV and combined with Energy Dispersive Spectroscopy (EDS) was used to identify the intermetallic phases present in both Al-Ti-C and Al-Ti-B master alloys. The size, morphology, and

size distributions of the nucleant particles were also compared using the SEM observation.

## 3.2- Experimental for the evaluation of the hot tearing susceptibility in 6111 alloys

3.2.1- Hot susceptibility experimental procedure of the experimental alloys

In this second experimental part, the same base alloy 6111 as in the first part was used. However, only the master alloy Al-5%Ti-1%B was selected as the grain refiner for the hot tearing susceptibility evaluation of 6111 alloys. The hot tearing susceptibility of the alloy was tested before and after refiners addition. The refiners addition rates were of (1, 2 and 3 Kg/T) in the presence of 200 ppm Ti as a solute. The 5/1 (%Ti/%B) grain refiner was added after degassing and skimming the molten alloys (base alloy, the added titanium). After 2 min of holding(duration time of contact between refiners and Al melt), the melt was poured into a Constrained Rod Casting (CRC) mold coated with Boron Nitride and preheated to 250°C.

The CRC mold shown in **Figure 3-4** consists of 4 parallel bars with different lengths. All the bars are constrained at one end by a sprue and at the other end by a spherical geometry (ball). In the CRC mold, hot tears are caused by tensile stress along bars (the gauge area), due to the metal contraction by the solidifying ball at one end and by sprue at the other end, which experimentally simulate the hot tears formation in

DC castings during solidification. During our experiments, the pouring temperature was kept always at (720°C) with stirring prior to each casting. The constrained rod casting (CRC) mold was coated with Boron Nitride and preheated to 250°C. All the castings were removed from the mold after fixed time of 90 seconds to be evaluated thereafter for the hot tearing susceptibility.
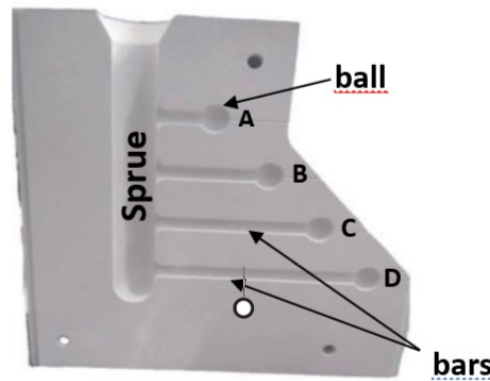
Figure 3-4. Constrained Rod Casting (CRC) mold used in the present tests

3.2.2- Hot tearing susceptibility evaluation and microstructure analyses

The equation (3-1) below was used in this experimental part to evaluate the hot tearing severity of the test alloys by calculating their hot tearing susceptibilities indexes, named 'HTS' [50]. The values of HTS are determined by the factors of: The crack severity in the bar (Ci), the bar length (Li), and the position (Pi) of the crack in the bar.

$$\text{HTS} = \sum_{i=A}^{D} (\text{Ci x Li x Pi}) \qquad (3\text{-}1)$$

Where i: (A, B, C and D) represent the 4 bars with different lengths, as shown in **Figure 3-4**. The detailed evaluation system is given by the following **Table 3-2**.

**Table 3-2**. HTS Evaluation System (open access) [50]

Bar Type (Length)	Li	Hot-tear Category	Ci	Hot-tear Position	Pi
A(3cm)	4	No crack	0	Sprue end	1
B(6.5cm)	3	Hair line crack	1	Middle bar	3
C(10cm)	2	Light crack	2	Ball end	2
D(14cm)	1	Severe crack	3		
		Complete crack(broken)	4		

The numerical values of Li were given based on the fact that the longer bars were less resistant and most likely to form hot tear. Thus, they were given the lower index. If tears are found in the shorter bar, they would reflect the higher severity of the hot tearing problem in the alloys. Each category of crack was assigned a numerical value C depending on the severity degree. Pi depends on the location of the crack in the bar as shown in **Figure 3-5**. Tears more easily form near the sprue-end because greater stress develops by the sprue on the bar.

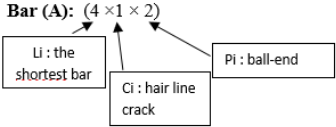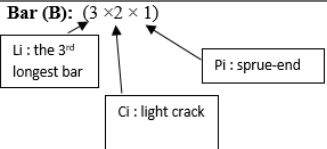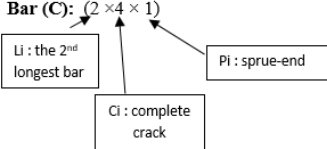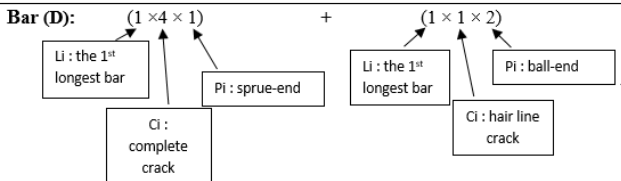**Figure 3-5**. Hot-tear position and the corresponding numerical value Pi.

An example of HTS casting is given in **Figure 3-6**, and its corresponding calculation of HTS index is given in **Table 3-3.**
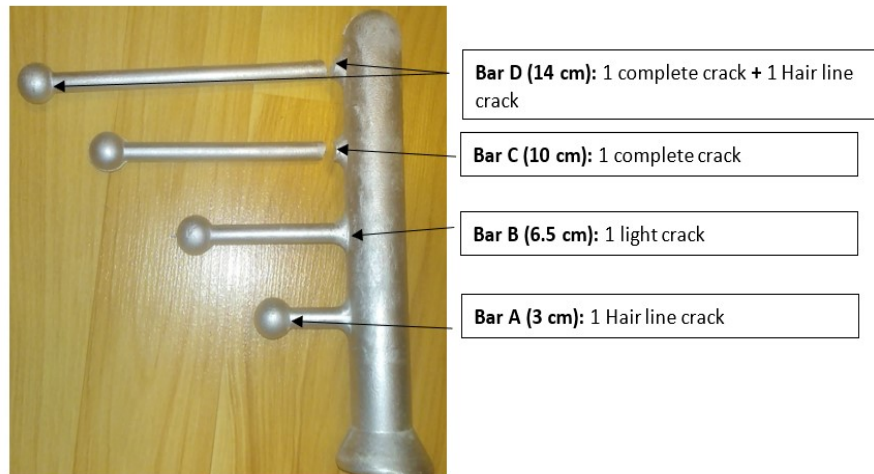

Figure 3-6. Example of HTS casting.

Table 3-3. Calculation of HTS index

Principle of calculation	HTS index for each bar	HTS index of the casting
Bar (A): $(4 \times 1 \times 2)$ Li : the shortest bar Pi : ball-end Ci : hair line crack	8	
Bar (B): $(3 \times 2 \times 1)$ Li : the 3rd longest bar Pi : sprue-end Ci : light crack	6	8+6+8+6 = 28
Bar (C): $(2 \times 4 \times 1)$ Li : the 2nd longest bar Pi : sprue-end Ci : complete crack	8	
Bar (D): $(1 \times 4 \times 1)$ + $(1 \times 1 \times 2)$ Li : the 1st longest bar Pi : sprue-end Ci : complete crack Li : the 1st longest bar Pi : ball-end Ci : hair line crack	6	

For each refiner addition rate, experiments were repeated 2 times and average HTS indexes were calculated. After that, microstructure evaluation was performed. Specimens for microstructure analysis were always taken from the longest bar, since it was completely separated in each condition due to its highest propensity for solidification stress [50]. Where the sectioned part was, exactly, taken from the area close to the junction between sprue and bar, as shown in **Figure 3-7**. Then, the transversal cross section was subjected to the grain structure evaluation and grain size measurement using optical microscopy and the standard linear intercept method (ASTM 112) after the electro-etching in order to relate the refiners addition rate and the resulting grain structure to the alloy cracking behavior.
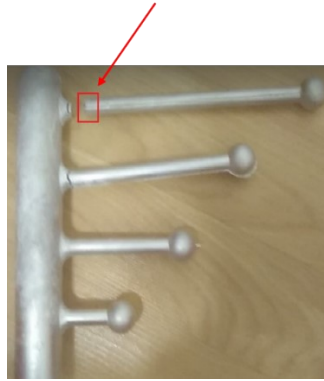
Figure 3-7. Casting from the CRC mold and the part sectioned for grain structure evaluation.

3.3- Experimental for studying the Cr effect on grain refinement

3.3.1- Grain refinement in 6111 alloys with/without chromium

3.3.1.2. Experimental alloys

To reveal the Cr effect on the refinement potency in 6111 aluminum wrought alloys, 2 different 6111 alloys were compared. The first one is without Cr (0.004%Cr), while the second one has a higher Cr percentage of (0.144%Cr). Both alloys with lower and higher (%) of Cr were received from the industrial partner. The chemical composition of the experimental alloys is listed in **Table 3-4**. The same three master alloys used before, were also used here as grain refiners for comparative studies: Al-3%Ti-1B, Al-5%Ti-1B and Al-3%Ti-0,15%C, and the same Al-6%Ti master alloy was used for titanium addition. Grain size measurements were performed at 2 different cooling rates (0.4 et 4°C/s), with modifying the addition rate of grain refiners (1 Kg/t, 2 kg/t and 3Kg/t) in the presence of 200 ppm Ti.

Table 3-4. Chemical composition of (wt.%) of the experimental alloys

Alloy	Mg	Si	Cu	Mn	Fe	Cr
6111 Base(0.004%Cr)	0.76	0.74	0.51	0.28	0.19	**0.004**
6111 High Cr(0.144%Cr)	0.79	0.76	0.52	0.28	0.19	**0.144**

3.3.1.2- Experimental procedure and grain size measurement

The experimental procedure already performed in the part (3-1 Experimental for Comparison of the grain refiners performance) was also performed in this part to compare the refinement efficiency in alloys (with/without) chromium.

3.3.2- Specimen preparation and analysis of interactions between Cr and grain refiners

3.3.2.1- Sample preparation

To study the interaction between Cr element and the intermetallic particles present in the 3 grain refiners (Al- 3%Ti-1B, Al-5%Ti-1B and Al-3%Ti-0.15%C), Al-20%Cr master alloy was added to each grain refiner master alloy to make each specimen containing 0.2% of Cr. The mixture was held at 720°C in 3 different holding times (2 min, 30min, 2 hours). After that, samples for microstructure observation were prepared by the same polishing procedure as in the previous section to be analyzed thereafter under the SEM-EDS. Analysis by SEM-EDS were mainly carried out to identify the change in the intermetallics compositions of grain refiners after the Cr addition, and therefore to check the possible diffusion of Cr into these particles. The

influence of contact time on this type of interaction was also studied using SEM-EDS tools.

3.3.2.2- Crystallographic analysis using E2EM

The fundamentals of the edge to edge matching model have been explained in detail in ref [79], and hence will not been detailed here in the same way. However, the key points that have been considered in this model have to be shown here prior to the model application. The basic principle of what is called (edge to edge matching model E2EM) is the energy minimization of the interface between two phases [79]. This energy is minimized when rows of atoms that present the edges of the meeting planes are close-packed or nearly close-packed atomic rows [79]. According to the E2EM, a number of planes of each phase meet each other edge to edge through the parallel rows of atoms. The important criteria of this model [79] is that this arrangement has to be in a way that the edges of the meeting planes must be close-packed or nearly close packed in each phase. For simplicity and to describe interface between phases A and B, we can say that each close-packed plane in phase A meets a close-packed plane of phase B, this meeting occurs in the interface across the edges and consists of a close-packed atomic rows [79].

To evaluate the crystallographic matching between 2 phases using the E2EM, requires basic knowledges of the crystal features, including the lattice parameters and the atomic positions of the studied phases [79, 80]. A crystallographic matching is

obtained when, at least, a pair of close packed rows and their corresponding pair of closed packed planes meet the criteria f_r <10 and f_d <10, respectively, where f_r is the interatomic spacing mismatch between the meeting rows and f_d is the interplanar spacing mismatch between the planes containing these rows [14, 81]. Applying the mathematical definition of f_r and f_d parameters on the interface particle/ metal matrix, the 2 key parameters are defined as follows [14, 82]:

$$f_r = \frac{|r_M - r_P|}{r_P} \text{ and } f_d = \frac{|d_M - d_P|}{d_P} \tag{3-2}$$

where r_M and r_p are the interatomic spacings along the close packed row in metal matrix and inoculant particle, respectively, while d_M and d_P are the interplanar spacings of close packed planes containing the matching rows inmetal matrix and inoculant particle, respectively. The smaller f_r and f_d are, the better crystallographic matching is [14].

Interestingly, this model consider that the matching rows should be parallel, and this parallelism is indicated based on the interfacial energy [14]. Crystallographic matching can further be refined by maximising the matching of atom rows in the interface. The refinement consists of the rotation of the meeting planes, one to another by a rotation angle Φ about the axis defined by the parallel matching close-packed atomic rows.

Following this, a resulting orientation relationship between the 2 phases will be defined by [79]:

$$(h_1k_1l_1)_A \text{ at angle } \Phi \text{ to } (h_1k_1l_1)_B$$

$$[u \ v \ w]_A \ // \ [u \ v \ w]_B$$

Where $[u \ v \ w]_{A,B}$ are the matching atomic rows of both phases A and B, while $(h \ k \ l)_{A,B}$ are the matching planes containing these directions. The final situation is illustrated in **Figure 3-8** [79].
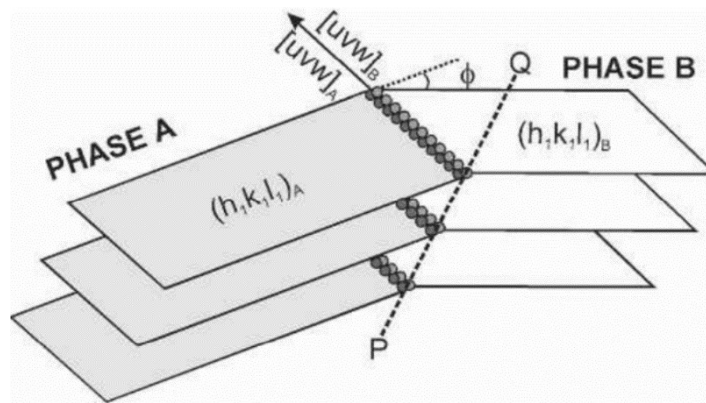
Figure 3-8. Illustration of the edge to edge model (E2EM), highlighting the matching atomic rows in the interface **[79]**.

To applicate the model, the crystallographic matching evaluation using E2EM involves two major steps: (1) identification of the close-packed atomic rows and identification of close-packed planes containing these atomic rows. (2) calculation of the interatomic spacing mismatch along the matching rows and the interplanar spacing mismatch between the corresponding matching planes (f_r) and (f_d), respectively. Practically, to identify the close packed planes, the International Powder Diffraction

Files should be very helpful. The planes with highest diffraction intensity, generally, are the close packed or nearly close packed planes. However, close packed directions identification in these planes requires geometrical calculation based on the positions of atoms in the lattice. A computer program called PTCLAB (Phase Transformation Crystallography Lab), a free and open source software was developed to evaluate the crystallographic matching and predict the possible orientation relationships between phases based on the edge to edge model proposed by Zhang et al. [76, 83]. Software calculations requires as input the crystallographic data of each phase.

In the present work, the PTCLAB was used for the crystallographic matching evaluation between the different nucleant particles of the grain refiners and the Al matrix. CIF files (Crystallographic Information Files) were used as input in the software for providing the crystallographic features for each phase including the lattice parameter and the atoms positions. As output, we could figure out the matching planes, rows and combination between them. The possible nominal rational orientation relationships were also identified. Furthermore, the refinement of some nominal rational ORs can be automatically performed by PTCLAB, showing the value of the deviation angle through which a maximum matching between phases can be obtained.

CHAPTER 4: THE EFFECT OF GRAIN REFINERS ON REFINING PERFORMANCE AND HOT TEARING SUSCEPTIBILITY OF ALUMINUM AA6111 ALLOYS

4.1-   Effect of the cooling rate and refiners addition on the grain structure: (refiner: 5/1(%Ti/%B), addition rate 2Kg/t, CR=(0.4°C/s, 4°C/s))

The samples before and after refinement were examined at the macro and micro-scale to reveal the detailed grain structure. With no addition of grain refiner, the base alloy 6111 presents a large columnar dendritic structure consisting of α–Al and interdendritic areas in both cooling rates (0.4 and 4°C/s). A small reduction effect was obtained on the grain size by the increased cooling rate before refinement, where the grains had an average value of 2030 μm at 0.4°C/s as shown in macrograph of **Figure 4-1 (a)** compared to 2022 μm at 4°C/s (**Figure 4-1(b)**). The quantitative measurement of SDAS was also performed before refinement. A significant coarsening of the dendrite arms was found at the lower cooling rate (0.4°C/s) and shown in the **micrograph(a-1)** of **Figure 4-1** with value of 117±35.5 μm compared to 47±2 μm after increasing the cooling rate to 4°C/s (**Figure 4-1 micrograph b-1**).

The reduction of SDAS observed in the absence of refinement was mainly caused by the difference in cooling rates. It is well known that the Dendrite Arm Space is strictly controlled by the solidification rate through a reverse correlation. Therefore, a higher cooling rate and a shorter solidification time leads to a finer dendritic structure.

The relationship between SDAS and cooling rate (CR) is given in literature as follows [84, 85]:

$$SDAS = K (CR)^{-n} \qquad (4\text{- }1)$$

Where K depends on the alloy constituents, and the power index n should be in the range of [0.33-0.5]. Solving for n from the equation (4-1) above and using the present experimental results obtained between CR and SDAS, we get n= 0.39, which fits well the typical range of n variation.

Furthermore, the present results confirm that both grain size and SDAS may be refined by increasing the cooling rate without refiner addition, showing bigger influence of the CR on the SDAS.

The addition of 2kg/T of the (5/1(%Ti/%B) refiner to the base alloy 6111 produced a drastic refinement where the coarse grains of the base alloy were totally replaced by smaller grains in both cooling rates, as shown in the **Figure 4-1 (macrographs c and d)**. Further improvement in grain refinement was obtained under the combined effect of both higher cooling rate and the refiner addition, where an average gain size of 146.6μm was achieved by the 5/1 (%Ti/%B) addition at 4°C/s **(Figure 4-1 (micrograph d-1)** compared to 160.4μm at 0.4°C/s as illustrated in **micrograph(c-1)** of **Figure 4-1**.
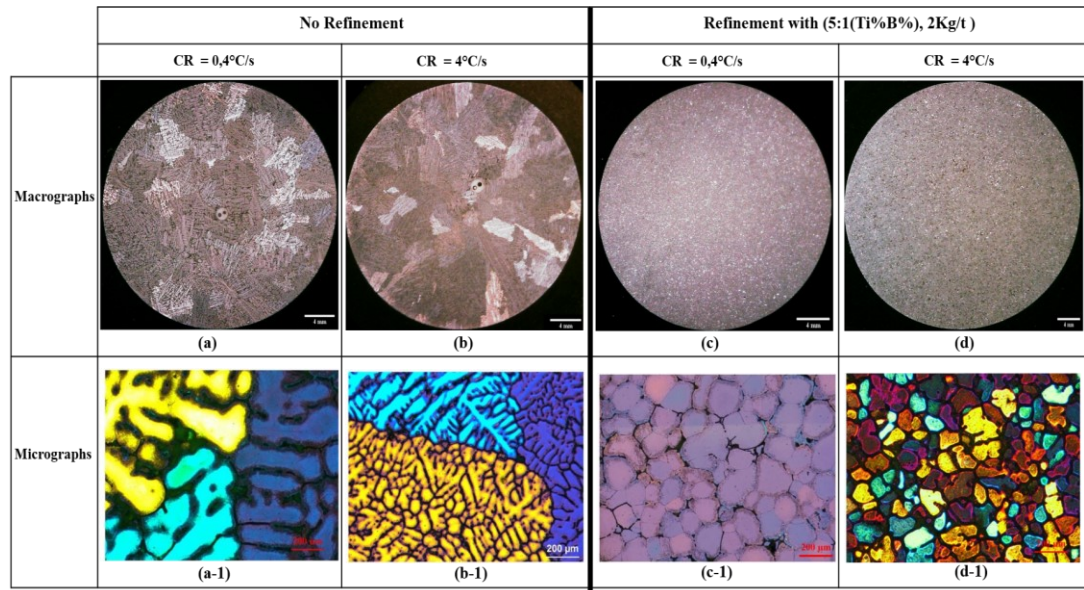
Figure 4-1. Optical macro and micrographs of the grain structure before and after refinement with (5/1(%Ti/%B), 2Kg/t), at different cooling rates (0.4°C/s, 4°C/s).
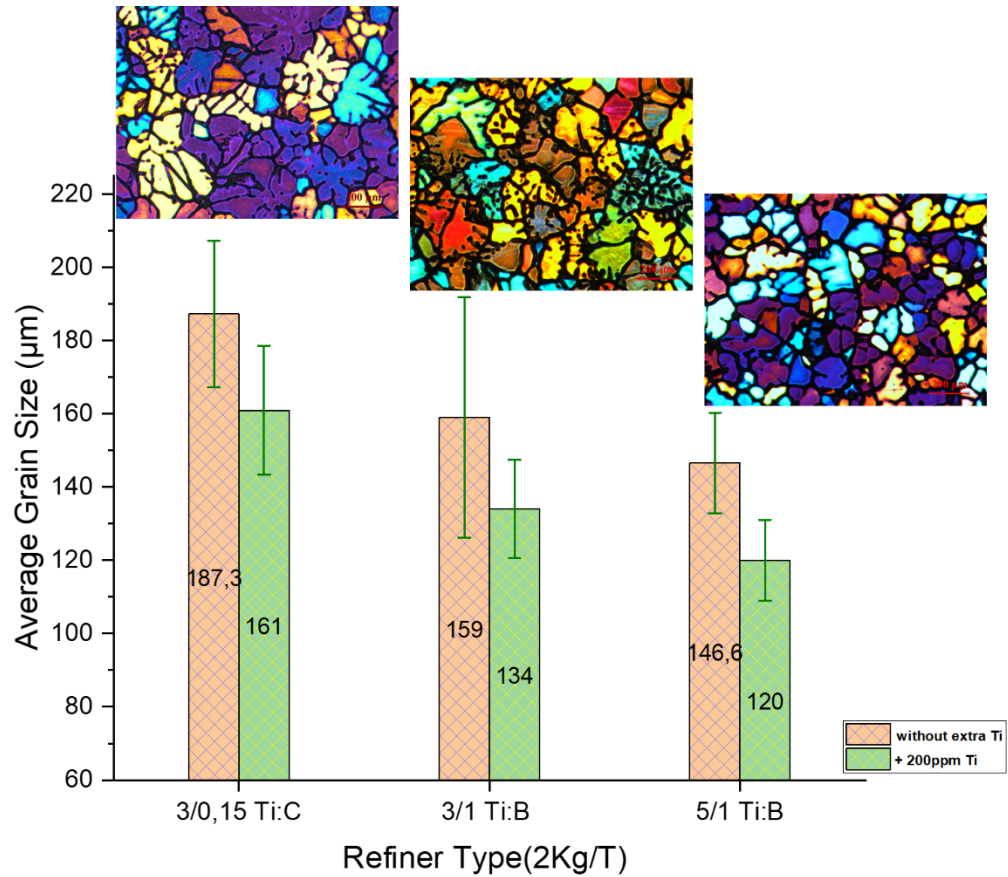
4.2- Comparison of the refining performance of the three refiners (at addition rate of 2Kg/T) and effect of Ti addition on grain refinement

For comparative studies of the refinement potency, three different types of grain refiners were tested: Al-3%Ti-1%B, Al-5%Ti-1%B and Al-3%Ti-0.15%C. In the beginning, an addition rate of 2 Kg/t of each refiner type was performed to the basic alloys. The refined grain size was analyzed thereafter, showing that the addition of 2kg/T of each refiner totally replaced the coarse grains of the base alloy by smaller grain structure. However, differences in refinement effect resulted from the three different refiners were clearly visible, resulting in different grain sizes and different grain morphologies. **Figure 4-2 (**bars in pink color) show the grain size measurements and the corresponding micrographs for each (2Kg/T) refiner addition and before Ti addition. The 5/1 (%Ti/%B) master alloy exhibited the greatest refinement effect,

inducing the smallest average grain size of 146.6μm with equiaxed grains with rosette-like morphology that show fewer dendrites. While the 3/1 (%Ti/%B) master alloy produced an intermediate average grain size of 159μm with larger dendritic grains, compared to more larger dendritic grains with an average gain size of 187.3μm when using 3/0.15 (%Ti/%C).

200 ppm of Ti as a solute was added thereafter to the refined alloys. **Figure 4-2** (bars in green color) show the experimental results obtained under the combined effect of master alloys (2Kg/T) and Ti solute additions on the grain size at the higher cooling rate(4°C/s). The measurements clearly confirm that the presence of free Ti as a solute contributes to a further reduction in the grain size in each case. The 5/1 (%Ti/%B) master alloy keeps his higher performance in terms of grain size reduction, where the size of grains was further reduced under the Ti effect to 120μm compared to 134 μm and 161 μm using the 3/1 (%Ti/%B) and 3/0.15 (%Ti/%C) refiners, respectively. The same tendency of Ti effect was confirmed in lower cooling rate (0.4°C/s).

Figure 4-2. Comparison of the refiners performance and effect of Ti addition (200ppm) on grain size (Addition rate of refiners:2Kg/T, Cooling Rate: 4°C/s), the micrographs correspond to the condition (2Kg/T of each refiner before 200 ppm Ti addition).

The importance of solutes in refinement has been known for a long time, particularly the contribution of Ti as a solute in grain refinement which has been investigated by several researchers [86, 87]. In the present work, Ti-controlled grain size of α-Al grains is attributed to the growth restriction factor (Q) of this Ti element on the growing grains. In fact, Ti has been reported to have the largest growth restriction factor in dissolved state with a value of Q ~ 245, compared to most other

alloying elements which are below ten. Hence, a minor modification in the Ti content may lead to a significant variation in grain size in wrought aluminum alloys [88, 89]. The Q parameter used to quantify the restriction effect of Ti solute on the grain size is defined as shown in the following equation [88, 89]:

$$Q = mc_0(k-1) \qquad (4\text{-}2)$$

Where m is the slope of the liquidus, c_0 is the concentration of the solute in the melt and K is the partition coefficient between the equilibrium concentrations of the solid and liquid at the growing interface ($K=C_s/C_l$ at the interface temperature).

The equation developed by Easton and StJohn [90] shows that the average grain size (d) is proportional to the inverse of Q restriction factor:

$$d=a+b/Q \qquad (4\text{-}3)$$

Where the coefficients a and b depend on the potency of the master alloys of the added refiners. To obtain better restriction condition, the necessary Ti addition rate depends on the composition of the actual alloy. For example, more Ti is required for the 1xxx and 3xxx compared to the case for the 6xxx alloys.

4.3- The comparison of the refining performance in different addition rates (1, 2 and 3kg/T) in the presence of Ti as a solute

The combined effect of master alloys and Ti solute addition on the grain refinement is studied in this part with modifying the addition rate of grain refiners and keeping Ti solute at a constant level of 200 ppm. **Figure 4-3** shows the variation of the grain size with three different levels of the three master alloys (1 Kg/T, 2 kg/T and 3Kg/T) in the presence of 200 ppm of titanium as a solute at a higher CR(4°C/s). For each refiner type, the grain size reduction was favored by the increase of the addition rate as shown in the curves of **Figure 4-3.** Increasing the addition rate from 1Kg/T to 3Kg/T with keeping Ti at a constant level of 200 ppm reduced significantly the grain size, which by evidence, due to the presence of more inoculants particles that promote the nucleation event in the melt. In each addition rate, the efficiency of the refiners increases in the order Al-3Ti-0.15C < Al-3Ti-1B < Al-5Ti-1B.
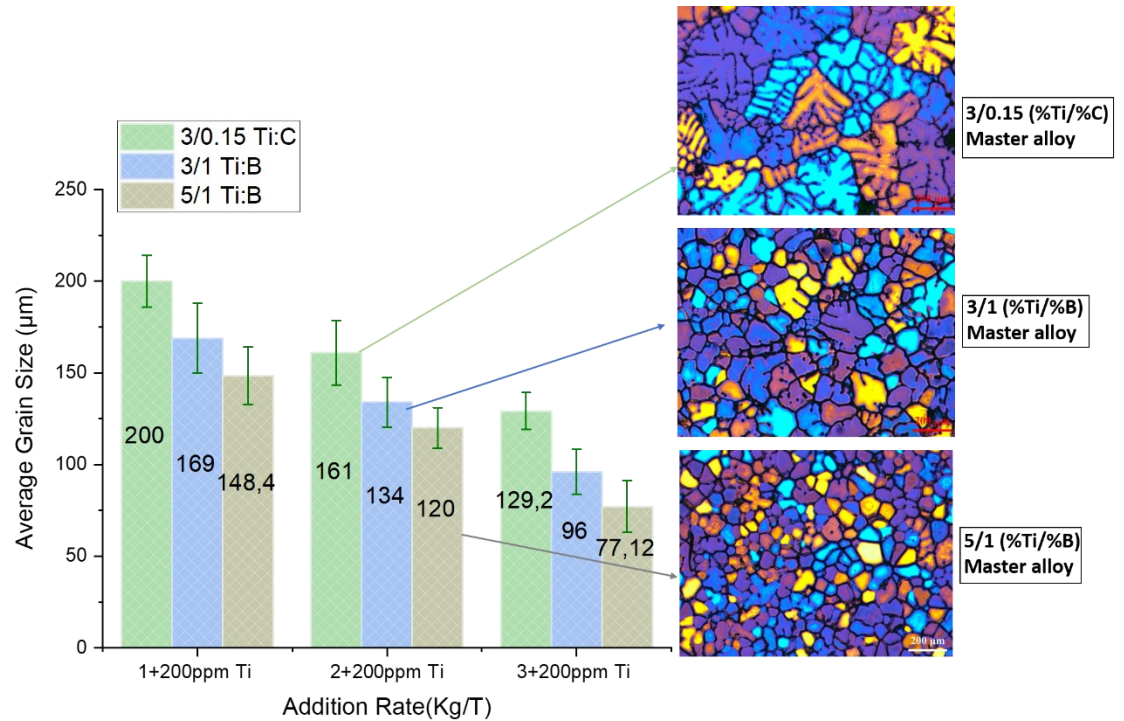
Figure 4-3. Evolution of the grain size with the refiner addition rate for the three different grain refiners in the presence of 200ppm Ti, (CR=4°C/s).

Micrographs at the addition rate of (2Kg/T) in the presence of 200ppm Ti are also shown in the same **Figure 4-3**. The 3/0.15 (%Ti/%C) refiner clearly exhibited the largest columnar dendritic grains, compared to smaller and equiaxed rosette-like grains with only few dendrites, when using the 3/1 (%Ti/%B) refiner. However, the use of the 5/1 1 (%Ti/%B) refiner produced the smallest grain size, presenting equiaxed and globular morphology.

The same tendency of refiners potency in grain size reduction was found in the lower CR (0.4°C/s), confirming that in each condition, the 5/1 (%Ti/%B) master alloy produced the smallest grain size followed by the 3/1 (%Ti/%B) and then the 3/0.15

(%Ti/%C) master alloys. Results are summarised in **Table 4-1**. Therefore, it is fair to conclude from the foregoing that the 5/1 (%Ti/%B) master alloy is the best grain refiner in terms of grain size reduction for the 6111 alloys in similar casting conditions.

Table 4-1. Grain size variation with the refiner type and refinement addition rate, (CR=0.4°C/s)

Refinement condition	3/0.15 (%Ti/%C)	3/1 (%Ti/%B)	5/1 (%Ti/%B)
1Kg/T+200ppm Ti	207±19.6 μm	198±13.6 μm	162±12 μm
2Kg/T+200ppm Ti	165±12 μm	155±9 μm	135.6±10 μm
3Kg/T+200ppm Ti	133.6±6 μm	116.4±8 μm	87±2 μm

4.4- The refinement and cooling rate effect on the morphology evolution in 6111 alloys

It is worth noting that the morphology of the resulting microstructure after refinement and the associated distribution of solute have a critical impact on the properties of the solidified alloys. Hence, controlling the grain morphology is of considerable practical importance in industries. To highlight the relationship between the casting factors (cooling rate, refiners addition rate) and the solidified structure, the morphology evolution was studied and results are shown in **Figure 4-4** at the higher CR (4°C/s). The present results show that by changing the grain size, the grain morphology also changes. Before refinement, the grains were coarse columnar and highly dendritic as shown in **Figure 4-4(a)**. After the first refinement by adding 1kg/T of refiners in the presence of 200 ppm of titanium as a solute, an equiaxed dendritic

grain morphology was obtained (**Figure 4-4(b)**). A further addition of the grain refiner (2kg/T+200ppm Ti) continues the grain size reduction and the grain morphology became rosette-like, termed also cellular (**Figure 4-4(c)**). Adding more grain refiner (3kg/T+200ppm Ti) leads to a very smaller size with a globular grain morphology(**Figure 4-4(d)**). Each refiner typeof the 3 master alloys (Al-3%Ti-1B, Al-5%Ti-1B and Al-3%Ti-0.15%C) was found to exhibit the same evolution in the grain morphology starting from being coarse columnar to final globular grains.
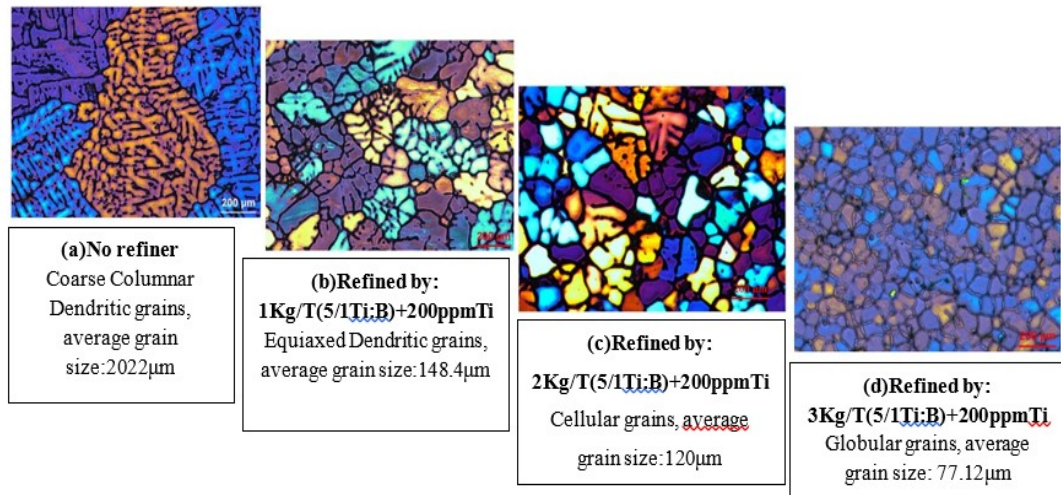
Figure 4-4. Variation of the grain morphology with the grain size in 6111 alloy under the increased addition rate of refiners, CR: 4°C/s.

For a given addition rate, almost the same morphology was found when using the three different refiners, but with a difference in grain size due to the potency difference of refiners. **Table 4-2** present more details about the morphology and size evolution of each refiner.
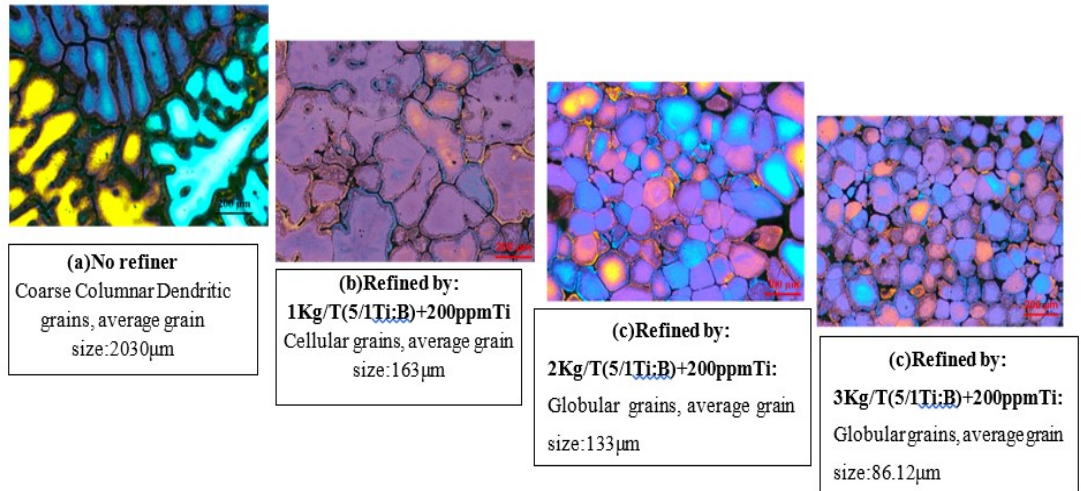
Table 4-2. Grain size and morphology evolution for each grain refiner, CR=4°C/s.

Refinement conditions	3/0.15 (%Ti/%C)	3/1 (%Ti/%B)	5/1 (%Ti/%B)
1Kg/T+200ppm Ti	-Average grain size: 200µm -Morphology:Equiaxed Dendritic grains	- Average grain size:169µm -Morphology:Equiaxed Dendritic grains + some cellular grains start to appear	- Average grain size:148.4µm -Morphology:Equiaxed Dendritic grains + some cellular grains start to appear
2Kg/T+200ppm Ti	Average grain size:161µm Morphology: Cellular grains	Average grain size:134µm Morphology: Cellular grains	Average grain size:120µm Morphology: Cellular grains + some globular grains
3Kg/T+200ppm Ti	Average grain size:129.2µm Morphology: Cellular grains + some globular grains start to appear	Average grain size:96µm Morphology: Cellular grains + some globular grains start to appear	Average grain size:77.12µm Morphology: totally globular grains

Furthermore, for a given cooling rate, increasing the refiner addition rate was found to influence only the grain size and grain morphology, while the SDAS remains almost stable with value of 47±7 µm. Thus, there was no interaction obtained between the grain refiner addition rate and the SDAS values [10, 11]. However, it became difficult to continue measuring the SDAS when the morphology became cellular due to the significant reduction in the size of the primary dendrite arm while the SDAS remained the same [10].

The same morphology evolution of the grains was obtained using each refiner at the lower cooling rate (0.4°C/s), starting from being coarse columnar to final globular grains. However, the higher cooling rate (4°C/s) was found to favor a very highly dendritic structure compared to the lower cooling rate. **Figure 4-5** shows the

morphology evolution at lower cooling rate of (0.4°C/s), where only fewer arms are observed or even not observed at all compared to a higher dendritic structure in the higher cooling rate and already shown in the precedent **Figure 4-4**.

(a)No refiner
Coarse Columnar Dendritic grains, average grain size:2030μm

(b)Refined by:
1Kg/T(5/1Ti;B)+200ppmTi
Cellular grains, average grain size:163μm

(c)Refined by:
2Kg/T(5/1Ti;B)+200ppmTi:
Globular grains, average grain size:133μm

(c)Refined by:
3Kg/T(5/1Ti;B)+200ppmTi:
Globular grains, average grain size:86.12μm

Figure 4-5. Variation of the grain morphology with the grain size in 6111 alloy under the increased addition rate of refiners, CR: 0.4°C/s.

This dendritic preference at a higher cooling rate (4°C/s) is known to be because of the instability of the planar interface solid-liquid during the rapid growth of crystals from the melt, resulting in highly complex branched structure. Moreover, if the solidification time is shorter, the SDAS will be very fine producing grain structure with more dendritic morphology [84]. Interestingly, at a lower cooling rate (0,4°C/s) the transition of grain morphology from columnar dendritic to fully equiaxed globular was achieved at earlier rate of refiners addition. Under CR of 0.4°C/s, (2Kg/T+200 ppm Ti) was always sufficient to produce fully globular grains while higher addition rate of (3Kg/T+200ppm Ti) was needed to obtain this final globular structure at CR=4°C/s. It was reported that the grain shape of the interface depends on the cooling rate, where

the lower cooling rate leads to more uniform and globular grain structure since there is more time for solutes diffusion from liquid to solid phase [91]. It appears therefore that for increased cooling rates, it is required to grain refine well to obtain this final equiaxed globular morphology.

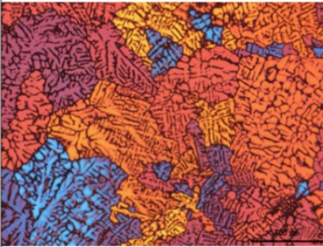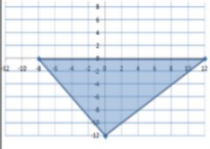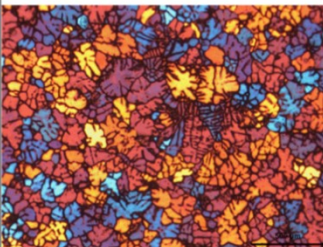### 4.5- Effect of the refinement on the hot tearing susceptibility
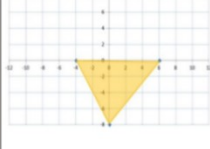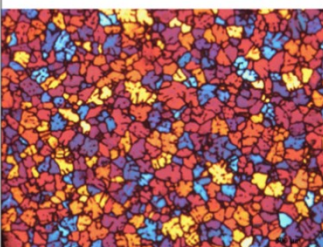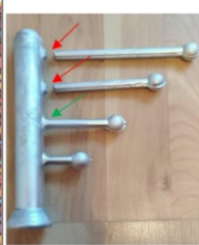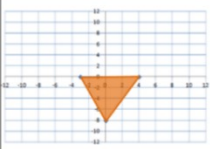
This experimental part has been conducted in order to relate the refiner addition rate and the obtained grain structure to the resulting hot tearing susceptibility of the alloy. The hot tearing tendency of the 6111 alloy was evaluated using the 5/1 Ti:B grain refiner since it was the preferred one in terms of grain size reduction in our previous results. Experimental results are illustrated in **Table 4-3** where indexes (HTS) for hot tearing evaluation were calculated based on the method already explained in the methodology part. Further description of the hot tearing susceptibility is provided graphically in the same table by a Foot Print Chart [22, 50], where the area represents the global hot tearing tendency of the alloy in each condition.

At the beginning, the non refined alloy with mainly columnar dendritic grains and average grain size of 471 µm had the highest hot tearing susceptibility index (32) with the greatest hot tearing area,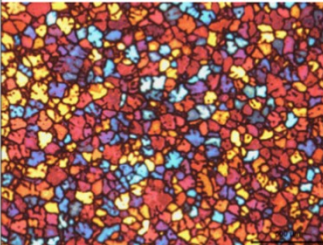 which reflects the higher hot tearing susceptibility of this condition. Then, after the refiner addition of (1Kg/T+200ppm Ti) the hot tearing index decreased significantly from 32 to 18, and hence a reduction in the resulting hot tearing area was obtained when equiaxed dendritic grains formed with average grain size of 99,3 µm. The addition of more grain refiner (2Kg/T+200 Ti) continues to

decrease the grain size to 68 µm and the grain morphology changes from being equiaxed dendritic to being rosette-like(cellular) reaching the minimum hot tearing susceptibility index (8) and the minimum corresponding area. With a further addition of grain refiner (3kg/T+200 Ti), grain morphology became totally globular reaching the minimum average grain size (51 µm), but the hot tearing susceptibility index increased again to reach a value of 15 with an increase in the corresponding tearing area. Tests were performed 2 times for each condition, where all results confirm the same tendency. When the grain morphology is dendritic, reducing the grain size decreases the hot tear susceptibility.

However, smaller grains with globular morphology may in fact increase the hot tear susceptibility of the alloy. Furthermore, the microstructures shown in **Figure 4-6** present an example of hot tearing defects (in micro-scale) found in the tested 6111 alloy after adding 3Kg/T+200 ppm Ti of 5/1(%Ti/%B). Micrographs of **Figure 4-6** are coming from specimens that were sectioned as shown in the experimental chapter, section (3-1). The microstructures show several intergranular cracks (hot tears) despite the highest addition rate of refiners (3Kg/T+200 ppm Ti) and the globular and smaller microstructure with average grain size of 77.12 µm.

Table 4-3. Experimental conditions and Results for the hot tearing evaluation of the 6111 alloy.

6111 alloy conditions	The resulting Grain structure	The hot tearing susceptibility casting	Foot Print Chart of the HTS	Average HTS Index
- No grain refiner - No Ti addition	 - Columnar Dendritic grains - Average grain size : 471µm	 - 3 Complete Cracks - 1 Light Crack in the 1st bar - 1 Hairline Crack in the 2nd bar		32
5/1 Ti:B(1Kg/T) + 200ppm Ti	 - Equiaxed Dendritic grains - Average grain size : 99,3 µm	 - 2 Complete Cracks - 1 Light Crack		18
5/1 Ti:B(2Kg/T) + 200ppm Ti	 - Rosette-like grains (cellular) - Average grain size : 68	 - 1Complete Crack - 1 Light Crack		8
5/1 Ti:B(3Kg/T) + 200ppm Ti	 - Globular grains - Average grain size : 51 µm	 - 2 Complete Cracks - 1 Hairline Crack		15
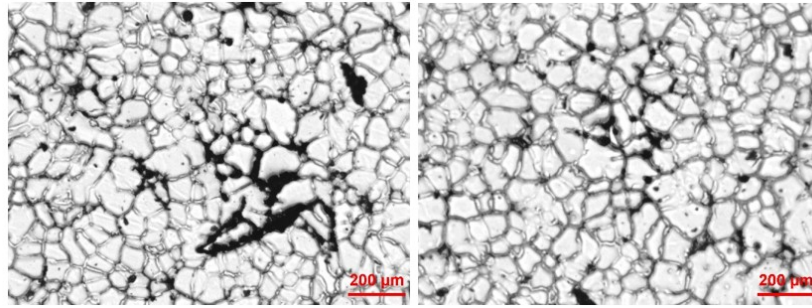
Figure 4-6. Microstructure revealing the hot tearing defect, Refiner: 5/1(%Ti/%B), Addition Rate: 3Kg/T+200ppmTi.

4.6- Discussion

4.6.1- The effect of the grain refiner microstructure on the refinement efficiency

Much theoretical and practical investigation has been performed to investigate the more potent master alloy of the grain refiner. Several works have been carried out on the influence of the processing parameters such as contact time, addition temperature and cooling rate on grain refiner efficiency [92]. However, other fewer studies considered the microstructure effect of the master alloys on their refining behavior [92]. The refiners microstructure, including the size, morphology and quantity of the particles present in the master alloys, is believed to be one of the critical facts influencing the grain refining response [92-94]. This discussion part is dedicated to suggest the possible causes behind the efficiency order of the 3 grain refiners obtained in our experiments based on their microstructure comparison and facts mentioned in the literature.

Figure 4-7 (a,b,c) shows microscope images of the tested refiners (5/1(% Ti/%B), 3/1(%Ti/%B) and 3/0,15(%Ti/%C)). From the EDS analysis, it can be noted that each refiner contains bigger aluminide (Al_3Ti) particles, surrounded with lots of smaller sub-micron size particles. These smaller particles were identified as TiB_2 in the 3/1 and 5/1 (%Ti/%B) master alloys and as TiC in the 3/0.15 (%Ti/%C) master alloy. Al_3Ti particles were found to be bigger with blocky shape in the 5/1(%Ti/%B) compared to finer needle-like Al_3Ti particles in the 3/1 (%Ti/%B) master alloy and also to the finer rod-like particles Al_3Ti in the 3/0.15(%Ti/%C) master alloy. This difference in morphology is found to be caused by the different melting temperatures and cooling rates during the forming process of the master alloys [92]. Al_3Ti particles have often been considered as the more suitable substrates for the Al nucleation than any other heterogeneous nucleating substrate [11, 70]. Al_3Ti possess a greater number of planes with a good orientation relationship with aluminum [3, 10, 11]. And, if they are stable, they act well as nucleation sites. However, when the master alloy is added, the amount of titanium in the melt is present at hypoperitectic amounts (less than 0.15%). Therefore, the Al_3Ti particles are prone to dissolve after a certain melt holding time [3]. Interestingly, literature has shown that the time required for complete dissolution of the aluminide Al_3Ti is highly dependent on the diffusivity time of Ti into Al, on particle size and morphology of the Al_3Ti particles and melt temperature [10, 11]. Al_3Ti particles with blocky morphology showed in studies [92, 95] better refinement potency than the other morphologies, and they were found to exist for longer time of 30 min in the Al melt and act as nucleating sites even when they are present at hypoperitectic concentration. It was thought that the compacted and blocky structure reduces the dissolution tendency, and therefore makes them resist or partially dissolve within the

104

contact time, acting as a nucleating site. The holding time of the present work was shorter and of 2 min with the same melt temperature as in ref [92], which ensure the longer existence of the Al_3Ti particles. From a crystallographic point of view, ref [96] found that the blocky morphology exhibit more suitable planes that contribute to the Al nucleation, when comparing to the other commercial available morphologies. Furthermore, in the Al-Ti-B master alloy, the stoichiometric ratio for TiB_2 formation is (%Ti/%B = 2.22). The remaining Ti contributes to the Al_3Ti formation in the master alloy [2, 61]. The 5/1(%Ti/%B) master alloy contains greater ratio, which provides more Al_3Ti particles in this master alloy compared to case in the 3/1(%Ti/%B). The variation in ratio was confirmed to have strong influence on the refining potency [61]. It appears therefore that the blocky morphology with larger number of the Al_3Ti particles may be one of the facts behind the higher efficiency of the 5/1 (%Ti/%B) master alloy as a grain refiner. A detailed comparison of Al_3Ti particles present in the 3 tested refiners is given by **Table 4-4**. Results clearly show that the 5/1(%Ti/%B) master alloy present the highest number density of particles with the largest mean equivalent diameter of particles.

Table 4-4. Number density and size of Al_3Ti particles in the three master alloys of the grain refiners

	Morphology of Al_3Ti particles	Number density of Al_3Ti particles	Average equivalent diameter of Al_3Ti particles
3/1(%Ti/%B)	needle-like	1.73×10^2 mm^{-2}	$9.7 \pm 6.4\mu m$
5/1(%Ti/%B)	Blocky	3.6×10^2 mm^{-2}	34 ± 14.2 μm
3/0.15(%Ti/%C)	needle-like	2.1×10^2 mm^{-2}	28.6 ± 7.4 μm

Given the instability of the Al_3Ti particles, several theories have been developed to describe the alternative grain refinement mechanism. Earlier, the boride/carbide theory was proposed by Cibula and supported by Jones and Pearson [3, 10, 62]. According to this theory, TiB_2 and TiC act as nucleating centers for aluminum due to their higher stability in the Al melt compared to Al_3Ti. However, it has been shown that the lattice matching between the aluminum and the borides/carbides is large which indicates that they are poor nucleants, while Al_3Ti possess a greater number of planes with a good orientation relationship with aluminum [2, 11]. Of all the grain refinement mechanisms proposed so far, the duplex nucleation theory is the most recent one, proposed by Mohanty et al. and supported by Schumacher and Greer [10, 11]. This theory suggests the existence of Al_3Ti layer between the surface of TiB_2 and α-Al, where this layer is formed by the segregation of titanium to the melt\TiB_2 interface [62].

SEM images at high magnification of 10 000x are used in the present section to show more details of the smaller particles TiB_2 and TiC. The TiC particles (**Figure 4-7 (c-1)**) were individual with faceted polygon and near spherical morphologies, exhibiting the smaller mean equivalent diameter in the 3/0.15 (%Ti/%C) master alloy. The TiB_2 particles in the 5/1 (%Ti/%B) (**Figure 4-7 (a-1)**) were almost individual and bigger, with faceted polygon morphology, while they were found in the 3/1(%Ti/%B) (**Figure 4-7 (b-1)**) either as agglomerates with faces touching morphology or individual with rod-like particles and faceted polygon morphologies, exhibiting the biggest mean equivalent diameter.

TiB_2 agglomeration is thought to be caused by factors coming from salts used in the manufacture of Al-Ti-B during their forming process. The Al-Ti-B master alloys are typically made by a mixture of fluoride salts(K_2TiF_6 and KBF_4) added to the molten aluminum [64, 97]. As a reaction, Al reduces these added salts to form the Al-Ti-B master alloy (Al containing dispersed $TiAl_3$ and TiB_2), and a KF-AlF3 flux. The problem of TiB_2 agglomeration may occur during this addition stage by the wetting and engulfment of the KF – AlF_3 flux [64]. Such agglomeration often leads to significant variation in the microstructure and refiners properties [97]. If such borides clusters enter in the finished product, this doesn't only reduce the refiners potency but also leads to several quality problems like the surface defects in lithographic sheets and porosity in foils for packaging [2, 64].

In the same context of comparative study, the number density of nucleant particles (TiB_2/TiC) in each refiner was calculated. It was found that the 5/1(%Ti/%B)

master alloy contains larger number of nucleant particles with value of 3.36×10^5 mm^{-2} compared to 2.52×10^5 mm^{-2} and 1.9×10^5 mm^{-2} for 3/1 (%Ti/%B) and 3/0.15(%Ti/%C), respectively. This fact may also be another reason behind the higher efficiency of the 5/1 (%Ti/%B) master alloy since it is known by evidence that the heterogeneous nucleation mechanism is promoted by the presence of more particles in the melt.
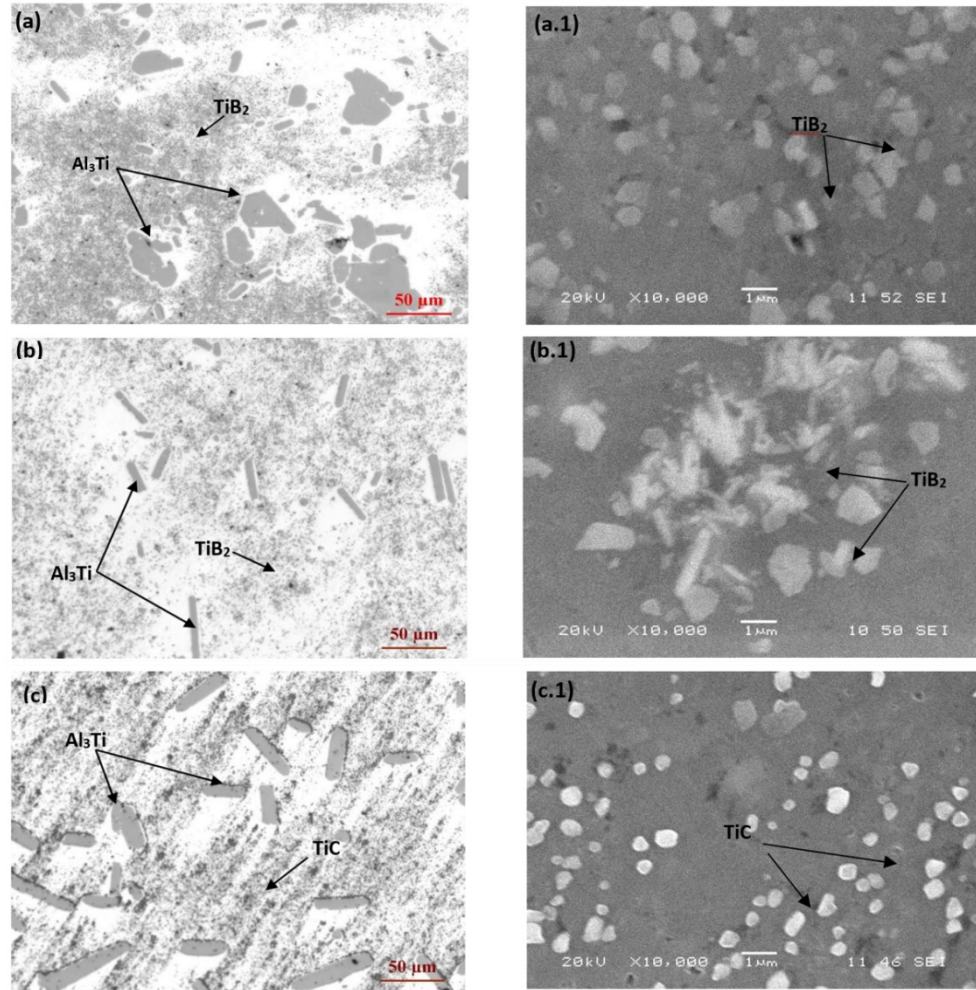
Figure 4-7. (a),(b)and (c) optical microscope images of the master alloys of the grain refiners: 5/1(%Ti/%B), 3/1(%Ti/%B) and 3/0.15(%Ti/%C), respectively. (a.1) and (b.1)SEM images of TiB_2 submicrons particles in 5/1(% Ti/%B) and 3/1(% Ti/%B),respectively. (c.1)SEM images of TiC submicrons particles in 3/0.15(% Ti/%C)

In addition to the number density, the size distribution of the nucleant particles (TiB_2/TiC) is reported also to influence the final grain size of the solidified alloy [98]. The size distribution of the nucleant particles in the 3 master alloys was examined and results are shown in **Figure 4-8.** A good fitting to the measured distributions was provided by log-normal curves in the same **Figure 4-8**. Lognormal functions are often

reported to fit well to the commercial refiner microstructures [99-101]. This distribution is characterized by the geometric mean diameter d_0 and the width of the size distribution σ (i.e., the geometric standard deviation), describing how spread out the nucleant size values are. The 2 distribution characteristics (σ and d_0) were determined for each tested grain refiner and values are shown also in **Figure 4-8**. An optimized combination of the width distribution σ and mean diameter (d_0) was reported to result in finer grain size [98].

Interstingly, the distribution range of size is often reported to be more important than the size of nucleants itself, where Greer et al., [13, 87] cited that a high potency of refinement can be obtained, if the nucleant particles present a narrow size range. The free growth model has been developed considering this concept, highlighting the importance of the nucleant size distribution. This model has been proven to have good match with experiments and has stimulated successful work in enhancing the nucleant performance by changing their size distribution in refiners [102]. According to this model, each nucleant particle represents a center for free growth(nucleation), where a critical undercooling is required for a given nucleant size.

In fact, nucleant substrate remains inactive until reaching the critical undercooling required for the free growth model of the grain. The required undercooling for the free growth onset is related to the nucleant diameter as given by the following equation [87, 103] :

$$\Delta T = \frac{4E}{\Delta S \, d} \qquad\qquad (4\text{-}4)$$

Where ΔT is the critical under cooling for the onset of the free growth, d is the particle diameter, E is the solid-liquid interfacial energy, ΔS is the entropy of fusion per unit volume. It is clear from the relation above that the undercooling necessary for the nucleation onsetvaries inversely with the particle diameter d. Therefore, larger particles could be activated more easily as a response to the smaller undercooling [28]. And the number of the grain initiation is controlled only by the maximum undercooling reached in the melt and doesn't depend on time [102]. Since the nucleant particles in commercial refiners have a log normal size distribution, and hence a corresponding spread of the critical undercooling, thus a spectrum of efficiency would be a result of this distribution [102]. In the free growth model, the free growth happens first on larger particles, then on smaller ones with the increase in the undercooling. The point to well consider here is the latent heat produced by the growing grains, which causes an increase in the melt temperature (coalescence). Then, no more grain initiation will occur due to the temperature increase, and this limits the refinement action due to the inactive particles. As a result, the rest of smaller particles will be pushed by the growing grains and end up in the grain boundaries of the final structure [28, 87]. Based on the model, only the larger particles in the size distribution play a part in nucleation event. Reference [3] has confirmed that larger particles were the ones found in grain centers, confirming the free growth model concept that larger particles would be active at smaller undercooling. For the reasons mentioned above, a narrowest distribution is preferred since it ensures a maximum possible number of particles to act as nucleating

grains at a certain undercooling [102]. In addition to the narrow size distribution required for an efficient refinement, studies have found that there exists an optimum mean diameter of nucleant particles by which a minimum solidified grain size is obtained [28, 102]. Ref [101] confirmed that a mean diameter in the range of [0.3-0.5 µm] can result in greater improvement of refinement. While, 0.7 µm was suggested to be the ideal mean particle size for an efficient refinement in ref [104]. In the present study, the TiB_2 particles were found in the the 5/1 (%Ti/%B) master alloy to have a facts combination of a relative narrow size distribution σ =0.48 and a relative intermediate mean diameter of 0.46 µm **(Figure 4-8(a))**. Experiments show that 74% of TiB_2 particles population in the 5/1 %Ti/%B master alloy are in the range of [0.3-0.7 µm] and are concentrated near the mean value, exhibiting smaller spread of diameter values. In contrast and because of the agglomerates presence, the 3/1 %Ti/%B master alloy **(Figure 4-8(b))** is found to present the largest size distribution σ=0.6 and the biggest mean particle diameter d_0= 0.62 µm. Around 63% of Ti particles population in the 3/1 (%Ti/%B) master alloy was in the range of [0.3-0.7 µm], while the rest size extends farther to reach a bigger diameter of 4.2µm, exhibiting more larger variation in diameters. Such large size distribution would activate the nucleation event first on the larger particles, while the rest of the smaller particles will be pushed by the growing grains to the grain boundaries as explained by the free growth model above [28, 87]. In return, the 3/0.15 (%Ti/%C) **(Figure 4-8(c))** shows TiC particles with the narrowest size distribution σ =0.3, but also the smallest mean diameter d_0= 0.4 µm, where 78.4% of the TiC particles population was in the range of [0.3-0.7µm]. TiC particles were found with smaller size compared to the TiB_2 particles. Therefore, greater undercooling is required for grain initiation based on the free growth model [76].
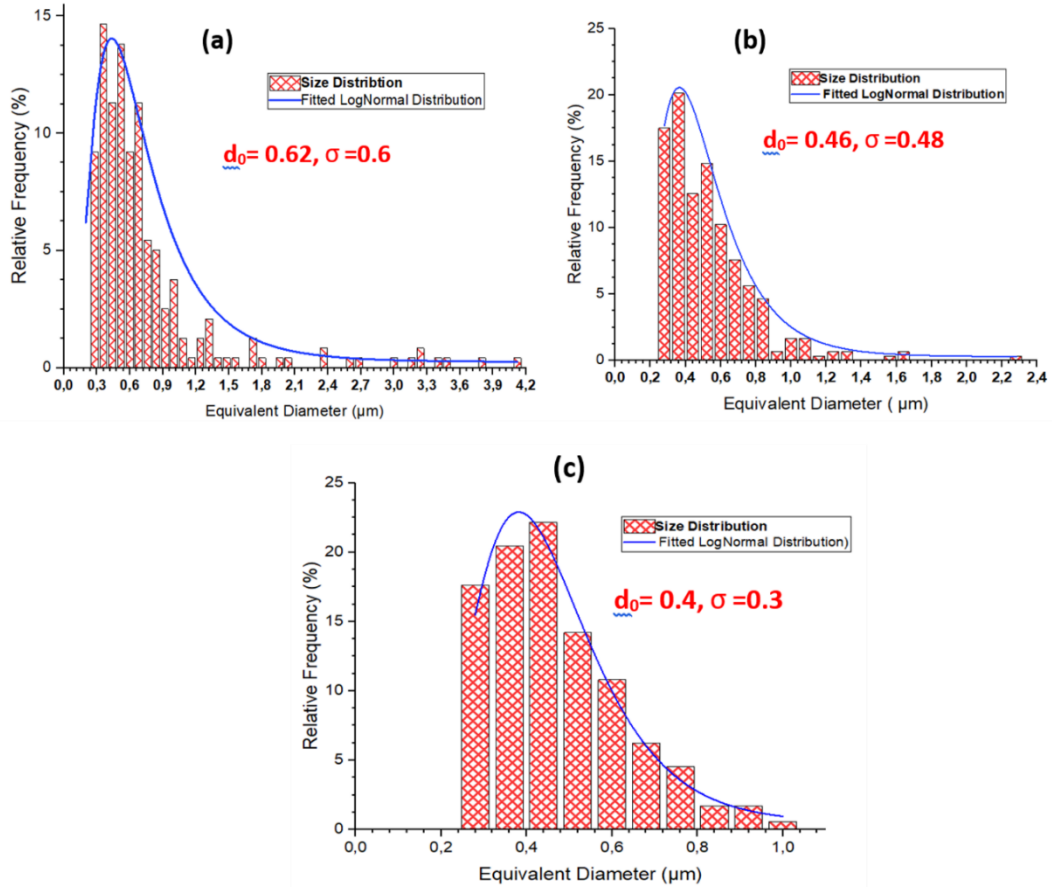
Figure 4-8. The size distribution of the nucleant particles in the three master alloys: TiB_2 in the (a) 3/1(%Ti/%B) and (b)5/1(%Ti/%B) and TiC paticles in the (c) 3/0.15(%Ti/%C).

In addition to the size distribution analysis performed above, TiC was often reported to be unstable at typical addition rates in Al melt due to its transformation to Al_4C_3 or SiC or Ti_2AlC [3, 76, 105]. Such transformation decreases the particle efficiency. Moreover, it is significantly sensitive to the temperature of the melt [3, 76]. Interestingly, our melt temperature was fixed at 720°C, and this temperature was reported to ruin the excellent lattice matching between TiC and Al [105]. When melt temperature are higher than 670-675°C, Al-Ti-C showed less efficiency than Al-Ti-B [61, 105]. Furthermore, the TiB2 is more preferred than TiC from crystallographic

view, since TiB$_2$ involve the much more compatible Al$_3$Ti layer for Al nucleation. However, TiC is known to nucleate directly Al without involving that Al$_3$Ti layer, resulting in lesser crystallographic matching with Al. More details about the crystallographic matching will be provided in the following chapter 5, section (5.3.1), figures (31 and 34).

In summary, it is fair to conclude that several facts were found to may explain the order in refinement potency of the 3 tested master alloys. In fact, higher potency of the 5/1 (%Ti/%B) master alloy may arise from the bigger and blocky aluminide Al$_3$Ti, the higher number density, the relative narrow size distribution and intermediate mean diameter of nucleant particles TiB$_2$. It is worth noting that the present study couldn't cover all the aspects that influence the refinement response of refiners including the different holding times of refiners in the melt, the wetting angle, the crystallographic matching or the different melt temperatures. However, the present interpretations tried at least to build a comparison study based on the properties of the tested refiners and the fixed experimental parameters in our study.

4.6.2- The correlation between grain refinement and hot tearing susceptibility

In general, it is believed that grain refinement reduces the hot tearing susceptibility of alloys. However, a heavy grain refinement was reported to result in a hot tearing increase [78]. In a practical use, there is no agreement on the optimum

refiners quantity. And subsequently the optimum grain structure (morphology and size) that leads to the maximum hot tearing resistance. Our experimental results of the hot tearing evaluation in 6111 alloys have confirmed that the hot tearing susceptibility is influenced by the refiners addition rate and the resulting structure. Before refinement, a higher hot tearing tendency was found in the test alloys with columnar structure. Columnar grains are very prone to hot tearing because of load concentrations at grain boundaries and the easy crack propagation through such coarse dendritic microstructure [20]. In addition, 6111 series alloys are reported to be very sensitive to the hot tearing due to their solidification characteristics including the wide freezing range, when comparing to other alloys [22]. After that, the addition of grain refiners decreased the grain size with an important decrease in the hot tearing susceptibility when the grain morphology changed from being columnar dendritic to being rosette-like (fewer arms are observed).

It is extensively reported that the change from coarse dendrites to fine equiaxed dendrites lead to an effective decrease in hot tearing severity [78]. The significant reduction in hot tearing severity with grain size when grains are dendritic can be explained by several mechanisms: (1) Enhancing the strain accommodation. In fact, an important strain concentration in semisolid alloy was found at grain boundaries [106], and finer grains provide larger number of grain boundaries to accommodate this strain, resulting in a decrease in the strain concentration [107, 108]. (2) Whilst the grain morphology is dendritic, the decrease of the highly branched structure improves the permeability and facilitates the diffusion of the liquid film in the semi-solid zone between grains to fill the voids [109]. (3) Delaying the onset of the transition point

from mass feeding to the interdendritic feeding which improves healing of the tears. (4) Reducing the critical temperature range, which is between the coherency temperature (when feeding starts to be interdendritic) and the coalescence temperature (when the metal starts to act as a solid), resulting in less accumulation of the thermal strain during solidification [110]. However, adding more refiners increases the hot tearing susceptibility when gains become cellular (more globular than dendritic). References [17, 21, 111]share the same results, where an excessive grain refiners addition increased the hot tearing for globular grain morphology. Such increase in hot tearing susceptibility despite the further refinement may only be explained from the permeability point [78]. The permeability was often considered as a critical factor in the hot tears formation. And it is used in itself as an indicator of hot tearing susceptibility [21, 112].

Hot tears are believed to occur during the last solidification stage according to all developed hot tearing models [112]. During this vulnerable stage, the solidifying grains exhibit thermal contractions that generate tensile stress and strain accumulation on the semi -solid zone [113]. The structure of this stage consists mainly of liquid film around solidified grains, known by the mushy zone[21, 112]. If tensile stress is greater than the mushy zone strength, then hot tearing (cracks) occur. However, the hot tearing problem can be prevented if the hot tear is compensated by the surrounding liquid film [113]. Therefore, the permeability or the feedability is the ability of the melt to compensate the solidification shrinkage in the semi-solid zone [112]. Quite simply, permeability is how easily will the metal liquid flow through the intergranular path to heal the hot cracks. The length scale of permeability was reported to be the grain size

(d) when grains have more globular than dendritic grain morphologies [20]. The well-known Carman-Kozeny equation that determines the permeability K of the liquid flow have different expressions, depending on the structure parameters (grains size and morphology). This equation is extensively used by scientists and industry for the permeability estimation in the semi-solid zone. When the grain morphology is more globular (i.e, rosette-like or globular morphology), then permeability is given by the following equation [112, 114].

$$K = \frac{d^2}{180} \frac{(1 - f_s)^3}{f_s^2} \qquad (4\text{-}5)$$

where f_s is the solid fraction and d is the mean grain size of particles.

Mathematically spoken, reducing the globular grain size (d) should reduce the permeability (K) for a given solid fraction based on the Carman-Kozeny equation above. A reduced permeability limits the required liquid flow, resulting in non-healed hot tears. The basis of the Carman Kozen equation was established on the fact that the resistance applied by particles against the flow of liquid in any permeable median is governed by the specific surface area of those particles, where smaller grains will provide larger specific surface area in contact between the flowing liquid and the surrounding grains [115]. This fact would generate greater resistance to the liquid movement, reducing the permeability. The Carman-Kozeny permeability K has different expressions in literature, where K is inversely proportional to the specific

surface area (S). And therefore, proportional to the particle size (d) as shown in the equation above, based on the fact that smaller d exhibits larger S.

In addition, the mushy zone has been considered as a porous medium [116]. And the connection between pores was known to influence the permeability in a porous medium [117, 118]. A grain structure is permeable if liquid flow is able to pass from one pore to another through pores throat (channels between neighboring pores) that are wide enough for allowing more liquid movement [119]. Coarser globular grains are believed to be more permeable for the liquid flow than the finer grains because they present larger pores throats, allowing more liquid flow to pass through voids [117]. This was explained by the fact that larger particles are not able to pack tightly as smaller particles can. Therefore, the structure arrangement of larger grains induces more voids and more interconnections between pores making the structure more permeable [120]. **Figure 4-9** present an example for confirming that permeability is favored by larger grains due to the larger and well-connected voids between those solid grains. A very tight voids throat will block the liquid path, reducing or even hindering the required feeding for hot tears healing. In contrast, additional flow will be allowed to pass due to the larger hole openings in between larger grains.
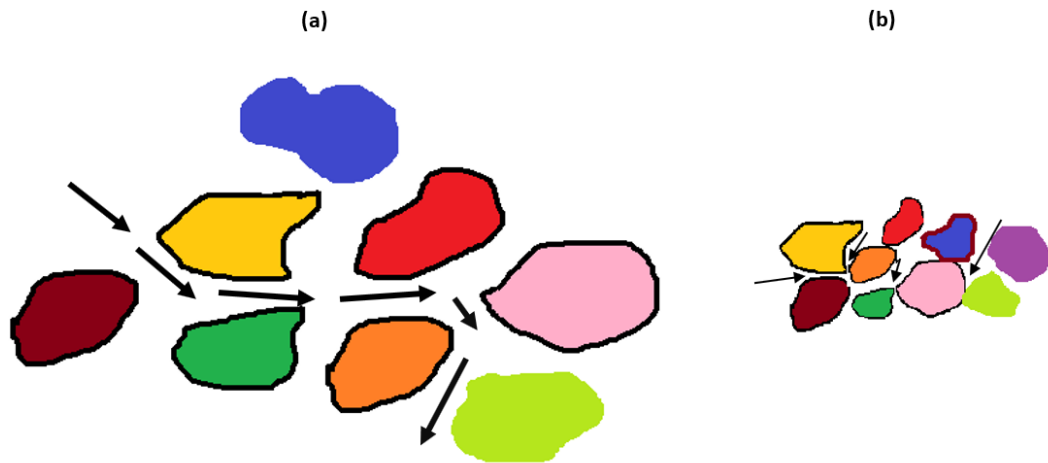
Figure 4-9. Effect of grain size on the permeability of liquid film during metal solidification in (left):larger grain structure and (right) smaller grain structure

It can be concluded from the ongoing work that the hot tearing prevention depends on enhancing the permeability of the mushy zone. This fact is largely controlled by the grain structure (size and morphology) during the last stage of solidification. And it was hypothesized that grain refinement is beneficial for the hot tearing resistance until the grains become cellular. Further refiners will decrease the hot tearing resistance. Hence, optimizing the casting factors that control the grain structure including the solidification conditions (cooling rates, etc…) and the alloy constitution should be considered as a key factor for production improvement.

CHAPTER 5 : Cr POISONING EFFECT ON GRAIN REFINEMENT OF ALUMINUM AA6111 ALLOYS

5.1- The effect of Cr on the grain refinement

The grain refinement efficiency was evaluated with increasing the addition rate of refiners from 1 to 3Kg/T in the presence of 200 ppm Ti. In terms of comparison, 3 grains refiners were used (Al-3%Ti-1%B, Al-5%Ti-1%B and Al-3%Ti-0.15%C). The experimental results that reveal the Cr effect on the grain size in the 6111-aluminum alloy at both cooling rates (0.4°C/s and 4°C/s) are shown in **Figure 5-1** and **Figure 5-2**, respectively. At higher CR (4°C/s), for each tested refiner and in each addition rate, the presence of (0.144%Cr) in the alloy resulted in a coarser grain size. The same tendency of grain coarsening was found in the lower cooling rate (0.4°C/s) due to higher percentage of Cr, which confirm that the refining potency of grain refiners was weakened by the Cr presence. The present findings indicate clearly that none of the 3 tested grain refiners is immune to this adverse effect of Cr on grain refinement. However, for each refiner type, the increase in addition rate from 1 to 3 Kg/T (+200ppmTi) compensates significantly the grain size gap between alloy containing (0.004%Cr) and alloy with (0.144%Cr).

This result is especially clear in the case of TiC grain refiner at both cooling rates, where the higher addition rate of refiners (3Kg/T+200 ppmTi) resulted in very smaller gap of 3.2 and 2 μm at 4°C/s and 0.4°C/s, respectively.
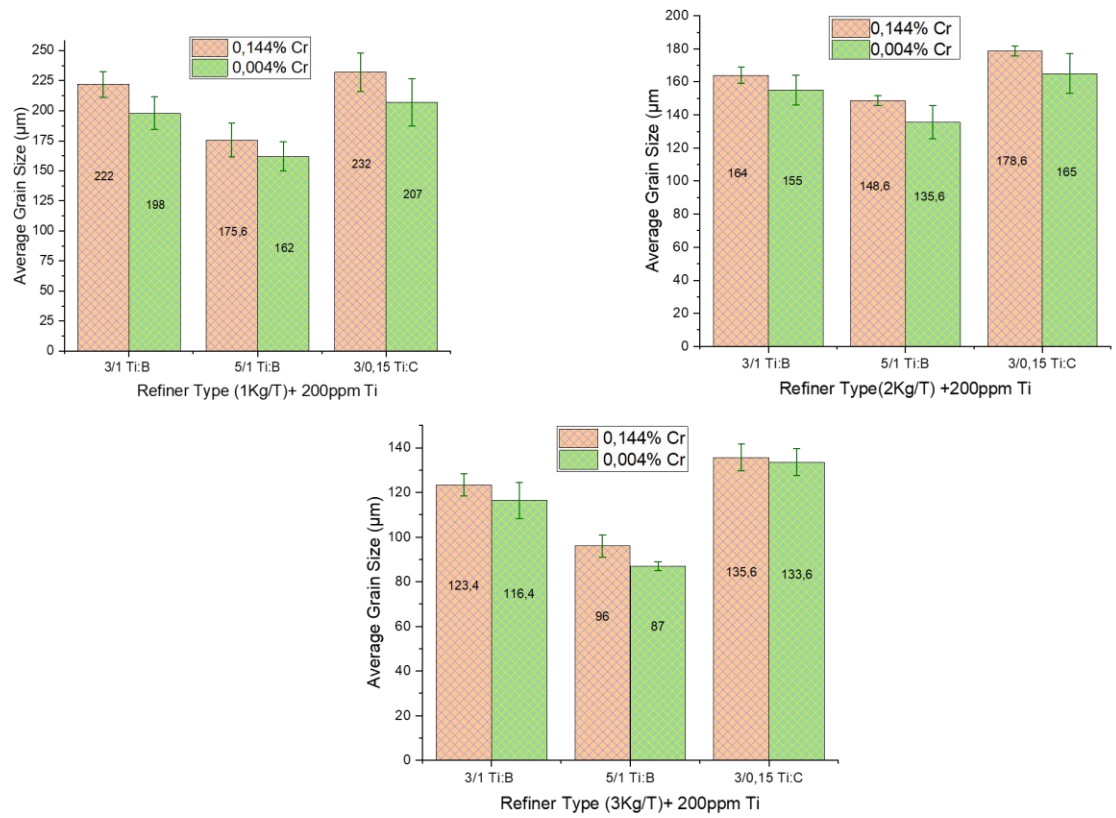
Figure 5-1. The variation in grain size in base alloy 6111(0.004%Cr) Vs alloy 6111 with higher Cr (0.144%Cr), after refinement using 3 different refiners, CR=0.4°C/s.
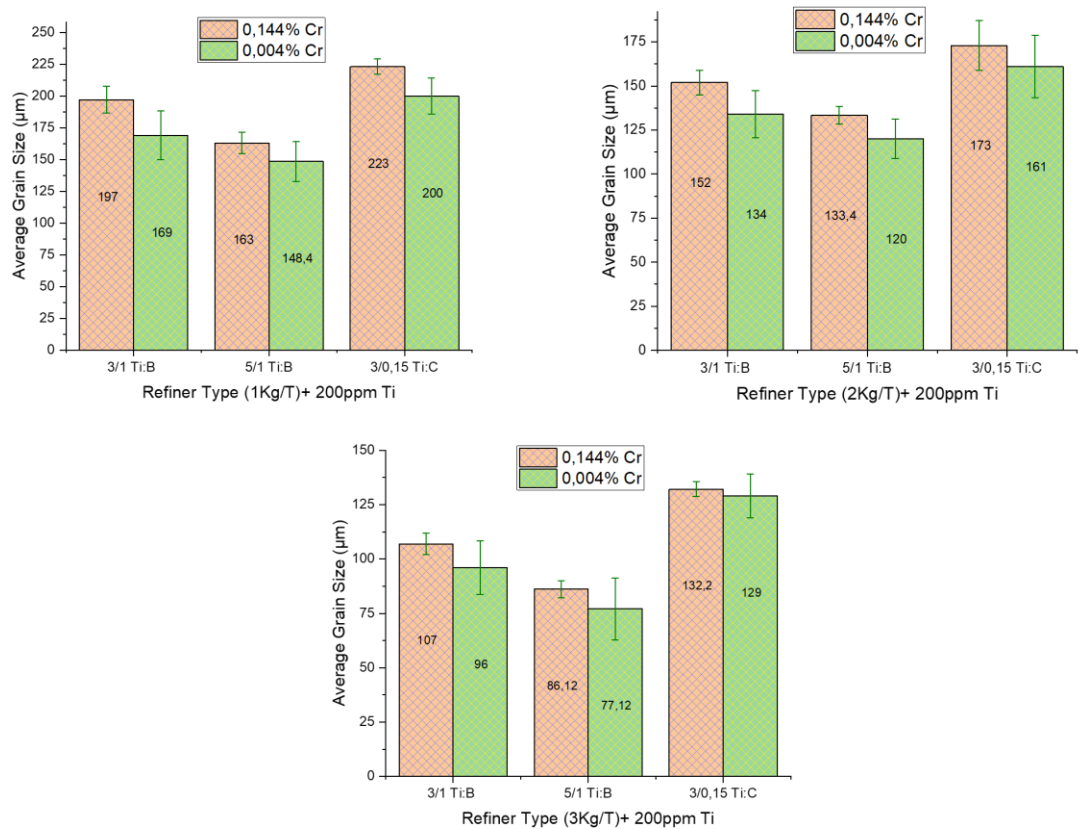
Figure 5-2. The variation in grain size in base alloy 6111(0.004%Cr) Vs alloy 6111 with higher Cr (0.144%Cr), after refinement using 3 different refiners, CR=4°C/s.

The effect of Cr on the refinement efficiency was also studied in the absence of Ti as a solute in the melt. Two Kg/T of each refiner of the 3 test refiners (Al-3%Ti-1%B,Al-5%Ti-1%B and Al-3%Ti-0.15%C) was added to both alloys (with/without)Cr. Results are shown in **Figure 5-3** under the higher cooling rate 4°C/s. **Figure 5-3(a-b-c)** correspond to the resulted micrographs after refinement of the alloy(0.004%Cr). While **Figure 5-3(a-1,b-1,c-1)** are the micrographs resulted after refinement of the alloy containing 0.144%Cr. As can be seen, for each refiner the

presence of 0.144% Cr limited the refinement effect, resulting in a coarser grain size. The difference in size between alloys (with/without) Cr resulted also in a difference in the morphology when using the same refiner in the same addition rate. A 2Kg/T of 3/1 (%Ti/%B) and 5/1 (%Ti/%B) refined significantly the 6111alloy(0.004%Cr), resulting in grains of cellular morphology with smaller grain sizes of 159 and 146.6 μm, respectively **(Figures 5-3-a, 5-3-b)**. While grains in the presence of higher % of Cr are still with equiaxed dendritic morphology and larger sizes of 188.1 and 177.3μm using 3/1 (%Ti/%B) and 5/1 (%Ti/%B), respectively **Figures (5-3(a-1), 5-3(b-1))**. Refining with 2Kg/T of 3/0.15 (%Ti/%C) resulted in dendritic grains for both 6111 alloys (with/without) chromium **Figures (5-3(c) and 5-3(c-1))**. However, alloy without Cr produced smaller equiaxed dendritic grains with size of 189 μm, compared to very larger dendritic grains with size of 221μm in the presence of higher % of Cr. It appears from the ongoing results that higher % of Cr increased the grain size, and hence delayed the morphological transformation.
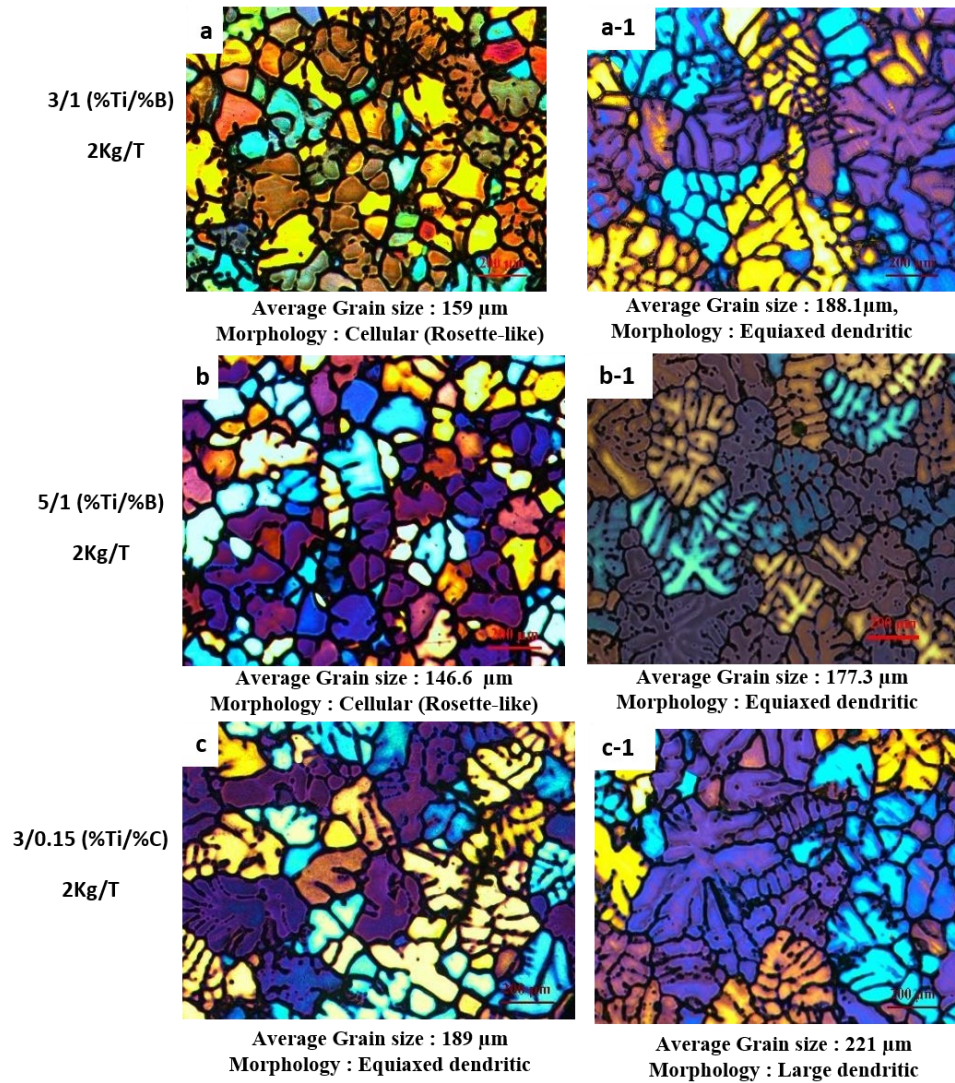
Figure 5-3. a,b,c: Micrographs after refinement in base alloy 6111(0,004%Cr), a-1,b-1,c-1: Micrographs after refinement in alloy 6111(0.144%Cr), CR=4°C/s, scale bar in all figures is 200 µm.

5.2-   Results of interaction between Cr and grain refiners

Given the weakening effect made by Cr presence on the refinement, further investigation was required. For that, the refiners Al-Ti-B and Al-Ti-C have been mixed, each one, with the master alloy Al-Cr. The Al-20%Cr master alloy was used to make

each experimental specimen contains 0.2% of Cr. Then, a scanning electron microscope operated at 20kV combined with Energy Dispersive Spectroscopy (EDS) was used to reveal whether there is some interaction of Cr element with the intermetallic phases present in both Al-Ti-C and Al-Ti-B master alloys.

The obtained results are shown in **Figure 5-4** , and were as the following: **(1)** The chromium could diffuse into each kind of intermetallic particles of the grain refiners (Al_3Ti, TiB_2 and TiC). However, not all the particles were subjected to this Cr diffusion in such conditions. **(2)** In the case of Cr presence, the chromium was present preferentially in the Al_3Ti particles, where the aluminides Al3Ti particles contain always higher percentage of Cr compared to Cr% in TiB_2 and TiC particles. **(3)** In the case of Cr presence in the nucleant particles, Cr was always detected in the particle surface layer. EDS analysis in **Figure 5-4 (a)** show that the Al_3Ti particles contain 1.48 wt% of Cr in the particle surface layer, while the interior was Cr free (0 wt%). Same thing for TiB_2 and TiC particles as shown in **Figure 5-4 (b)** and **(c)**, respectively, where the particles surface show certain Cr % and the particle center was free from Cr. This fact confirm that the Cr segregation was happened on the external surface of particles in such conditions. Moreover, for the Al_3Ti particles, the increase in holding time resulted in an increase in Cr concentration in the surface layer of particles. This effect may confirm the selective diffusion of Cr on such intermetallic compounds Al_3Ti compared to others. As indicated in **Table 5-1**, the Cr% increased from 0.41 to 1.48wt% in the surface layer of Al_3Ti , when increasing the contact time from 2min to 2 hours.
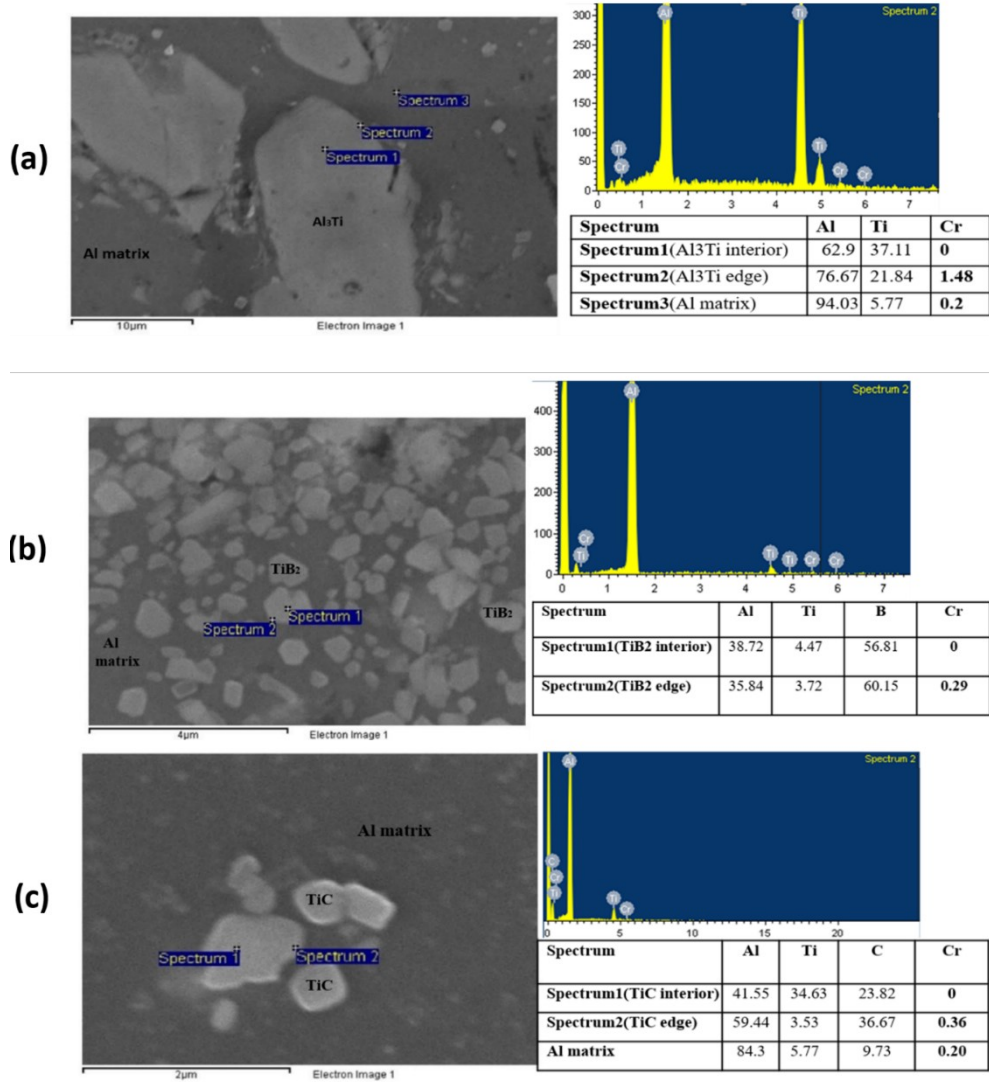
Figure 5-4. SEM-EDS results revealing the % of Cr in the nucleant particles ((a)Al3Ti(b)TiB2 and (c) TiC), All results in weight%

Table 5-1. The effect of contact time on Cr% in Al$_3$Ti particles

Holding Time	2 min	30 min	2 Heures
Cr % in the Al$_3$Ti edge	0.41(wt%)	0.75(wt%)	1.48 (wt%)
Cr % in the TiB$_2$ edge	0(wt%)	0.14(wt%)	0.29(wt%)
Cr % in the TiC edge	0(wt%)	0.18(wt%)	0.36(wt%)

5.3- Discussion

5.3.1- Crystallographic misfit analysis before Cr diffusion

The grain refiners Al-Ti-B and Al-Ti-C have been mixed with the master alloy Al-Cr. Therefore, no other solutes,except the Cr, can involve in the interactions with the refiners constituents. When they are in contact with poisoning elements like (Cr and Zr), nucleant particles (Al$_3$Ti and TiB$_2$) were reported to form ternary particles Al$_3$(Ti$_{l-x}$,Me$_x$) and (Ti$_{l-x}$, Me$_x$)B$_2$ where Me = Cr or Zr, where this transformation was proposed to be an atomic substitution of Ti by poisoning elements. This concept was proposed by Abdel-Hamid [16], and has been supported based on experimental evidence by Johnsson et al., and also by Arjuno et al., [121-124].

Our SEM-EDS results have confirmed the presence of Cr element in the superficial layer of nucleant particles. This motivated us, in addition to literature, to suggest that the hybrid compounds that may form in the present work by the Cr diffusion are: (Ti$_{l-x}$ Cr$_x$)Al$_3$ and (Ti $_{l-x}$Cr$_x$)B$_2$ and (Ti$_{l-x}$ Cr$_x$) C. The concept in the present section is to apply the E2EM criteria in order to findout whether this diffusion leads really to poisoning impact from a crystallographic matching view. For that, the matchingdegree of different particles with Al will be examined before and after Cr diffusion.

Hence, the possible orientation relationships ORs between Al and (Al$_3$Ti,TiB$_2$ and TiC) will be found, and also the ones between Al and the completely modified particles Al$_3$Cr, CrB$_2$ and CrC. While the matching degree of the ternary compounds(Ti$_{l-}$

$_x$,Cr$_x$)Al$_3$, (Ti$_{l-x}$Cr$_x$)B$_2$ and (Ti$_{1-x}$ Cr$_x$)C with the Al matrix will be predicted in the present work as a value in between.

5.3.1.1- Misfit of Al/Al₃Ti

The prediction of the possible orientation relationships ORs between 2 phases using the edge-to-edge model requires some specific crystallographic Data including the crystal structure, the lattice parameters and the atoms positions in each phase. Al alloys have FCC structures with a change in the lattice parameters based on the variation in chemical composition. However, the solutes effect can be neglected because of the very low percentage of solutes in the alloy [76]. Therefore, the crystallographic data used in the present investigation for Al matrix is the same as the one of pure aluminum metal, where the crystal structure is cubic with a=4,049Å, and space group of Fm3m [76]. Al₃Ti has tetragonal structure with a =3,854 Å, b=3,854 Å, c=8,584 Å, and space group of I4/mmm [14]. For both phases(Al and Al₃Ti), the atomic positions were provided from the Database of the PTCLAB software [83] and confirmed by literature [14, 76]. Based on those atomic configurations, close packed planes and the corresponding close packed directions were identified in each phase by the program. After that, the possible matching direction pairs and the interatomic spacing misfit along these directions between Al matrix and Al₃Ti particles were calculated. The interplanar spacing mismatch was also calculated between the possible matching planes in Al matrix and Al₃Ti particles.

In the prediction of a possible orientation relationship, 10% was selected in the present work as the critical value for both interatomic and interplanar spacing misfits f_r and f_d. Based on extensive statistic studies, Zhang and Kelly [14, 81] defined an empirical criterion to ensure a reproducible crystallographic orientation relationship (OR) between two phases, where 10% was proposed to be the up-limit of both interatomic and interplanar spacing misfits (f_r and f_d). Moreover, investigations indicated that all the potent grain refiners in Al and Mg cast alloys have at least one pair of matching rows and matching planes that meet the criteria fr< 10% and fd< 10% respectively [14]. Furthermore, ref [76] cited that the value of 10% was proposed based on the variation calculation of Van der Merwe's energy combined with empiric studies performed on over 20 ORs observed experimentally in various systems [76]. Therefore, combination of interatomic and interplanar misfit with respecting the criterion f_r and f_d has been found and figured out for the system Al₃Ti/Al as shown in **Figure 5-5**.
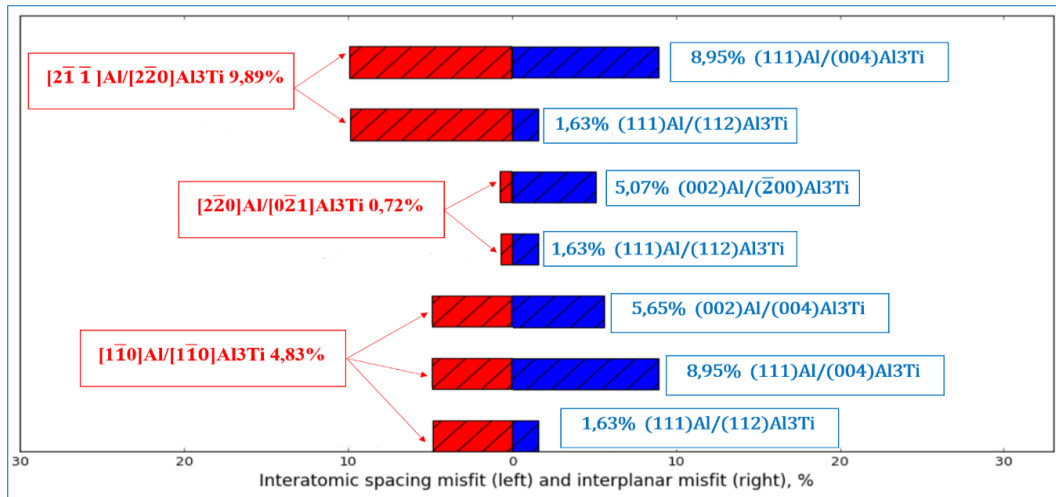

Figure 5-5. Combination of interatomic and interplanar misfits in the Al/Al₃Ti system, with criterion fr and fd <10%.

For a given system(matrix/particle), an orientation relationship is defined by the matching directions and their corresponding matching planes [125]. Therefore, 7 total possible orientation relationships (ORs) can be predicted in the Al/Al$_3$Ti system based on the program results and as shown in **Figure 5-5.** As can be seen from the same **Figure 5-5**, Al/Al$_3$Ti system contains 1 pair of very excellent matching rows ([220]Al/[021]Al$_3$Ti) with very smaller f_r=0.72%, while one of the corresponding matching planes were found to have also very good f_d smaller than 2 with value of (1.63%). This excellent matching was further confirmed by refs [76] and also [14, 126], having the same f_r and f_d values as in the present work. In addition to the critical value of 10%, further restriction on f_d value was fixed, where 6% of f_d was announced as the critical value that indicate an already parallelism of the matching planes or just a small rotation of the matching planes from each other is required to ensure the parallelism [76]. However, when the f_d is greater than 6 %, the matching planes should deviate by a refinement angle to ensure the atom row matching along the interface [76]. Interestingly in the present Al/Al$_3$Ti system, we can see from **Figure 5-5** that 3 pairs of matching planes were found to have f_d values smaller than 6%, reflecting the very good matching, and therefore the important stable state of the Al/Al$_3$Ti from an energetic point of view.In fact, 1.63%, 5.07% and 5.65 % were found as the f_d values that are smaller than 6% in the present study, whencomparing to 1.6%, 5% and 6.1% found by ref [76] as interplanar spacing mismatch f_d. A few differences can befound in calculation results from one crystallography program to another, arising from the different expressions of the same orientation relationship in Miller indices, and also

from some differences in lattice parameters of thesame phase coming from the different available crystallographic databases.

Furthermore, the present software was able to predict some of the rotation angle values that should be rotated by the matching planes, resulting in a refined orientation relationship with a total parallelism between the matching planes.

The calculation was done here on just 1OR and the refined OR resulted by the program is as the following:

[111]Al   0.221deg from [112]Al_3Ti ; (1-10)Al // (1-10)Al_3Ti
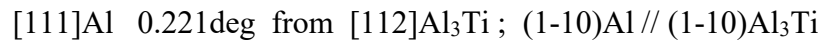
The very smaller deg of rotation required for refining this OR is a further confirmation of the strong crystallography relationship in the Al/Al_3Ti system. Same rotation value was found by ref [76] when studying the refinement angle between those 2 matching planes.

An example of a simulation of the superimposed diffraction patterns along the matching directions is shown in **Figure 5-6**.
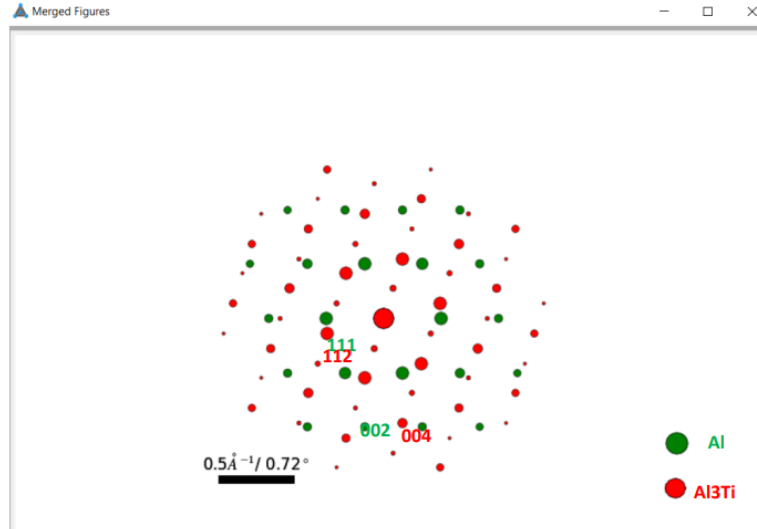
Figure 5-6. Simulated, superimposed diffraction patterns along the zone axes (matching directions) (1 -1 0)Al // (1 -1 0)Al$_3$Ti , showing two predicted OR along this zone axe.

5.3.1.2-   Misfit of Al/TiB$_2$

TiB$_2$ has an hexagonal structure with a =3,035 Å, c=3,223 Å, and belongs to the space group of P6/mmm. The atomic positions for this phase weren't available in the PTCLab software Database, and was provided instead from the Crystallographic Information Files (CIF) in another software, named (The Material Project). Based on the atomic configurations, close packed planes and close packed directions were identified in each phase of the Al/TiB$_2$ system by the PTCLab program. After that and in the same way as for the previous system, combination of interatomic and interplanar misfit with respecting the criterion f_r and f_d has been therefore figured out as shown in **Figure 5-7**.
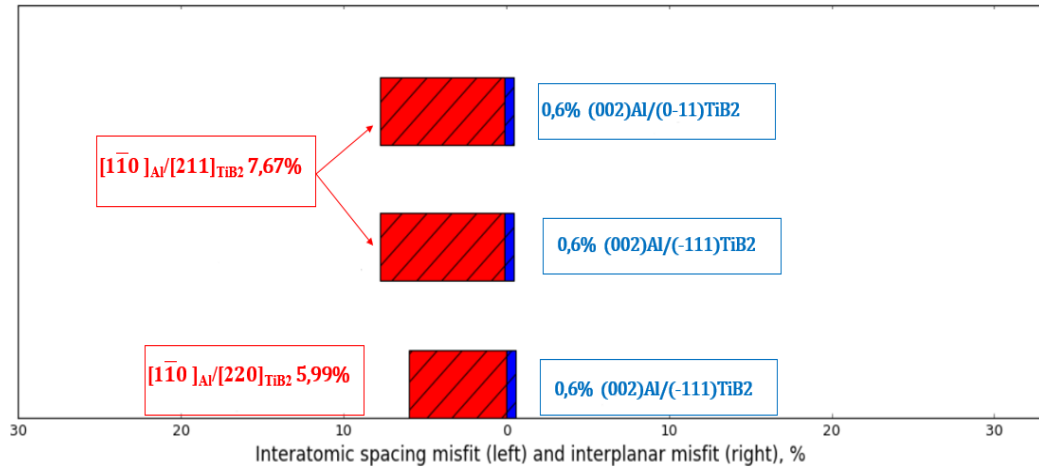
Figure 5-7. Combination of interatomic and interplanar misfits in the Al/TiB$_2$ system, with criterion fr and fd <10%.

As can be seen in **Figure 5-7**, the extent of matching along the close-packed direction pairs in the Al/TiB$_2$ system is not as good as the case in the Al/Al$_3$Ti system. However, we still can find 3 possible ORs in the light of the present criteria of E2EM, where the 5,99% was found as the smallest f_r value as interatomic spacing along the matching rows with a corresponding f_d equal to 0,6%. This possible OR in Al/TiB$_2$ system was confirmed in ref [76], where the most qualified matching directions were found to have 6,1% as f_r and f_d of 0,9% as interplanarmisfit. Moreover, 5.5% was indicated as f_r by another ref [14] for the most qualified matching directions.

5.3.1.3- Misfit of Al/TiC

TiC has a cubic structure with a =4.335 Å, and belongs to the space group of Fm3m. The Crystallographic Data was provided from the Information Files (CIF) in The Material Project software. Following the same steps as before, the calculation

concerning the interatomic spacing and interplanar misfit in the Al/TiC system are shown in the **Figure 5-8.**
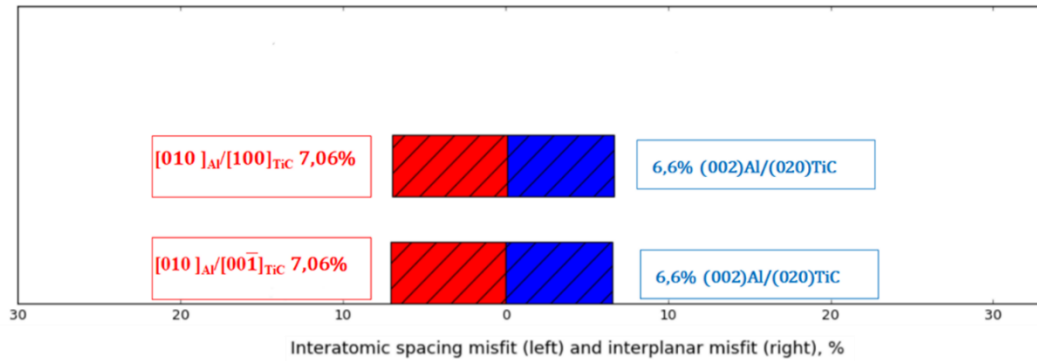

Figure 5-8. Combination of interatomic and interplanar misfits in the Al/TiC system, with criterion fr and fd <10%.

Based on the software results, two ORs are possible in the Al/TiC with f_r and f_d values of 7.06% and 6.6%, respectively, for both possible ORS. For the same system Al/TiC, whena(TiC)=4.32 Å, two preferred matching ORS were also found by ref [76], where 6.9% was as f_r and 6.4% as f_d.

5.3.2- Comparison of the crystallographic misfit before and after Cr diffusion

5.3.2.1- Misfit comparison (Al/Al₃Ti) Vs (Al/Al₃Cr)

Al₃Cr has a tetragonal structure with a=3.78Å, b=3.78Å and c=8.09Å. It belongs to the space group of I4/mmm. The crystallographic Data was also provided from the Crystallographic Information Files (CIF) in The Material Project software. Evaluation of the crystallographic matching based on the edge to edge model criteria has shown that both Al₃Ti and Al₃Cr have a number of ORs with Al. And therefore,

can act as grain refiners, but with a variation in the nucleation potency that raise from the different extents of crystallographic matching between each compound with Al matrix. As can be seen from **Figure 5-9** (a Vs b), Al_3Ti particles are clearly more potent when comparing to Al_3Cr from crystallographic point of view for several reasons: (1) The total possible matching ORs are 7 in the first one, while they are just 5 in the latter system. (2) The both interatomic spacing misfit along the matching directions f_r and the corresponding interplanar spacing misfit f_d in Al/Al_3Ti are very smaller than values in Al/Al_3Cr. The most preferred f_r and f_d in Al/Al_3Ti were predicted to be 0,72% and 1,63%, respectively, against 3,3% as f_r value and 4,81% as f_d value found for the most preferred OR in the Al_3Cr system. It appears therefore that the crystallographic matching with Al matrix of the completely transformed particles Al_3Cr decreased. In the present work, Cr is believed to substitute Ti atoms to form the ternary particles $Al_3(Ti_{1-x}Cr_x)$ [16, 121-124]. The crystallographic matching of $Al/Al_3(Ti_{1-x}Cr_x)$ would be lower than Al/Al_3Ti based on the crystallographic matching comparison of (Al/Al_3Ti vs Al/Al_3Cr). Hence, the nucleation potency of the hybrid compound $Al_3(Ti_{1-x}Cr_x)$ would be weakened with f_r and f_d values between Al/Al_3Ti and Al/Al_3Cr systems.
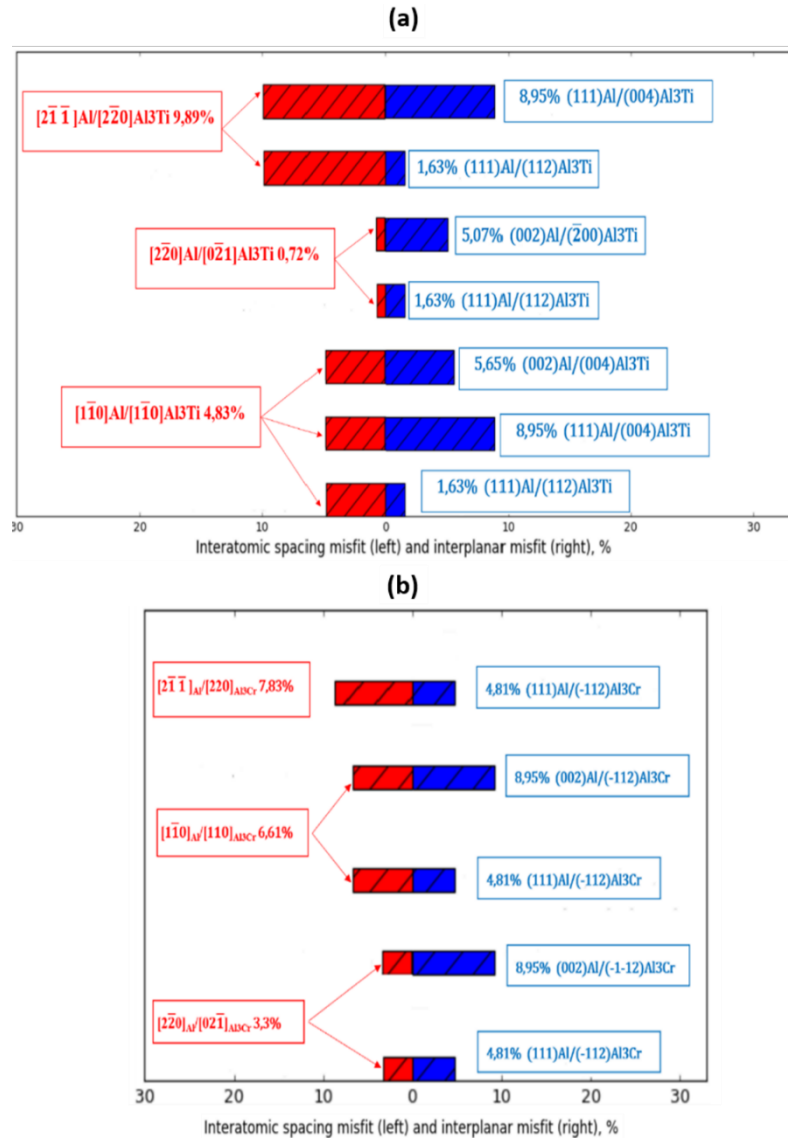
Figure 5-9. Interatomic and interplanar misfits in systems: (a) Al/Al$_3$Ti, (b) Al/Al$_3$Cr.

5.3.2.2-   Misfit comparison (Al/TiB$_2$) Vs (Al/CrB$_2$)

CrB$_2$ has an hexagonal structure with a =2.96 Å, b= 2.96 Å and c= 3.03 Å. It belongs to the space group of P6/mmm. The Crystallographic Data was provided from the Information Files (CIF) in The Material Project software. For TiB$_2$ and CrB$_2$, it was

predicted that both of them have 3 possible ORs **(Figure 5-10 (a Vs b))**. However, the TiB$_2$ compound showed a smaller f_d mismatch value between the closest packed planes (0,6% Vs 3,5%), but with a larger misfit along the closest matching directions f_r (5,99% Vs 3,3%). Such finding unlikely to result in serious poisoning, since the completely transformed (CrB$_2$) didn't show a decrease in the crystallographic misfit.
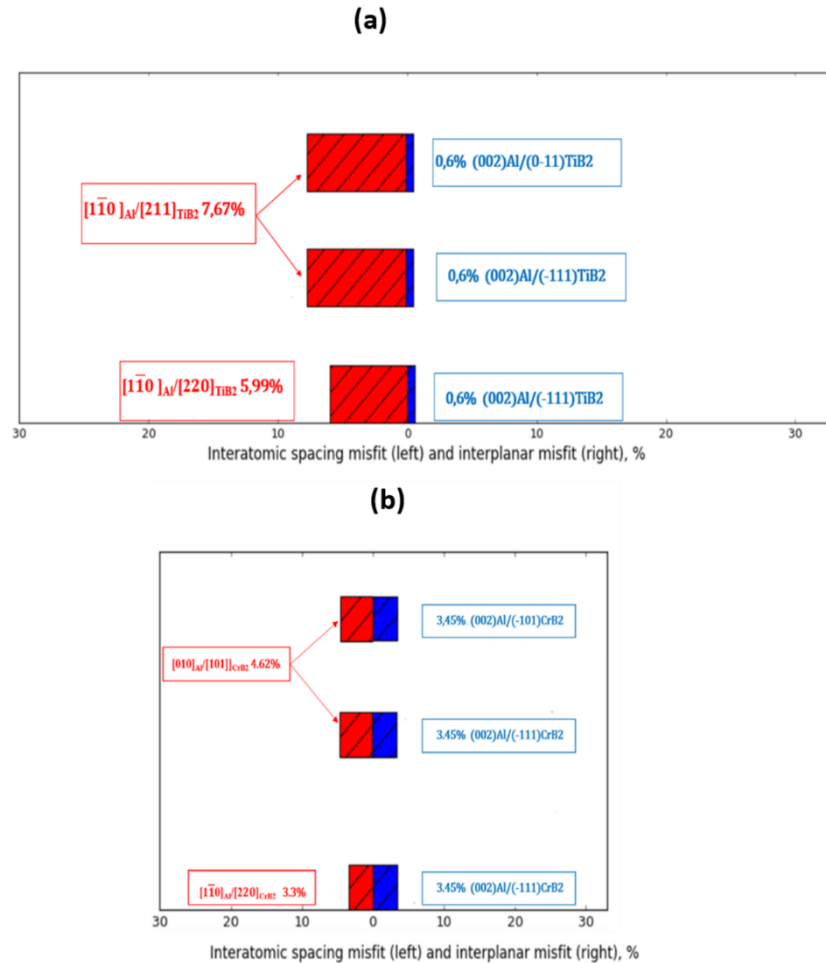
Figure 5-10. Interatomic and interplanar misfits in systems: (a) Al/TiB$_2$, (b) Al/CrB$_2$.

5.3.2.3- Misfit comparison (Al/TiC) Vs (Al/CrC)

CrC has an hexagonal structure with a =2.71Å, b= 2.71Å and c= 2.62 Å. It belongs to the space group of $\overline{P}$6m2. The Crystallographic Data was provided from the Information Files (CIF) in The Material Project software. When comparing TiC and CrC we can see from **Figure 5-11 (a Vs b)** that the crystallographic matching decreased from being 2 possible ORs in the system (Al/TiC) to become no possible OR for the system (Al/CrC) in the light of the edge to edge model (since the up-limit misfit criteria in the E2EM=10%). However, increasing the up-limit values of f_d and f_r could result in possible ORs in the Al/CrC system, where a f_d value of 13,63% was found in this system. Such finding could reveal that the completely transformed particles CrC are not as good as the TiC particles in terms of crystallography, indicating the decrease, to some extent, of the crystallography matching of the hybrid compound $(Ti_{1-x} Cr_x)C$. Hence, the nucleation potency will be also weakened.
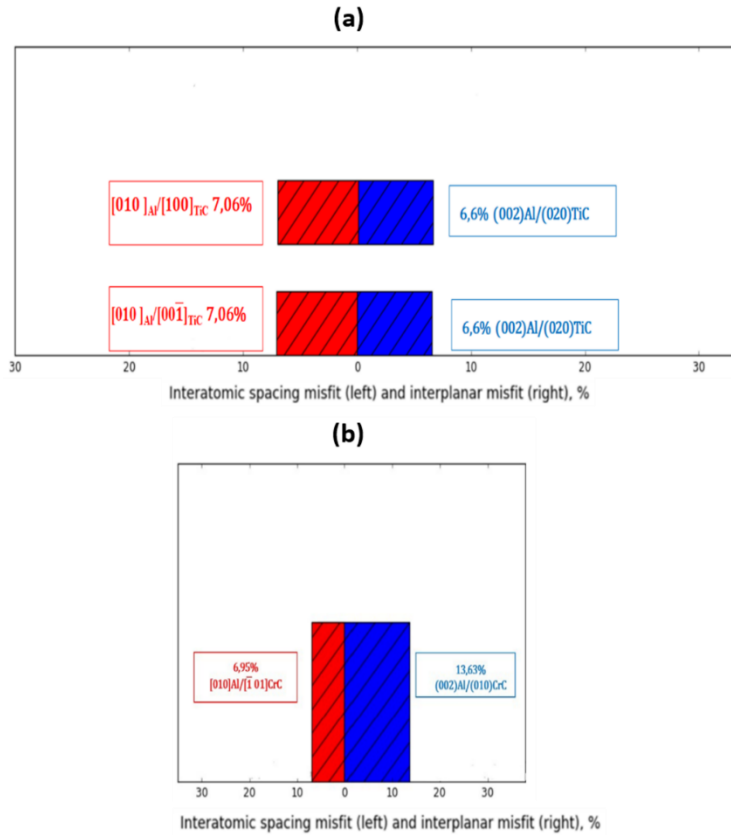
Figure 5-11. Interatomic and interplanar misfits in systems: (a) Al/TiC, (b) Al/CrC

To sum up, predictions have confirmed that each particle (Al_3Ti, TiB_2, TiC, Al_3Cr, CrB_2, and CrC) can have possible number of ORs with Al matrix, but with different extent in crystallographic matching. And such difference would result in different extent in nucleation potency.

5.3.3- Possible mechanism of Cr poisoning

Coupling the crystallography calculations above with findings in literature, this section is dedicated to provide the possible mechanisms that explain the poisoning effect made by Cr when adding grain refiners (Al-Ti-B and Al-Ti-C). When using the Al-Ti-B grain refiner, poisoning mechanism can be explained by considering the duplex nucleation theory [10, 11]. It is the most recent theory that describes the grain refinement mechanism [10, 11]. According to this theory, the TiB_2 particles are not the direct nucleant for Al grains. An Al_3Ti layer is required to form on these TiB_2 particles to nucleate α-Al. Such layer is formed by Ti segregation that takes place in the melt\TiB_2 interface [62]. The duplex nucleation theory was proposed based on the fact that Al_3Ti are often found as the most efficient nucleant sites thanks to the multiple and better orientation relationships with aluminum [3, 10, 11]. However, they are not stable in the melt and they are prone to dissolve. Therefore, TiB_2 particles were proposed to stabilize on their surfaces the Al_3Ti layer to form the delicate epitaxial relationship (TiB_2/Al_3Ti/ α-Al), where Al_3Ti are in direct contact with Al [3]. Our present calculations have also confirmed that (Al_3Ti) are the most capable of Al nucleation, presenting the highest number of ORs(7) with Al. Software predictions showed that Al/Al_3Ti system has the excellent interatomic and interplanar misfits, exhibiting the smallest f_r and f_d (0.72% and 1.63%, respectively). While Al/Al_3Cr system showed a decrease in the possible ORs from (7) to (5), exhibiting larger interatomic and interplanar misfits (3.3% and 4.8%, respectively). Cr was found in SEM results to interact with particles present in master alloy. And therefore, may modify the terminal surface of the newly formed Al_3Ti layer, resulting in an hybrid $Al_3(Ti_{1-x}Cr_x)$ layer with

lesser qualified orientation relationship with Al (towards that of Al$_3$Cr) [16]. This explanation could be supported by TEM observations [3], where it was found that some poisoning solutes may contribute to the destruction of the newly formed layer Al$_3$Ti, where the Al$_3$Ti layer was found to suffer from a progressive substitution from poisoning solutes [3]. Ti substitution by poisoning elements in Al$_3$Ti particles was suggested by Abdelhamid [16] and have proven thereafter experimentally by Johnsson, Arjuna and others [74, 121-123].

In addition, such Al$_3$Ti layer was reported to be stabilized by chemical attraction (adsorption) at the TiB$_2$ surface, since the phase diagram Al-Ti could not explain such layer formation [127]. In our SEM observations, Cr was found also to diffuse into the surface layer of TiB$_2$ particles. The modification of the terminal surface of TiB$_2$ by Cr diffusion would most probably modify the chemical properties of TiB$_2$ surface, influencing the adsorption of Al$_3$Ti required for Al nucleation. Moreover, the lattice parameter of the modified TiB$_2$ (after Cr diffusion) is different compared to the TiB$_2$ one, since the Ti and Cr atomic radius are different, which would reduce the stability of Al$_3$Ti layer on the modified surface of TiB$_2$due to the lattice modification. All these mentioned facts present reasonable causes that would impose limitation and impact on the relationship required for nucleation event(TiB$_2$/Al$_3$Ti/Al).

Moreover, the blocky and bigger Al$_3$Ti particles found in the 5/1 %Ti/%B master alloy were suggested in literature to hold more time in the melt and may act as nucleant particle as discussed before. Our SEM investigations revealed that Cr interacts, preferentially, with Al$_3$Ti particles, where it was found with higher

percentage into the surface layer of these particles (1.48% Vs 0.46%, in the edge of Al$_3$Ti Vs TiB$_2$, respectively). This fact would decrease the crystallographic matching in the system Al/Al$_3$Ti by transforming Al$_3$Ti particles behavior towards Al$_3$(Ti$_{1-x}$Cr$_x$), leading to decrease crystallographic matching as shown above.

Al-Ti-C grain refiner is also found, in the present work, not to be immune to the poisoning effect of Cr. TiC particles in literature, unlike the TiB$_2$, are believed to nucleate directly the Al melt without involving the Al$_3$Ti layer. Where the Ti provided by the Al$_3$Ti dissolution contributes to the growth restriction of the growing grains [2, 3, 10]. Based on our crystallography calculations, Al/TiC system was found to have 2 ORs with f_d =6.6% and f_r=7.06%. In contrast, Al/CrC resulted in no ORs in the light of the E2EM criteria. According to the E2EM an OR can be defined in a system, only when both of up-limits f_d and f_r are less than 10%. Increasing the up-limit of the software predictions to values that exceed the E2EM criteria, The Al/CrC system was found to have only one OR with (f_d=13.63% corresponding to f_r=6.95%). The diffusion of Cr into the TiC particles transform the system Al/TiC toward Al/(Ti$_{1-x}$Cr$_x$)C, wich would reduce the crystallographic matching based on predictions. The decrease in crystallographic matching of CrC with Al reveal that (Ti$_{1-x}$ Cr$_x$)C is also less potent with lesser extent compared to CrC. This decrease in matching can be explained by the lattice parameters modifications, resulting from difference in atomic radius.

SEM investigations have revealed that increasing the contact time between refiners and Cr element increased the % content of Cr in the nucleant particles, which

would increase the deviation of the lattice parameters of particles from being more efficient nucleants (Al_3Ti, TiB_2 and TiC) towards the poor or less efficient particles ($Al_3(Ti_{1-x}Cr_x)$, $(Cr_xTi_{1-x})B_2$ and $(Ti_{1-x}Cr_x)C$) [16]. Therefore, the holding time is a critical factor that control the poisoning extent when refining alloys that contain poisoning elements. Moreover, the increase in refiners addition rate from 1 Kg/T to 3Kg/T in our grain size measurement decreased significantly the poisoning effect in each refiner type. This fact supports well the fact that the addition of more refiners will provide more unaffected particles, resulting in refinement enhancement [16].

Based on all the facts above, increasing the refiners quantity with minimum contact time would represent one solution for overcoming the poisoning effect. However, an optimization is always required to reduce the high costs of refiners from industrial view.

CHAPTER 6 : CONCLUSIONS

1. The Al-5Ti-1B grain refiner is the most efficient grain refiner for aluminum AA6111 alloys in all conditions studied compared to Al-3Ti-1B and Al-3Ti-0,15C in terms of grain size reduction. This difference in grain refinement efficiency may arise from the difference in morphology, size, size distribution and number density of the nucleant particles in the master alloys.

2. In combination with a grain refiner, the addition of titanium further reduces grain size due to its growth restriction effect in all three grain refiners.

3. Grain refinement affects the hot tearing susceptibility of AA6111 alloys by the changes of a number of important factors (grain size and morphology). The grain refinement significantly decreased the hot tearing susceptibility relative to the base alloy free of grain refiner. However, an excessive grain refinement reduced the resistance of the hot tearing when grain morphology become globular.

4. The presence of high Cr level (0.144wt%) in aluminum AA6111 alloy showed an adverse effect on the grain refinement, when using both Al-Ti-B ad Al-Ti-C master alloys. The poisoning extent was found to decrease by the increase in the refiner addition rate, with keeping the same contact time of 2 min.

5. Tendency of Cr diffusion into the surface layer of refiners intermetallics (Al_3Ti, TiB_2 and TiC) was confirmed through SEM-EDS investigation, where the Al_3Ti particles were the most likely to be affected by such diffusion. A longer contact time increased the diffusion, resulting in higher concentration of Cr in the particles surfaces.

6. Software calculations in the light of E2EM criteria revealed that the transformed ternary compounds: $Al_3(Ti_{1-x}Cr_x)$ and $(Ti_{1-x}Cr_x)C$ are less potent in the nucleation event of Al based on the comparison of crystallographic matching with Al matrix of the initial particles (Al_3Ti, TiB_2 and TiC) and the particles totally substituted by Cr (Al_3Cr, CrB_2 and CrC).

7. The poisoning mechanism in Al-Ti-B was explained by the fact that the possible diffusion of Cr in the Al_3Ti may modify the newly formed layer Al_3Ti, which supposed to form on TiB_2 particles. Also, the Cr diffusion into TiB_2 may influence the chemical potency, known by adsorption and required to fix Al_3Ti layer on TiB_2. And hence, the preferred epitaxial orientation relationship between the TiB_2, the titanium aluminide layer Al_3Ti and aluminium will be impared.

CHAPTER 7: RECOMMENDATIONS

According to the different parts of the present work, the following recommendations can be made:

1- The hot tearing susceptibility evaluation has shown that the 6111 alloy follows a decreasing trend with grain refinement. However, obvious increase in hot tearing tendency was also obtained when grain size dropped to a certain level, which confirms the complicated and the multi-factor nature of hot tearing susceptibility. In fact, in addition to the grain size and morphology dependency, it is also associated with the liquid-solid transformation and the thermal contraction behavior during solidification. Therefore, it is highly recommended to use in the future the more developed experimental setup that can evaluate simultaneously the temperature evolution, the contraction amount during the freezing range and the load development due to the solidification shrinkage and thermal contraction. The setup will mainly contain the (CRC) mold equipped with a load cell and displacement sensor. Temperature and load measurements for different refinement conditions (different types and addition rates of refiners) can lead to many pieces of important information including the load onset, the crack initiation and propagation, and furthermore the remaining liquid fractions at these points. Moreover, measuring the total contraction

during solidification will present also a helpful index to correlate the thermal contraction amount to the refinement condition.

Coupling all these results with the microstructure (morphology and size) variation under different refinement conditions can describe more the solidifying environment. And, hence provide more experimental explanation concerning the effect of refinement condition on the hot tearing tendency phenomenon.

2- To understand the poisoning nature of Cr on the grain refining efficiency, it was difficult to identify the exact poisoning compound using scanning electron microscopy. However, a crystallographic investigation was performed on the most probable and possible compounds that can form with proposing different poisoning mechanisms. In this context, an advanced electron microscopy known by scanning transmission electron microscopy (STEM) is recommended to perform a direct atomic scale examination of this new segregation layer that forms in the interface between grain refiner and Al matrix. This can be very helpful to select the most possible mechanism that can explain the adverse effect of Cr presence on the refinement efficiency.

REFERENCES

[1]   K. Kashyap and T. Chandrashekar, "Effects and mechanisms of grain refinement in aluminium alloys," *Bulletin of Materials Science,* vol. 24, no. 4, pp. 345-353, 2001.

[2]   P. Moldovan and G. Popescu, "The grain refinement of 6063 aluminum using Al-5Ti-1B and Al-3Ti-0.15 C grain refiners," *JOM,* vol. 56, no. 11, pp. 59-61, 2004.

[3]   B. Cantor and K. O'Reilly, *Solidification and casting* (Series in Materials Science and Engineering). CRC Press, 2003.

[4]   P. Hoefs, W. Reif, A. Green, P. Van Wiggen, W. Schneider and D. Brandher, "Development of an improved AlTiC master alloy for the grain refinement of aluminium," *LIGHT METALS-WARRENDALE-,* pp. 777-784, 1997.

[5]   M. Yun, S. Lockyer, J. Hunt, R. Cook and D. Bristow, "A Study of TiCAl 315TM Grain Refinement in a Roll Cast AA8111 Aluminum Alloys," *Light Metals,* pp. 857-862, 2000.

[6]   A. Hardman and D. Young, "The grain refining performance of TICAR master alloys in various aluminum alloy systems," *Light metals 1998,* pp. 983-988, 1998.

[7]   M. Jaradeh, "The effect of processing parameters and alloy composition on the microstructure formation and quality of DC cast aluminium alloys," Doctoral Thesis, Materials Science and Engineering, School of Industrial Engineering and Management, Royal Institute of Technology, Stockholm, Sweden, 2006.

[8]   A. Whitehead and S. Danilak, "The Development of a Commercial Al-3% Ti-0.15% C Grain Refining Alloy," *Light Metals,* vol. 2, pp. 972-785, 1997.

[9]   A. Detomi, A. Messias, S. Majer and P. Cooper, "The impact of TiCAl and TiBAl grain refiners on cast house processing," *Light metals,* pp. 919-925, 2001.

[10]   B. Murty, S. Kori and M. Chakraborty, "Grain refinement of aluminium and its alloys by heterogeneous nucleation and alloying," International Materials Reviews, vol. 47, no. 1, pp. 3-29, 2002. copyright © Institute of Materials, Minerals and Mining and ASM International, reprinted by permission of Taylor & Francis Ltd, http://www.tandfonline.com on behalf of Institute of Materials, Minerals and Mining and ASM International.

[11]   M. Easton and D. StJohn, "Grain refinement of aluminum alloys: Part I. the nucleant and solute paradigms—a review of the literature," *Metallurgical and Materials Transactions A,* vol. 30, no. 6, pp. 1613-1623, 1999.

[12]   M. Guzowski, G. Sigworth and D. Sentner, "The role of boron in the grain," *Metallurgical and Materials Transactions A,* vol. 18, no. 4, pp. 603-619, 1987.

[13]   R. Vainik, J. Courtenay and B. Saglam, "Optimisation of grain refinement," in *Light Metals 2013*: Springer, 2016, pp. 1001-1008.

[14]   D. Qiu, J. Taylor and M.-X. Zhang, "Understanding the co-poisoning effect of Zr and Ti on the grain refinement of cast aluminum alloys," *Metallurgical and Materials Transactions A,* vol. 41, no. 13, pp. 3412-3421, 2010.

[15]   S. Kori, V. Auradi, B. Murty and M. Chakraborty, "Poisoning and fading mechanism of grain refinement in Al-7Si alloy," in *Proceedings of 3rd international conference on advanced materials processing (ICAMP-3)*, 2004: Processing (ICAMP-3), Melbourne, Australia, pp. 387-393.

[16]   A. Abdel-Hamid and A. Zaid, "Poisoning of grain refinement of some aluminium alloys," in *Current Advances in Mechanical Design and Production VII*: Elsevier, 2000, pp. 331-338.

[17]   M. Easton, J. F. Grandfield, D. H. StJohn and B. Rinderer, "The effect of grain refinement and cooling rate on the hot tearing of wrought aluminium alloys," in *Materials science forum*, 2006, vol. 519: Trans Tech Publ, pp. 1675-1680.

[18]   S. Li, K. Sadayappan and D. Apelian, "Role of grain refinement in the hot tearing of cast Al-Cu alloy," *Metallurgical and Materials Transactions B,* vol. 44, no. 3, pp. 614-623, 2013.

[19]   Y. Li, Q. Bai, J. Liu, H. Li, Q. Du, J. Zhang and L. Zhuang, "The influences of grain size and morphology on the hot tearing susceptibility, contraction, and load behaviors of AA7050 alloy inoculated with Al-5Ti-1B master alloy," *Metallurgical and Materials Transactions A,* vol. 47, no. 8, pp. 4024-4037, 2016.

[20]   M. Easton, H. Wang, J. Grandfield, D. St John and E. Sweet, "An analysis of the effect of grain refinement on the hot tearing of aluminium alloys," in *Materials forum*, 2004, vol. 28, pp. 224-229.

[21]   M. Easton, D. H. StJohn and L. Sweet, "Grain refinement and hot tearing of aluminium alloys-how to optimise and minimise," in *Materials Science Forum*, 2010, vol. 630: Trans Tech Publ, pp. 213-221.

[22]   S. Lin, "A study of hot tearing in wrought aluminium alloys," Master Thesis, University of Quebec in Chicoutimi, Chicoutimi, Canada, 1999.

[23]   D. StJohn, M. Qian, M. Easton and P. Cao, "The Interdependence Theory: The relationship between grain formation and nucleant selection," *Acta Materialia,* vol. 59, no. 12, pp. 4907-4921, 2011.

[24]   T. Quested, "Understanding mechanisms of grain refinement of aluminium alloys by inoculation," *Materials Science and Technology,* vol. 20, no. 11, pp. 1357-1369, 2004.

[25]   R. P. Sear, "Nucleation: theory and applications to protein solutions and colloidal suspensions," *Journal of Physics: Condensed Matter,* vol. 19, no. 3, p. 033101, 2007.

[26]   X. Liu, "Heterogeneous nucleation or homogeneous nucleation?," *The Journal of Chemical Physics,* vol. 112, no. 22, pp. 9949-9955, 2000.

[27]   M. A. Easton and D. H. StJohn, "A model of grain refinement incorporating alloy constitution and potency of heterogeneous nucleant particles," *Acta Materialia,* vol. 49, no. 10, pp. 1867-1878, 2001.

[28]   R. Haghayeghi, "Grain refinement and nucleation processes in aluminium alloys through liquid shearing," Doctoral Thesis, Brunel University School of Engineering and Design United Kingdom 2009.

[29]   K. Kelton, A. Greer, D. Herlach and D. Holland-Moritz, "The influence of order on the nucleation barrier," *MRS bulletin,* vol. 29, no. 12, pp. 940-944, 2004.

[30]   F. C. Campbell, *Elements of metallurgy and engineering alloys*. ASM International, 2008.

[31]   L. Baeckerud and M. Johnsson, "The relative importance of nucleation and growth mechanisms to control grain size in various aluminum alloys," 1996.

[32]   G. E. Totten and D. S. MacKenzie, *Handbook of aluminum: vol. 1: physical metallurgy and processes*. CRC press, 2003.

[33]   J. G. Kaufman, *Introduction to aluminum alloys and tempers*. ASM international, 2000.

[34]   J. R. Davis, *Aluminum and aluminum alloys*. ASM international, 1993.

[35]   M. Wang, "Joining Vacuum High Pressure Die Cast Aluminum Alloy A356 Subjected to Heat Treatment to Wrought Alloy 6061," Master Thesis, University of Windsor ,Windsor, Ontario, Canada, 2013.

[36]   R. D. Brown, F. Ambrose and D. Montagna, "Separation of Cast and Wrought Aluminum Alloys by Thermo-mechanical Processing," in "Report of Investigations 8960," Bureau of Mines,DEPARTMENT OF THE INTERIOR, UNITED STATES, 1985.

[37]   F. Iversen, "Meniscus Dynamics in Aluminium Extrusion Ingot Casting," Doctoral thesis, The Norwegian University of Science and Technology, Norway, 2002.

[38]   D. G. Eskin, *Physical metallurgy of direct chill casting of aluminum alloys*. CRC press, 2008.

[39]   R. E. O. Pelayo, "Direct Chill and Casting of Aluminum Alloys," Master Thesis, University of Waterloo, Waterloo, Ontario, Canada,, 2012.

[40]   K. Al-Helal, J. B. Patel, G. M. Scamans and Z. Fan, "Direct Chill Casting and Extrusion of AA6111 Aluminum Alloy Formulated from Taint Tabor Scrap," *Materials,* vol. 13, no. 24, p. 5740, 2020.

[41]   M. N. Jamaly, "The effects of microstructural features and process parameters on the hottearing in direct chill cast aluminum alloys," Master Thesis, University of British Columbia, Okanagan, Canada, 2012.

[42]   D. G. Eskin, V. I. Savran and L. Katgerman, "Effects of melt temperature and casting speed on the structure and defect formation during direct-chill casting of an Al-Cu alloy," *Metallurgical and Materials Transactions A,* vol. 36, no. 7, pp. 1965-1976, 2005.

[43]   P. I. Sarafoglou, A. Serafeim, I. A. Fanikos, J. S. Aristeidakis and G. N. Haidemenopoulos, "Modeling of microsegregation and homogenization of 6xxx Al-alloys including precipitation and strengthening during homogenization cooling," *Materials,* vol. 12, no. 9, p. 1421, 2019.

[44]   J. Langlais, "Fundamental study of hot tearing mechanisms of aluminium-silicon alloys," Doctoral Thesis, Department of Mining, Metals and Materials Engineering, McGill University, Montreal , Canada, 2006.

[45]   D. Eskin and L. Katgerman, "Solidification phenomena related to direct chill casting of aluminium alloys: fundamental studies and future challenges," *Materials Technology,* vol. 24, no. 3, pp. 152-156, 2009.

[46]   F. D'Elia, "A Study of Hot Tearing during Solidification of B206 Aluminum Alloy," Doctoral Thesis, Ryerson University, Toronto, Ontario, Canada, 2015.

[47]   S. Li, "Hot tearing in cast aluminum alloys: measures and effects of process variables," Doctoral Thesis, Worcester Polytechnic Institute, Worcester,USA, 2010.

[48]   Y. Li, H. Li, L. Katgerman, Q. Du, J. Zhang and L. Zhuang, "Recent advances in hot tearing during casting of aluminium alloys," *Progress in Materials Science,* vol. 117, p. 100741, 2021.

[49]   J. Song, F. Pan, B. Jiang, A. Atrens, M.-X. Zhang and Y. Lu, "A review on hot tearing of magnesium alloys," *Journal of Magnesium and Alloys,* vol. 4, no. 3, pp. 151-172, 2016.

[50]   H. Akhyar, V. Malau and P. Iswanto, "Hot tearing susceptibility of aluminum alloys using CRCM-Horizontal mold," *Results in Physics,* vol. 7, pp. 1030-1039, 2017, doi: //doi.org/10.1016/j.rinp.2017.02.041

[51]   A. Phillion, S. Thompson, S. Cockcroft and M. Wells, "Tensile properties of as-cast aluminum alloys AA3104, AA6111 and CA31218 at above solidus temperatures," *Materials Science and Engineering: A,* vol. 497, no. 1-2, pp. 388-394, 2008.

[52]   A. Phillion, "Hot tearing and constitutive behaviour of semi-solid aluminum alloys," Doctoral Thesis, University of British Columbia, British Columbia,Canada, 2007.

[53]   J.-M. Drezet and M. Rappaz, "Prediction of hot tears in DC-cast aluminum billets," in *Essential Readings in Light Metals*: Springer, 2016, pp. 912-918.

[54]   D. Eskin and L. Katgerman, "Mechanical properties in the semi-solid state and hot tearing of aluminium alloys," *Progress in materials science,* vol. 49, no. 5, pp. 629-711, 2004, doi: 10.1016/S0079-6425(03)00037-9.

[55]   G. Razaz and T. Carlberg, "Hot tearing susceptibility of AA3000 aluminum alloy containing Cu, Ti, and Zr," *Metallurgical and Materials Transactions A,* vol. 50, no. 8, pp. 3842-3854, 2019.

[56]   S. N. Dubey, "Study of hot tearing evaluation methods and quantification of contraction forces in die casting alloys," Doctoral Thesis, The Ohio State University, Columbus, Ohio, USA, 2015.

[57]   G. Cao, I. Haygood and S. Kou, "Onset of hot tearing in ternary Mg-Al-Sr alloy castings," *Metallurgical and Materials Transactions A,* vol. 41, no. 8, pp. 2139-2150, 2010.

[58]   R.-G. Guan and D. Tie, "A review on grain refinement of aluminum alloys: progresses, challenges and prospects," *Acta Metallurgica Sinica (English Letters),* vol. 30, no. 5, pp. 409-432, 2017.

[59]   N. Reddy, A. P. Rao, M. Chakraborty and B. Murty, "Prediction of grain size of Al–7Si Alloy by neural networks," *Materials Science and Engineering: A,* vol. 391, no. 1-2, pp. 131-140, 2005.

[60]   S. Liu, C. Cui, X. Wang, N. Li, J. Shi, S. Cui and P. Chen, "Effect of cooling rate on microstructure and grain refining behavior of in situ CeB6/Al composite inoculant in aluminum," *Metals,* vol. 7, no. 6, p. 204, 2017.

[61]   I. A. Mwamba, "Characterisation of Al-Ti-B Grain Refiners Prepared by Aluminothermic Reduction of TiO2 and B2O3," Master Thesis, School of Process and Materials Engineering - Faculty of Engineering and the Built Environment, Witwatersrand,Johannesbourg,South Africa, 2005.

[62]   Z. Fan, Y. Wang, Y. Zhang, T. Qin, X. Zhou, G. Thompson, T. Pennycook and T. Hashimoto, "Grain refining mechanism in the Al/Al–Ti–B system," *Acta Materialia,* vol. 84, pp. 292-304, 2015.

[63]   J. Yang, S. Bao, S. Akhtar and Y. Li, "The interactions between oxide film inclusions and inoculation particles TiB2 in aluminum melt," *Metallurgical and Materials Transactions B,* vol. 52, no. 4, pp. 2497-2508, 2021.

[64]   M. Lee and P. Grieveson, "Production of Al–Ti–B grain refining master alloys," *Materials science and technology,* vol. 19, no. 6, pp. 769-772, 2003.

[65]   S. Jha, A. Mandal and P. Srirangam, "Optimization of Casting Process Parameters for Synthesis of Al-Nb-B Master Alloy," *JOM,* vol. 71, no. 1, pp. 397-406, 2019.

[66]   Y. Zhao, Z. Lu, L. Mi, Z. Hu and W. Yang, "Morphological Evolution of TiB2 and TiAl3 in Al–Ti–B Master Alloy Using Different Ti Adding Routes," *Materials,* vol. 15, no. 6, p. 1984, 2022.

[67]   G. V. Kumar, B. Murty and M. Chakraborty, "Development of Al–Ti–C grain refiners and study of their grain refining efficiency on Al and Al–7Si alloy," *Journal of Alloys and Compounds,* vol. 396, no. 1-2, pp. 143-150, 2005.

[68]   A. Standard, "E112–12: standard test methods for determining average grain size. ASTM Int E112–12: 1–27," ed, 2012.

[69]   G. P. Jones and J. Pearson, "Factors affecting the grain-refinement of aluminum using titanium and boron additives," *Metallurgical Transactions B,* vol. 7, no. 2, pp. 223-234, 1976.

[70]   M. Johnsson, L. Backerud and G. K. Sigworth, "Study of the mechanism of grain refinement of aluminum after additions of Ti-and B-containing master alloys," *Metallurgical Transactions A,* vol. 24, no. 2, pp. 481-491, 1993.

[71]   G. K. Sigworth, "Communication on mechanism of grain refinement in aluminum," *Scripta materialia,* vol. 34, no. 6, pp. 919-922, 1996.

[72]   I. Maxwell and A. Hellawell, "A simple model for grain refinement during solidification," *Acta Metallurgica,* vol. 23, no. 2, pp. 229-237, 1975.

[73]   D. StJohn, A. Prasad, M. Easton and M. Qian, "The contribution of constitutional supercooling to nucleation and grain formation," *Metallurgical and Materials Transactions A,* vol. 46, no. 11, pp. 4868-4885, 2015.

[74]   A. A. Rao, B. Murty and M. Chakraborty, "Response of an Al—Cr alloy towards grain refinement by Al—5Ti-1B master alloy," *International Journal of Cast Metals Research,* vol. 9, no. 3, pp. 125-132, 1996.

[75]   Y. Wang, C. Fang, L. Zhou, T. Hashimoto, X. Zhou, Q. Ramasse and Z. Fan, "Mechanism for Zr poisoning of Al-Ti-B based grain refiners," *Acta materialia,* vol. 164, pp. 428-439, 2019.

[76]   M.-X. Zhang, P. M. Kelly, M. A. Easton and J. A. Taylor, "Crystallographic study of grain refinement in aluminum alloys using the edge-to-edge matching model," *Acta Materialia,* vol. 53, no. 5, pp. 1427-1438, 2005.

[77]   F. Wang, D. Qiu, Z.-L. Liu, J. A. Taylor, M. A. Easton and M.-X. Zhang, "Crystallographic study of grain refinement of Al by Nb addition," *Journal of Applied Crystallography,* vol. 47, no. 2, pp. 770-779, 2014.

[78]   Q. Bai, Y. Li, H. Li, Q. Du, J. Zhang and L. Zhuang, "Roles of alloy composition and grain refinement on hot tearing susceptibility of 7××× aluminum alloys," *Metallurgical and Materials Transactions A,* vol. 47, no. 8, pp. 4080-4091, 2016.

[79]   P. Kelly and M.-X. Zhang, "Edge-to-edge matching—The fundamentals," *Metallurgical and Materials Transactions A,* vol. 37, no. 3, pp. 833-839, 2006.

[80]   Z. Liu, "Review of grain refinement of cast metals through inoculation: theories and developments," *Metallurgical and Materials Transactions A,* vol. 48, no. 10, pp. 4755-4776, 2017.

[81]   M. Li, J. Li, D. Qiu, Q. Zheng, G. Wang and M.-X. Zhang, "Crystallographic study of grain refinement in low and medium carbon steels," *Philosophical Magazine,* vol. 96, no. 15, pp. 1556-1578, 2016.

[82]   Y.-c. Huang, Z.-b. Xiao and Y. Liu, "Crystallography of Zr poisoning of Al-Ti-B grain refinement using edge-to-edge matching model," *Journal of Central South University,* vol. 20, no. 10, pp. 2635-2642, 2013.

[83]   X.-F. Gu, T. Furuhara and W.-Z. Zhang, "PTCLab: free and open-source software for calculating phase transformation crystallography," *Journal of applied crystallography,* vol. 49, no. 3, pp. 1099-1106, 2016.

[84]   M. Easton, C. Davidson and D. StJohn, "Grain morphology of as-cast wrought aluminium alloys," *Materials transactions,* vol. 52, no. 5, pp. 842-847, 2011.

[85]   M. Easton, C. Davidson and D. St John, "Effect of alloy composition on the dendrite arm spacing of multicomponent aluminum alloys," *Metallurgical and materials transactions A,* vol. 41, no. 6, pp. 1528-1538, 2010.

[86]   D. G. McCartney, "Grain refining of aluminium and its alloys using inoculants," *International Materials Reviews,* vol. 34, no. 1, pp. 247-260, 1989.

[87]   A. Greer, A. Bunn, A. Tronche, P. Evans and D. Bristow, "Modelling of inoculation of metallic melts: application to grain refinement of aluminium by Al–Ti–B," *Acta materialia,* vol. 48, no. 11, pp. 2823-2835, 2000.

[88]   M. A. Easton, D. H. StJohn and A. Prasad, "Grain refinement of aluminium alloys: recent developments in predicting the as-cast grain size of alloys refined by Al-Ti-B master alloys," *Light metals 2014,* pp. 939-944, 2014.

[89]   Z. Fan, F. Gao, Y. Wang, H. Men and L. Zhou, "Effect of solutes on grain refinement," *Progress in Materials Science,* vol. 123, p. 100809, 2022.

[90]   M. Easton and D. StJohn, "An analysis of the relationship between grain size, solute content, and the potency and number density of nucleant particles," *Metallurgical and materials transactions A,* vol. 36, no. 7, pp. 1911-1920, 2005.

[91]   K. Symeonidis, "The Controlled Diffusion Solidification Process--Fundamentals and Principles," Doctoral Thesis, Worcester Polytechnic Institute, Worcester, U.S.A, 2009.

[92]   W. Ding, T. Xia and W. Zhao, "Performance comparison of Al–Ti master alloys with different microstructures in grain refinement of commercial purity aluminum," *Materials,* vol. 7, no. 5, pp. 3663-3676, 2014.

[93]   P. Li, E. Kandalova and V. Nikitin, "Grain refining performance of Al–Ti master alloys with different microstructures," *Materials Letters,* vol. 59, no. 6, pp. 723-727, 2005.

[94]   J. Zhao, J. He, Q. Tang, T. Wang and J. Chen, "Grain refinement efficiency in commercial-purity aluminum influenced by the addition of Al-4Ti master alloys with varying TiAl3 particles," *Materials,* vol. 9, no. 11, p. 869, 2016.

[95]   G. Vinod Kumar, B. Murty and M. Chakraborty, "Effect of TiAl3 particles size and distribution on their settling and dissolution behaviour in aluminium," *Journal of materials science,* vol. 45, no. 11, pp. 2921-2929, 2010.

[96]   L. Arnberg, L. Bäckerud and H. Klang, "Intermetallic particles in Al–Ti–B–type master alloys for grain refinement of aluminium," *Metals Technology,* vol. 9, no. 1, pp. 7-13, 1982.

[97]   O. Yücel and F. Ç. Şahin, "Production of aluminum-titanium-boron master alloy by aluminothermic process," *High Temperature Materials And Processes,* vol. 20, no. 2, pp. 137-142, 2001.

[98]   T. Quested, A. L. Greer and P. Cooper, "The variable potency of TiB2 nucleant particles in the grain refinement of aluminium by Al-Ti-B additions," in *Materials Science Forum*, 2002, vol. 396: Trans Tech Publ, pp. 53-58.

[99]   Y.-Z. Zhao, X.-T. Liu and H. Hao, "Effect of Al4C3 Particle Size Distribution in a Al–2.5 C Master Alloy on the Refining Efficiency of the AZ31 Alloy," *Acta Metallurgica Sinica (English Letters),* vol. 30, no. 6, pp. 505-512, 2017.

[100] A. Greer, "Grain refinement of alloys by inoculation of melts," *Philosophical Transactions of the Royal Society of London. Series A: Mathematical, Physical and Engineering Sciences,* vol. 361, no. 1804, pp. 479-495, 2003.

[101] T. Quested and A. Greer, "The effect of the size distribution of inoculant particles on as-cast grain size in aluminium alloys," *Acta materialia,* vol. 52, no. 13, pp. 3859-3868, 2004.

[102] A. Greer, "Overview: Application of heterogeneous nucleation in grain-refining of metals," *The Journal of chemical physics,* vol. 145, no. 21, p. 211704, 2016.

[103] T. Quested and A. Greer, "Athermal heterogeneous nucleation of solidification," *Acta Materialia,* vol. 53, no. 9, pp. 2683-2692, 2005.

[104] P. Cooper, A. Hardman, D. Boot and E. Burhop, "Characterisation of a new generation of grain refiners for the foundry industry," in *LIGHT METALS-WARRENDALE-PROCEEDINGS-*, 2003: Citeseer, pp. 923-928.

[105] W. Schneider, M. Kearns, M. McGarry and A. Whitehead, "A comparison of the behaviour of AlTiB and AlTiC grain refiners," in *Essential readings in light metals*: Springer, 2016, pp. 400-408.

[106] J. Mitchell, S. Cockcroft, D. Viano, C. Davidson and D. StJohn, "Determination of strain during hot tearing by image correlation," *Metallurgical and Materials Transactions A,* vol. 38, no. 10, pp. 2503-2512, 2007.

[107] W. S. Pellini, "Strain theory of hot tearing," *Foundry,* vol. 80, no. 11, pp. 125-133, 1952.

[108] M. N. Esfahani and B. Niroumand, "Study of hot tearing of A206 aluminum alloy using Instrumented Constrained T-shaped Casting method," *Materials characterization,* vol. 61, no. 3, pp. 318-324, 2010.

[109] F. D'Elia and C. Ravindran, "09-055 Effect of Ti-B Grain Refiner on Hot Tearing in Permanent Mold Cast B206 Aluminum Alloy," *Transactions of the American Foundrymen's Society,* vol. 117, p. 139, 2009.

[110] D. Eskin, D. Suyitno, J. Mooney and L. Katgerman, "Contraction of Aluminum Alloys during and after Solidification," *Metallurgical and Materials Transactions-Series A,* vol. 35, no. 4, pp. 1325-1336, 2004.

[111] J. Langlais, "Fundamental study of hot tearing mechanisms of aluminium-silicon alloys," Doctoral Thesis, Department of Mining and Materials Engineering, McGill University, Montreal, Canada, 2006.

[112] M. A. Easton, M. A. Gibson, S. Zhu and T. B. Abbott, "An a priori hot-tearing indicator applied to die-cast magnesium-rare earth alloys," *Metallurgical and Materials Transactions A,* vol. 45, no. 8, pp. 3586-3595, 2014.

[113] J. Rakhmonov, M. Qassem, D. Larouche, K. Liu, M. Javidani, J. Colbert and X.-G. Chen, "A New Approach to Determine Tensile Stress-Strain Evolution in Semi-Solid State at Near-Solidus Temperature of Aluminum Alloys," *Metals,* vol. 11, no. 3, p. 396, 2021.

[114] H.-T. Li, P. Zhao, R. Yang, J. B. Patel, X. Chen and Z. Fan, "Grain refinement and improvement of solidification defects in direct-chill cast billets of A4032 alloy by melt conditioning," *Metallurgical and Materials Transactions B,* vol. 48, no. 5, pp. 2481-2492, 2017.

[115] K. Niesel, "Determination of the specific surface by measurement of permeability," *Matériaux et Construction,* vol. 6, no. 3, pp. 227-231, 1973.

[116] A. Kumar, M. Založnik, H. Combeau, G. Lesoult and A. Kumar, "Channel segregation during columnar solidification: Relation between mushy zone instability and mush permeability," *International Journal of Heat and Mass Transfer,* vol. 164, p. 120602, 2021.

[117] R. Nolen-Hoeksema, "Defining and determining permeability," *Oilfield Review,* vol. 26, no. 3, 2014.

[118] S. Earle, *Physical geology*. BCcampus, 2015.

[119]   L. Miaomiao, S. Benbiao, T. Changbing and M. Xianyu, "Relationship between pore throat and permeability of porous carbonate reservoir in the Middle East," *Arabian Journal of Geosciences,* vol. 15, no. 1, pp. 1-7, 2022.

[120]   M. S. A. Perera, "A comprehensive overview of CO2 flow behaviour in deep coal seams," *Energies,* vol. 11, no. 4, p. 906, 2018.

[121]   M. Johnsson, "Influence of Zr on the grain refinement of aluminium," *International Journal of Materials Research,* vol. 85, no. 11, pp. 786-789, 1994.

[122]   N. Lashko, G. Matveeva, G. Morozova and L. Zhorova, "Nucleation cellar dendrite crystallization of the Al-Mg-Ti-Zr alloy," *Izvestiya Akademii Nauk SSSR, Metally,* pp. 121-123, 1979.

[123]   A. Arjuna Rao, B. Murty and M. Chakraborty, "Influence of chromium and impurities on the grain-refining behavior of aluminum," *Metallurgical and Materials transactions A,* vol. 27, no. 3, pp. 791-800, 1996.

[124]   A. A. Rao, B. Murty and M. Chakraborty, "Role of zirconium and impurities in grain refinement of aluminium lNith AI-Ti-B," *Materials science and technology,* vol. 13, no. 9, pp. 769-777, 1997.

[125]   M.-X. Zhang and P. Kelly, "Edge-to-edge matching model for predicting orientation relationships and habit planes—the improvements," *Scripta Materialia,* vol. 52, no. 10, pp. 963-968, 2005.

[126]   Z. Chen and K. Yan, "Grain refinement of commercially pure aluminum with addition of Ti and Zr elements based on crystallography orientation," *Scientific Reports,* vol. 10, no. 1, pp. 1-8, 2020.

[127]   P. Schumacher and A. Greer, "Studies of the action of grain-refining particles in aluminium alloys," in *Essential Readings in Light Metals*: Springer, 2016, pp. 366-374.